CONTENTS

	Page	
INTRODUCTION	1	1/A4
SYMBOLS AND ABBREVIATIONS	2	1/A5
AIRCRAFT DESCRIPTION	5	1/A8
ELEMENTS OF FLIGHT CONTROL SYSTEM	6	1/A9
Air Data Sensors	6	1/A9
Air Data Computer	8	1/A11
Original Altitude and Mach Hold Control Systems	8	1/A11
FLIGHT INSTRUMENTATION	9	1/A12
SIMULATION SYSTEM	11	1/A14
Aerodynamic and Propulsion Dynamics	11	1/A14
Control System	12	1/B1
Air Data Computer	12	1/B1
RESULTS AND DISCUSSION	14	1/B3
Altitude Hold Autopilot	14	1/B3
Original Altitude Hold Operation	14	1/B3
Simulation Studies	16	1/B5
Pitch Flight Control System Hardware Changes	35	1/C10
In-Flight Performance of Modified Autopilot	37	1/C12
Mach Hold Autopilot	52	1/D13
Original Mach Hold Operation	53	1/D14
Simulation Studies	54	1/E1
Mach Hold Flight Results With ADC Connected to p_{s_3}	59	1/E6
CONCLUDING REMARKS	61	1/E8
APPENDIX A.—DETAILED DESCRIPTION OF FLIGHT CONTROL SYSTEM ELEMENTS	62	1/E9
APPENDIX B.—DEFINITION OF DAMPING INDEX AND RELATIONSHIP WITH SECOND-ORDER SYSTEM SUBSIDENCE RATIO	71	1/F4
APPENDIX C.—ANALYSIS OF MODIFIED AUTOPILOT HIGH FREQUENCY OSCILLATION	73	1/F6
REFERENCES	80	1/F13

NAS1.60:1180

APR 28 1978

NASA Technical Paper 1180

COMPLETED
ORIGINAL

Results From Flight and Simulator Studies of a Mach 3 Cruise Longitudinal Autopilot

Glenn B. Gilyard and John W. Smith

APRIL 1978

NASA

85

NAS 1.60: 1180

NASA Technical Paper 1180

Results From Flight and Simulator Studies of a Mach 3 Cruise Longitudinal Autopilot

Glenn B. Gilyard and John W. Smith
Dryden Flight Research Center
Edwards, California

NASA
National Aeronautics
and Space Administration

**Scientific and Technical
Information Office**

1978

RESULTS FROM FLIGHT AND SIMULATOR STUDIES OF A MACH 3 CRUISE LONGITUDINAL AUTOPILOT

Glenn B. Gilyard and John W. Smith
Dryden Flight Research Center

INTRODUCTION

For subsonic jet transports, accurate control of altitude and Mach number is necessary for such items as air traffic control and good ride qualities. For aircraft operating at high altitudes and supersonic Mach numbers, accurate control becomes increasingly necessary for maximum range performance. The aircraft of the YF-12 series present an excellent opportunity to document the interaction of various autopilot schemes, upper atmospheric effects, and aircraft dynamics for the advancement of supersonic cruise aircraft technology.

The precise control of flightpath and speed becomes increasingly difficult at high altitude, high speed flight conditions. Large excursions in altitude or speed, or both, have been experienced with the XB-70 (ref. 1), YF-12 (ref. 2), and Concorde (ref. 3) airplanes. Factors that contribute to such performance include decreases in aircraft stability, low static pressure, atmospheric disturbances such as temperature variations, and unfavorable aircraft-propulsion system interactions. Low atmospheric static pressure makes precise altitude control difficult because of poor pressure transducer resolution. In addition, the combination of high altitude and high speed contributes to an unfavorable balance between kinetic and potential energy, which in turn makes large altitude changes necessary to correct for small Mach number changes when the aircraft is flown in a Mach hold mode through the elevator. Interactions between the aircraft and the propulsion system also become a significant factor at high altitude, high speed flight conditions. Reference 2 presents flight data illustrating that longitudinally, the YF-12 aircraft's phugoid mode has a larger amplitude and less stability with the inlets operating automatically than with the inlet geometry fixed.

One aspect of the YF-12 research program is to identify the deficiencies of the original autopilot, which is approximately 10 years old, and to implement an autopilot improvement program. The first part of the improvement program was to update the existing altitude hold mode of the autopilot with minimal modification to reflect recent knowledge and experience. In subsequent phases, an autothrottle for speed control is to be implemented and an integrated airplane-propulsion system controller

(ref. 2) is to be developed to utilize previously identified lateral-directional airplane-propulsion system interactions (refs. 4 and 5).

This report presents flight data obtained with the original altitude hold and Mach hold control systems and the results of simulator studies, which include parametric variations of various gains. Flight test results for the modified altitude hold autopilot and the Mach hold autopilot when connected to an angle-of-attack-insensitive static pressure source are also presented. A condensed version of this report is presented in reference 6.

SYMBOLS AND ABBREVIATIONS

Physical quantities in this report are given in the International System of Units (SI) and parenthetically in U.S. Customary Units. The measurements were taken in Customary Units. The decibels in this report are $20 \log_{10} \frac{|\text{output}|}{|\text{input}|}$.

A	amplitude of sine wave oscillation
$A(N)$	actuator nonlinearity, ±0.15° hysteresis
$A_I(s)$	inboard actuator transfer function
$A_O(s)$	outboard actuator transfer function
ADC	air data computer
a_n	normal acceleration at center of gravity (unless otherwise noted), g
B	first bending mode
$\frac{B}{\delta_e}(s)$	first bending mode transfer function
D	nonlinearity width
DI	damping index, $\frac{X_2 - X_1}{X_0 - X_1}$ (derived in app. B)
F	$\equiv \frac{\Delta p_s / p_s}{\Delta M / M}$
$F_{HP}(s)$	high-pass filter
$F_{st}(s)$	structural filter

$F_1(s), F_2(s)$	shaping filter
f	frequency, Hz
G_D	describing function
$G_Y(N)$	backup gyro nonlinearity
$G'(s)$	equivalent system forward-loop elements
$H(s)$	SAS feedback loop filters
$H'(s)$	equivalent system feedback elements
h	altitude, m (ft)
j	$= \sqrt{-1}$
K	gain
M	Mach number
m	peak number of sine wave oscillation
PLA	power lever angle, deg
p_s	static pressure, N/m^2 (lb/ft^2)
$p_s(\alpha)$	variation of static pressure error with angle of attack, N/m^2/deg (lb/ft^2/deg)
p_{sl}	sea level static pressure, N/m^2 (lb/ft^2)
p_{t_2}	total pressure, N/m^2 (lb/ft^2)
q_c	impact pressure, $p_{t_2} - p_s$, N/m^2 (lb/ft^2)
R	$= p_{t_2}/p_s$
SAS	stability augmentation system
s	Laplace operator, 1/sec

t	time, sec
t_{30}	time required to reac and maintain altitude within ±9.1 meters (±30 feet) of steady state, sec
$X(t)$	$= Ae^{-\zeta\omega_n t}$
X_m	peak amplitude of sine wave oscillation; m = 0 is the reference peak and m = 1,2,3,... are the successive peaks
α	wing reference plane angle of attack, deg
δ	$= -\zeta/\sqrt{1-\zeta^2}$
δ_e	average elevon deflection, deg and rad
δ_{θ_L}, $\delta_{\dot{\theta}}$	autopilot gains
ζ	damping ratio
θ	pitch attitude, deg and rad
θ_c	controlled attitude, rad
θ_r	reference attitude, rad
$\frac{\dot{\theta}}{\delta_e}(s)$	aircraft transfer function
τ	time constant
τ_{sl}	ime constant referenced to sea level
τ_{θ_L}	autopilot time constant
φ	phase angle, deg
ω	frequency, rad/sec
ω_d	damped frequency, rad/sec
ω_n	natural frequency, rad/sec

Subscripts:

1,2	compensated static pressure location
3	uncompensated static pressure location

A dot over a quantity denotes the time derivative of that quantity.

AIRCRAFT DESCRIPTION

The YF-12 airplane is an advanced, twin-engined, delta-winged interceptor designed for long-range cruise at Mach numbers greater than 3.0 and altitudes above 24,400 meters (80,000 feet). A photograph and a three-view drawing of the airplane are shown in figures 1 and 2. Pertinent physical characteristics are given in reference 4.

E-23090

Figure 1. YF-12 airplane.

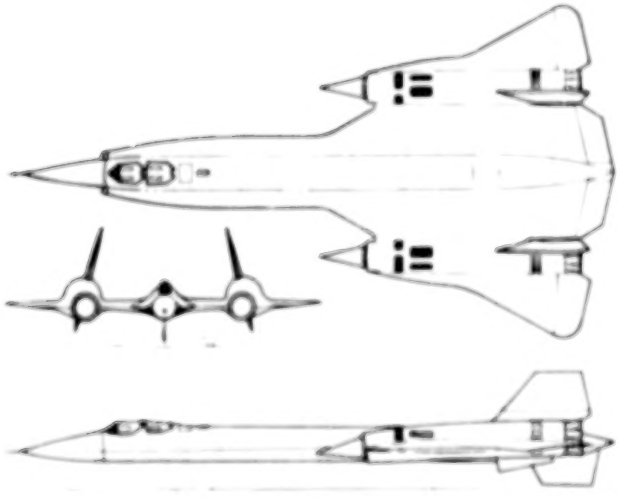

Figure 2. Three-view drawing of YF-12 airplane.

Two nacelle-mounted, all-movable vertical tails provide directional stability and control. Each vertical tail is canted inward and pivots on a small stub section attached directly to the top of the nacelle. Three ventral fins enhance directional stability; one is fastened along the fuselage centerline and two small fixed fins extend down from the nacelles below the two main vertical tails. The centerline ventral fin folds out of the way for landing.

Two elevons on each wing, one inboard and one outboard of each nacelle, perform the combined functions of ailerons and elevators.

The airplane has two axisymmetric, variable-geometry, mixed-compression inlets, which supply air to two J58 engines. Each inlet has a translating spike and forward bypass doors to control the position of the normal shock in the inlet. An automatic inlet control system varies the spike and bypass door position to keep the normal shock in the optimum position. Manual control of the spike and bypass doors is also available to the pilot.

ELEMENTS OF FLIGHT CONTROL SYSTEM

The main elements of the pitch-axis flight control system are the air data sensors, the air data computer, and the original autopilot control system. These items are briefly discussed in this section; a more detailed description is presented in appendix A.

Air Data Sensors

The air data parameters, static and total pressure, are obtained from the compensated nose boom illustrated in figure 3. A more detailed view of the three static pressure source locations is presented in figure 4. The air data computer is connected to p_{s_2}, which is compensated to minimize position error corrections, but is sensitive to angle of attack as shown in figure 5.

The variation of static pressure error with angle of attack in figure 5, which is referred to throughout this report as the nominal $p_s(\alpha)$, was determined from slow pullup-pushover maneuvers of approximately 20 to 30 seconds' duration. The nominal $p_s(\alpha)$ at Mach 3.0 and 23,600 meters (77,500 feet) at a typical trim angle of attack is equivalent to an altitude error of 49 meters (161 feet) per degree angle of attack or a Mach error of 0.011 per degree angle of attack.

The p_{s_3} source was not originally on the nose boom, but was added for research purposes. The p_{s_3} measurements require large position error corrections transonically but have negligible sensitivity to angle of attack.

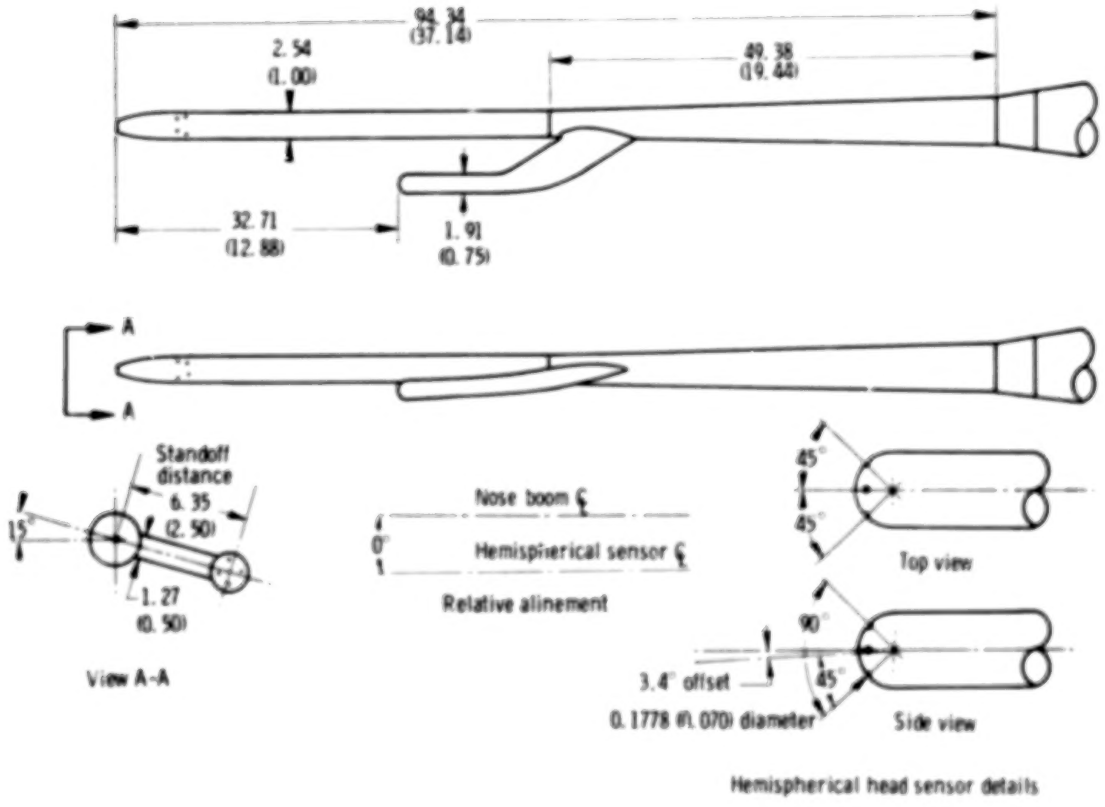

Figure 3. Three-view drawing of nose boom and pitot-static probe showing hemispherical head flow direction sensor. Dimensions in centimeters (inches).

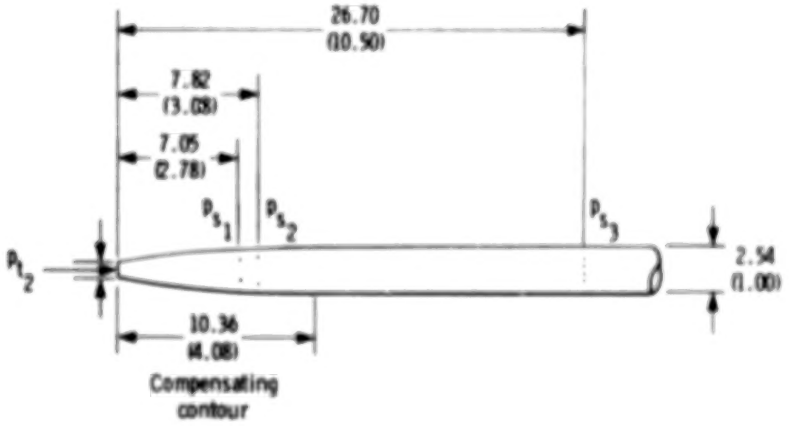

Figure 4. Static pressure source locations on compensated nose boom. Dimensions in centimeters (inches).

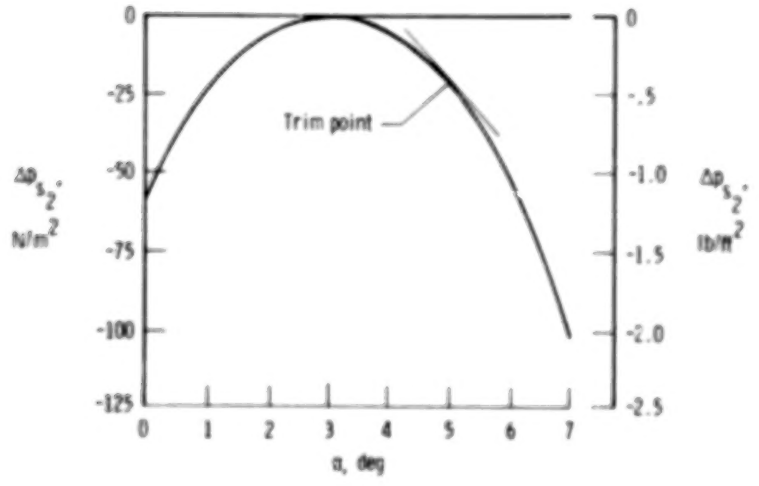

Figure 5. Variation of static pressure error with angle of attack, $p_s(\alpha)$. $M \approx 3.0$, $h = 23,600$ meters (77,500 feet). At the trim point, $\Delta p_{s_2}/\Delta\alpha = -23.9$ N/m^2/deg (-0.50 lb/ft^2/deg), which is equivalent to $\Delta h/\Delta\alpha = 49$ m/deg (161 ft/deg) or $\Delta M/\Delta\alpha = 0.011$/deg.

At 23,600 meters (77,500 feet), the approximate lags due to the tubing lengths of the static pressure and total pressure systems are 2.00 seconds and 0.75 second, respectively.

Air Data Computer

The air data computer (ADC) is an electromechanical device that receives total and static pressure from the nose boom and computes Mach number and altitude information for the cockpit display and the autopilot. The threshold of the static pressure loop at an altitude of 23,600 meters (77,500 feet) is approximately 3.7 meters (12 feet) and its frequency response is constant to approximately 0.5 radian per second.

Original Altitude and Mach Hold Control Systems

Figure 6 is a pitch-axis block diagram of the vehicle control system. At Mach 3.0 and an altitude of 23,600 meters (77,500 feet), the gains and time constant for the original autopilot, which are referred to throughout this report as the nominal settings, are as follows:

$$K_{\theta_{\dot{h}}} = 440 \text{ deg } \theta/\dot{\overline{ln\ p_s}}$$

$$K_{\theta_h} = 170 \text{ deg } \theta/\Delta ln\ p_s$$

$$K_{\theta \int h} = 14 \text{ (deg/sec } \dot{\theta})/\Delta ln\ p_s$$

$$K_{\theta \int M} = 20 \text{ (deg/sec } \dot{\theta})/\Delta ln\ (R - 1)$$

$$K_{\theta_M} = 61 \text{ deg } \theta/\Delta ln\ (R - 1)$$

$$K_{\theta_{\dot{M}}} = 0 \text{ deg } \theta/\overline{ln\ (\dot{R} - 1)}$$

$$K_\theta = 1$$

$$K_h = 1$$

$$\delta_{\dot{\theta}} = 0.295 \text{ deg } \delta_e/\text{(deg/sec } \dot{\theta})$$

$$\tau_{\theta_L} = 5.75$$

$$\delta_{\theta_L} = 3.50 \text{ deg } \delta_e/\text{deg } \theta$$

The pitch stability augmentation system (SAS) is used full time for normal aircraft operation and attitude hold is the primary autopilot mode. In addition to the basic attitude hold autopilot, the pilot can select either altitude hold or Mach hold as an outer loop of attitude hold.

The altitude hold autopilot receives altitude rate and altitude error information from the ADC and commands attitude changes proportional to the altitude rate, altitude error, and integral of altitude error. Similarly, the Mach hold autopilot receives Mach error information from the ADC and commands attitude changes proportional to the Mach error and the integral of Mach error.

Both the pitch SAS and attitude hold loops, which are inner loops for the altitude hold and Mach hold modes, performed satisfactorily.

FLIGHT INSTRUMENTATION

A standard set of stability and control parameters was recorded. The angular rate and linear acceleration instrumentation was alined with the body axes. The angle-of-attack indicator was attached as a dogleg on the nose boom, which also contained an airspeed-altitude probe (fig. 3). A fixed four-port pressure-sensing

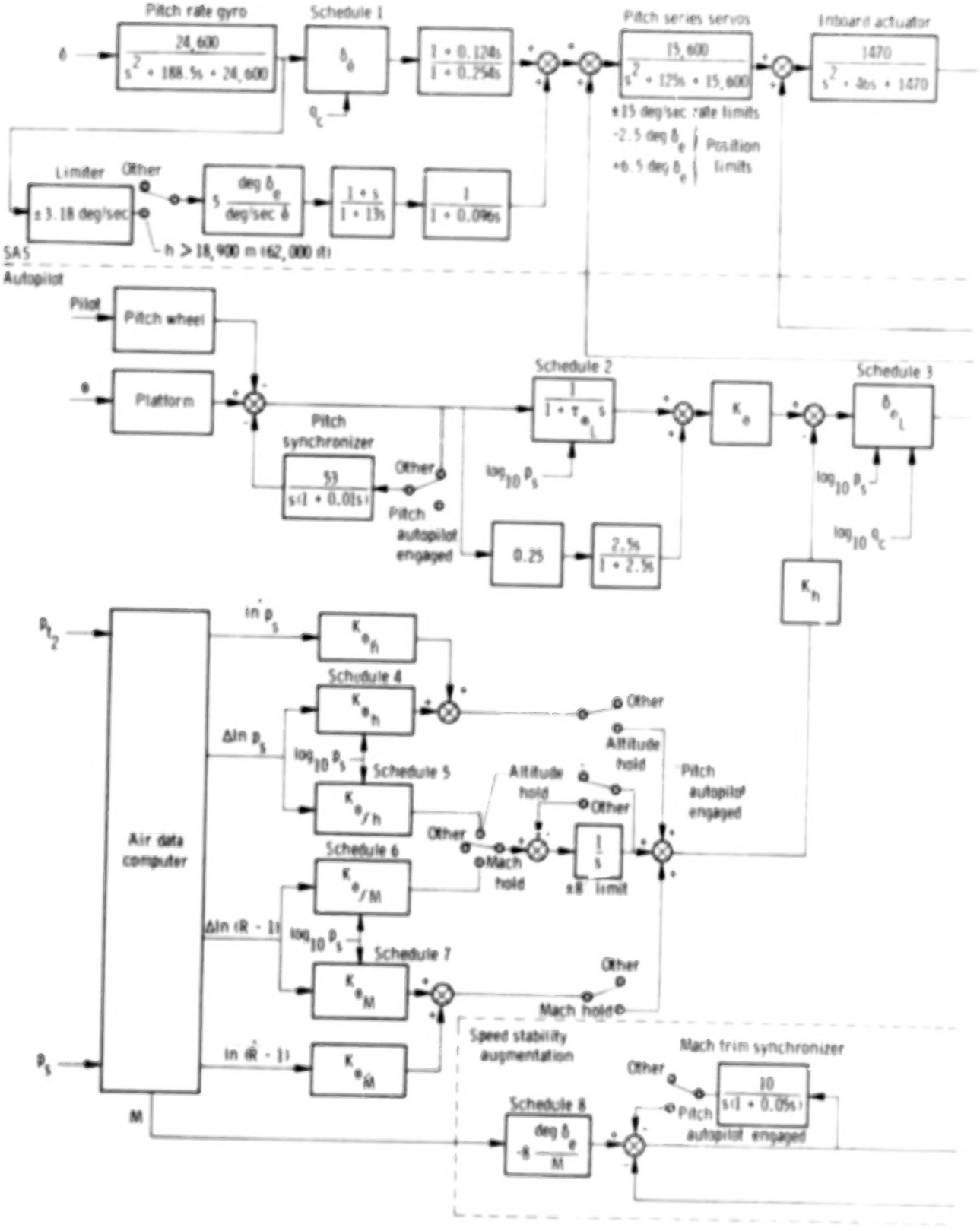

Figure 6. Pitch-axis block diagram for the YF-12 vehicle control system.

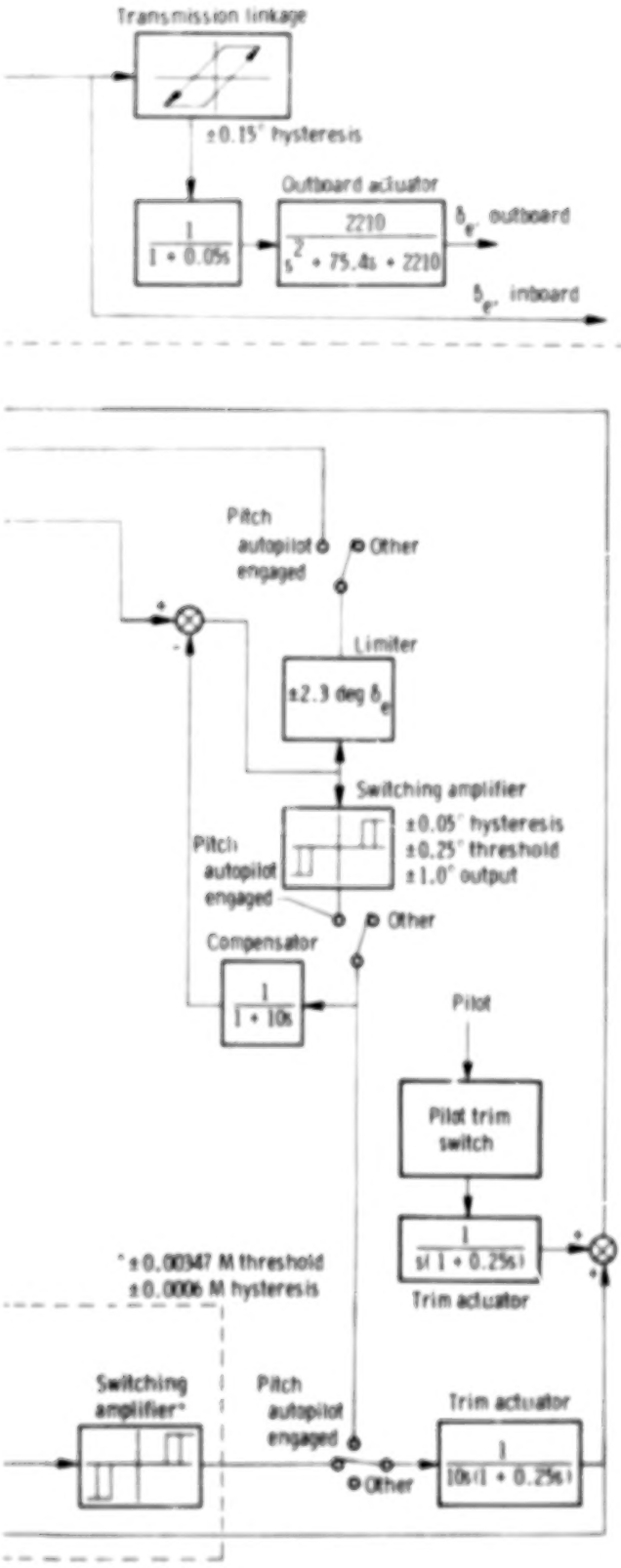

Schedules are given in figure 52.

hemispherical head was used to obtain angle-of-attack measurements on the airplane (ref. 7). The lag associated with the hemispherical head was significantly different from that predicted by first-order lag theory (ref. 8). The actual angle-of-attack system lag at Mach 3.0 flight conditions was approximately 0.4 second.

In addition, data were recorded at test points within the autopilot control system to analyze system performance and to detect system problems. All the data were recorded on magnetic tape at 200 samples per second.

SIMULATION SYSTEM

A digital simulation was implemented to investigate closed-loop aircraft-control system problems. The simulation included aircraft and propulsion dynamics, the control system, and an air data computer model. An integration interval of 20 milliseconds was used for the entire simulation.

Aerodynamic and Propulsion Dynamics

The simulation was modeled for the flight conditions at Mach 3.0 and an altitude of 23,600 meters (77,500 feet). The simulation was a modification of that described in reference 9 and included the three longitudinal degrees of freedom. Dynamic pressure flexibility corrections were included for pitch control, although no structural modes were simulated. The variation of density with altitude was also included.

High speed inlet operation and the afterburner range of engine operation were represented in sufficient detail to permit investigation of the aerodynamic and propulsion system interactions. Only normal inlet operation was modeled.

Control System

With the exception of the speed stability system, which has no effect at the flight condition of the study, the control system illustrated in figure 6 was implemented. The schedules were programed as functions of static or dynamic pressure, or both. All control system dynamics above 5 hertz were not modeled.

Air Data Computer

Accurate modeling of the ADC was required because the ADC generates the altitude and Mach signals input to the autopilot. Initial attempts at linearization proved inadequate in the complete closed-loop simulation. Figure 7 presents the complete

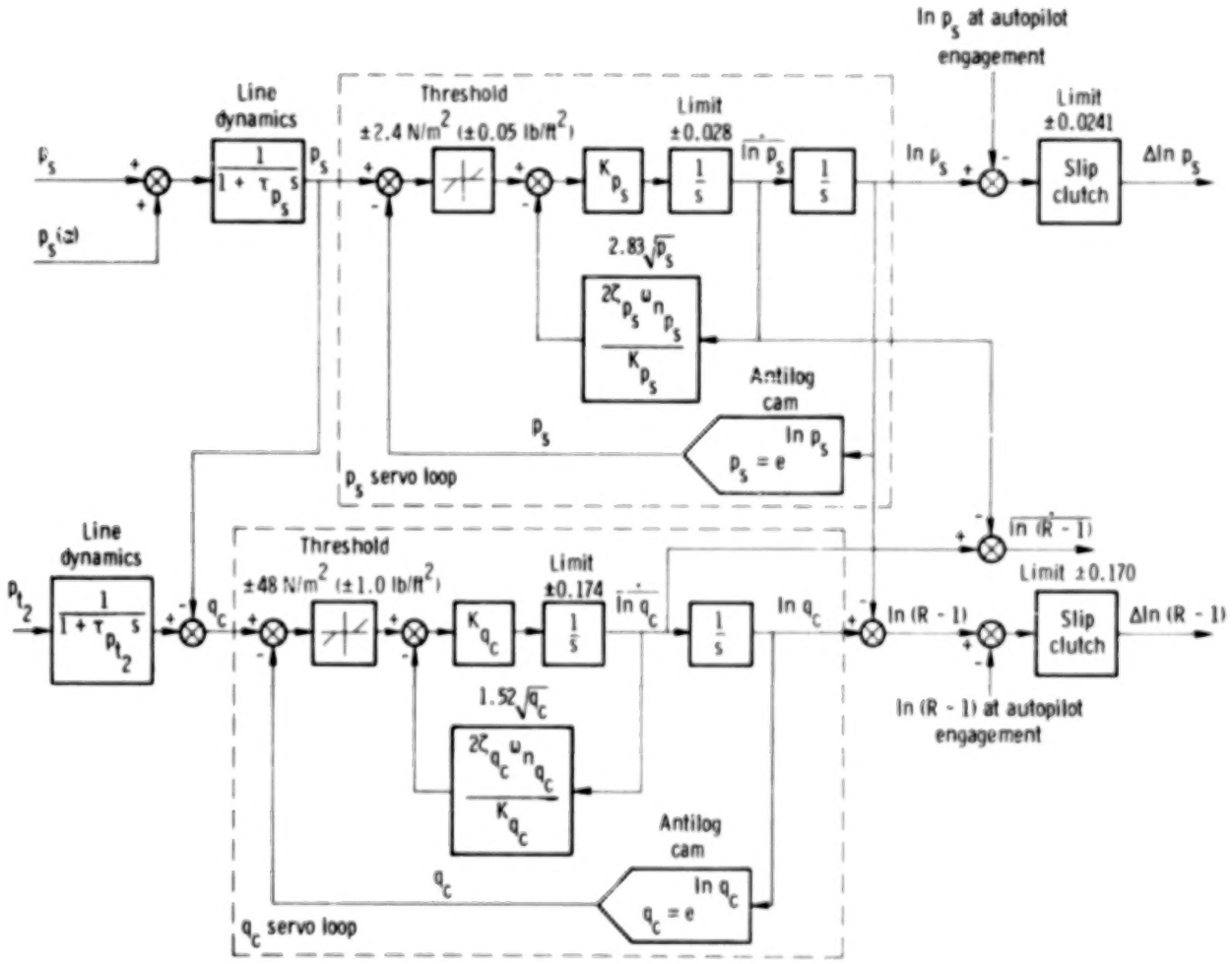

Figure 7. Simulation mechanization of air data computer.

ADC model (based on the ADC description in appendix A) used in the simulation. The system characteristics were defined as follows:

$$\tau_{p_s} = 1.8 \text{ sec}$$

$$\omega_{n_{p_s}} = 0.71 \sqrt{p_s}$$

$$\zeta_{p_s} = 1.0$$

$$K_{p_s} = \frac{\omega_{n_{p_s}}^2}{p_s}$$

$$\tau_{p_{t_2}} = 0.2 \text{ sec}$$

$$\omega_{n_{q_c}} = 0.83 \sqrt{q_c}$$

$$\zeta_{q_c} = 0.63$$

$$K_{q_c} = \frac{\omega_{n_{q_c}}^2}{q_c}$$

The limits in the servo loops were due to the rate limits of the motor used in the rebalancing hardware. The slip clutch limits were due to the limited range of the potentiometer, which was designed to get maximum resolution at the expense of a larger error output range.

The inputs to the ADC model were true static pressure, p_s, and total pressure, p_{t_2}. Angle-of-attack sensitivity was added to p_s and first-order line dynamics were added to p_s and p_{t_2}.

The outputs of the ADC were logarithmic functions, which were approximately linearly proportional to altitude and Mach number over the perturbation range of interest.

RESULTS AND DISCUSSION

Altitude Hold Autopilot

This section presents the results of the altitude hold autopilot investigation. The discussion covers the original altitude hold performance; simulation studies, which include parametric variations of the feedback gains; the actual hardware changes made to improve the autopilot; and the in-flight performance evaluation of the modified altitude hold mode.

Original Altitude Hold Operation

The altitude hold mode of the YF-12 autopilot was designed as a loiter mode for use at altitudes of approximately 9100 meters (30,000 feet), although operation was permitted at altitudes up to 18,300 meters (60,000 feet). The control system does not limit altitude hold operation to 18,300 meters (60,000 feet) since the autopilot gains extend to the altitude and speed capabilities of the aircraft. However, the U.S. Air Force performed a preliminary evaluation of the altitude hold mode at altitudes exceeding 21,300 meters (70,000 feet) and found its operation to vary considerably from day to day. Occasionally, altitude could be held within ±15 meters (±50 feet) while at other times altitude diverged in an unacceptable manner.

An example of acceptable altitude control at approximately Mach 3.0 and an altitude of 23,600 meters (77,500 feet) is presented in figure 8. The pilot described the atmosphere as stable as evidenced by the ease of maintaining Mach number and altitude conditions. The low frequency limit cycle, which has a period of approximately 32 seconds, is due to the air data computer's static pressure threshold; the high frequency oscillatory characteristics, which can be seen in δ_e, are due to the angle-of-attack sensitivity of the static pressure source, p_{s_2}. The normal acceleration parameter at the center of gravity was noisy and sensitive to engine power level.

An example of unacceptable altitude hold control at approximately Mach 3.0 and an altitude of 23,600 meters (77,500 feet) is presented in figure 9. The pilot described the atmosphere as unstable because of the difficulty in maintaining altitude and the sudden increases in the indicated Mach number. On this occasion the atmospheric disturbances apparently induced the erratic altitude behavior; however, other types of disturbances or untrimmed conditions can initiate the autopilot instability. The high frequency, divergent-convergent oscillations in this example are due to the angle-of-attack sensitivity of the static pressure ports, p_{s_2} (fig. 5). As angle of attack increases, $\Delta p_{s_2}/\Delta\alpha$ becomes more negative and the high frequency motion diverges; as angle of attack decreases, $\Delta p_{s_2}/\Delta\alpha$ becomes less negative and the high frequency motion converges.

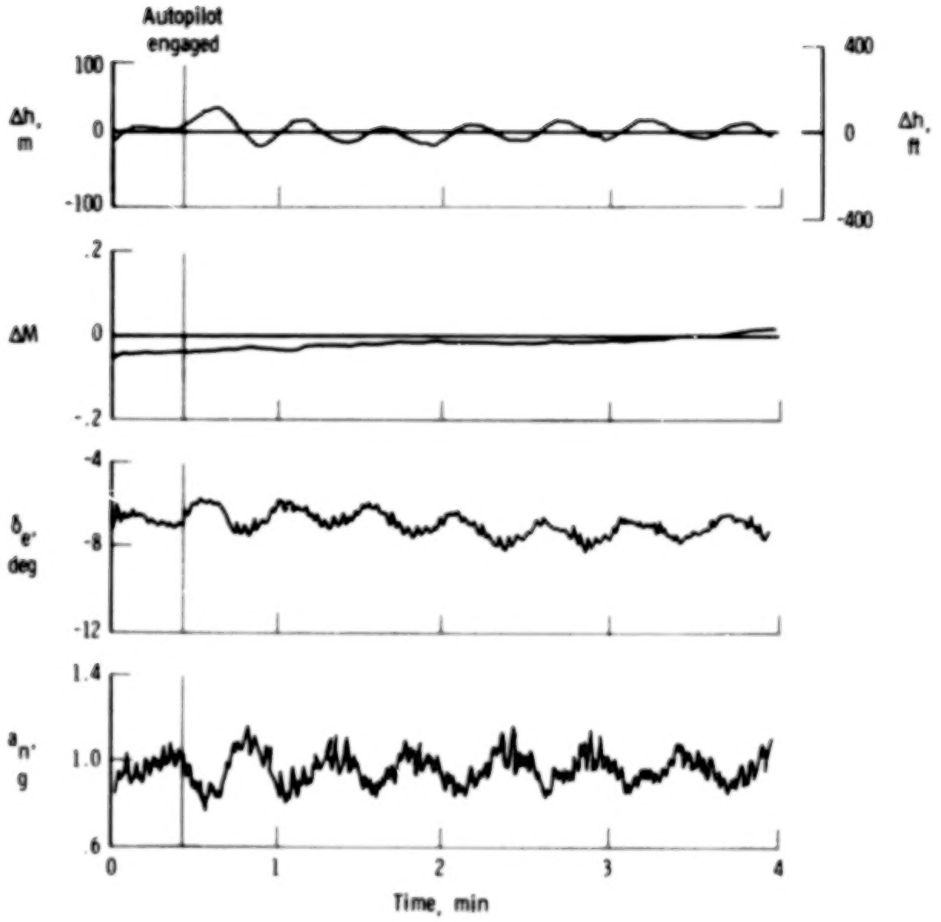

Figure 8. Good original altitude hold; stable atmosphere.

In both the previous examples, the static pressure sensitivity to angle of attack is evident. In the latter example, the divergent, high frequency, large amplitude oscillations were disturbing to the pilot.

A short evaluation of the altitude hold autopilot was conducted with the ADC connected to p_{s_3}, which is not sensitive to angle of attack. A typical example of altitude hold in this configuration is shown in figure 10. The high frequency oscillations were eliminated as expected; however, the low frequency mode was divergent. The time history shows that after 2 1/2 minutes the autopilot reached saturation (±2.3° elevator authority), as evidenced by the ramp type of elevon input caused by the autotrim feature of the autopilot.

These examples demonstrate two major problems with the original altitude hold autopilot: the neutral to divergent damping of the low frequency mode and the high

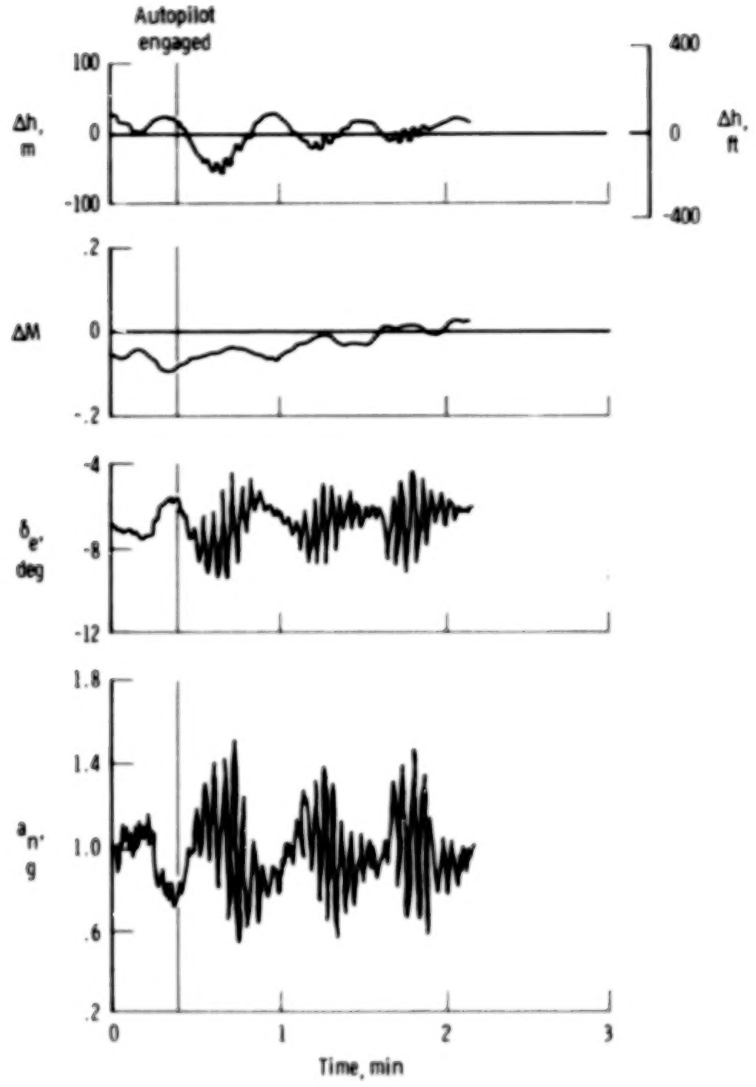

Figure 9. Unacceptable original altitude hold; unstable atmosphere.

frequency, divergent-convergent oscillations due to the sensitivity of static pressure to angle of attack.

Simulation Studies

The simulation was used to investigate the closed-loop aircraft-autopilot problems and, subsequently, to define autopilot improvement modifications. The effects of static pressure angle-of-attack sensitivity and outer-loop gains on autopilot performance were the primary areas of investigation.

For the study of the modified altitude hold autopilot, the SAS loop was not altered and autopilot hardware changes were kept to a minimum. In addition, because the

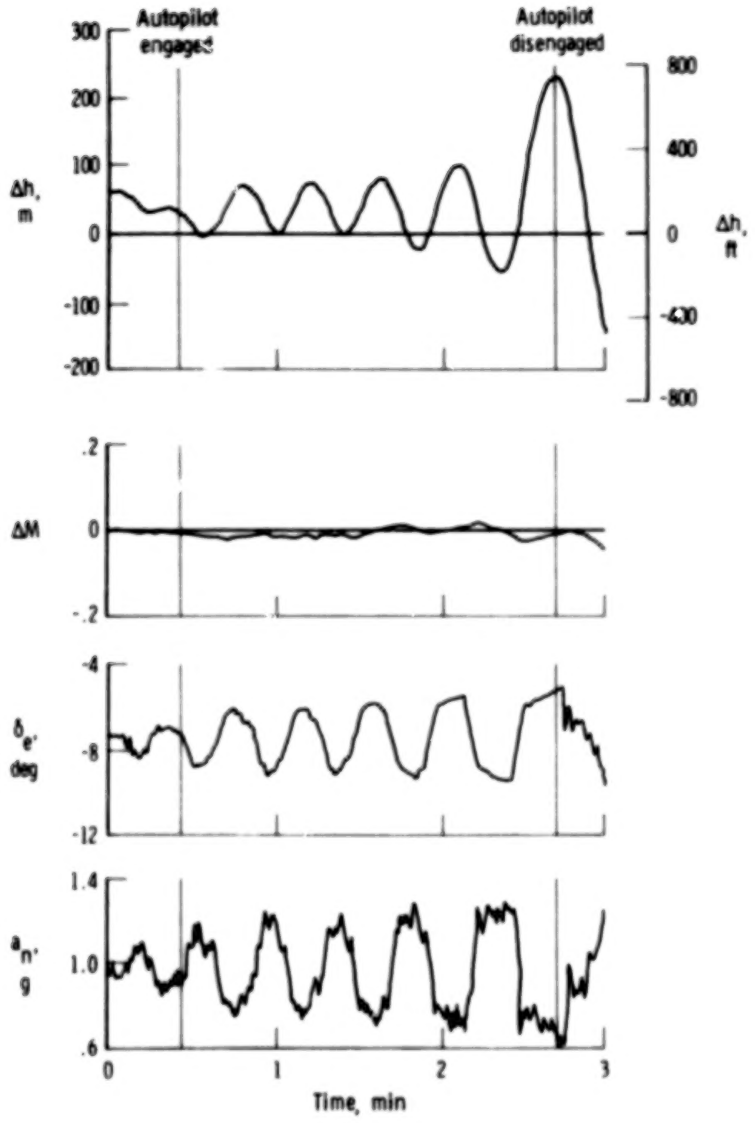

Figure 10. Original altitude hold operation with angle-of-attack-insensitive static pressure, p_{s_3}.

attitude hold mode of the autopilot performed well, the primary work on the autopilot was concentrated on the altitude control loops.

The altitude hold investigation consisted of two goals: to improve the damping of the low frequency mode and to eliminate the high frequency mode. The first series of parametric studies concentrated on improving the characteristics of the low frequency mode with static pressure ports having no sensitivity to angle of attack. Once acceptable low frequency mode characteristics were obtained, the studies were devoted to determining a way to eliminate the high frequency mode.

Simulation excitation.—A number of methods were used to excite the aircraft-autopilot simulation. The primary methods were a step elevon input for a defined length of time; autopilot engagement from an initial rate of climb, which is typical of flight experience; and a 0.9° $\Delta\theta$ step function input to the attitude loop of the autopilot, which is equivalent to a pilot pitch wheel input. The $\Delta\theta$ step function was incorporated in the final hardware to provide an error signal of constant value to test autopilot response characteristics; therefore, the $\Delta\theta$ step input was also used in the simulation for comparison purposes.

In addition to the above disturbances, the autopilot's sensitivity to atmospheric pressure and temperature variations was investigated.

Original altitude hold performance.—Because the lag and attenuation characteristics of the pitot-static system are not well defined, especially at the high frequencies of interest, the effective $p_s(\alpha)$ sensed by the ADC could vary from the values shown in figure 5. Therefore, the simulation of $p_s(\alpha)$ was varied by a factor until the data best matched the flight data, which occurred at a $p_s(\alpha)$ of approximately one-half of the nominal setting. A time history of the simulation response of the original altitude hold autopilot to a 5-second, 2° elevon step with the ADC connected to p_{s_2} is presented in figure 11.

Figures 12 and 13 are simulation responses of the original altitude hold mode with the ADC connected to p_{s_3} (no angle-of-attack sensitivity). In figure 12, the disturbance (a 5-second, 2° elevon step) was small and the aircraft reached a neutral limit cycle with altitude variations of ±18 meters (±60 feet). The limit cycle is due to the ADC threshold.

In the response shown in figure 13, the disturbance was an initial rate of climb of approximately 21 meters per second (70 feet per second). The pitch SAS was engaged during the climb and, as the aircraft passed through an altitude of 23,600 meters (77,500 feet), the attitude and altitude hold autopilot modes were engaged. In addition, in the simulation runs with initial rates of climb, a constant 2° excess power lever angle (PLA) from trimmed, Mach 3.0, 23,600-meter (77,500-foot) altitude flight conditions was used to partially minimize the Mach number loss. In this example, the disturbance was large and the aircraft entered a low frequency, saturated autopilot limit cycle. The δ_e simulation result was similar to the latter portion of the data in figure 10, which was obtained with the same autopilot-ADC configuration.

Parametric autopilot gain variations.—The parametric studies presented in this section are perturbations about the selected gains with $p_s(\alpha)$ equal to zero. All the gains are referred to in terms of a fraction of the nominal, or original, altitude hold autopilot gains. The disturbance was an initial rate of climb of approximately 21 meters per second (70 feet per second) with a 2° excess PLA and the autopilot engaged at an indicated altitude of 23,600 meters (77,500 feet).

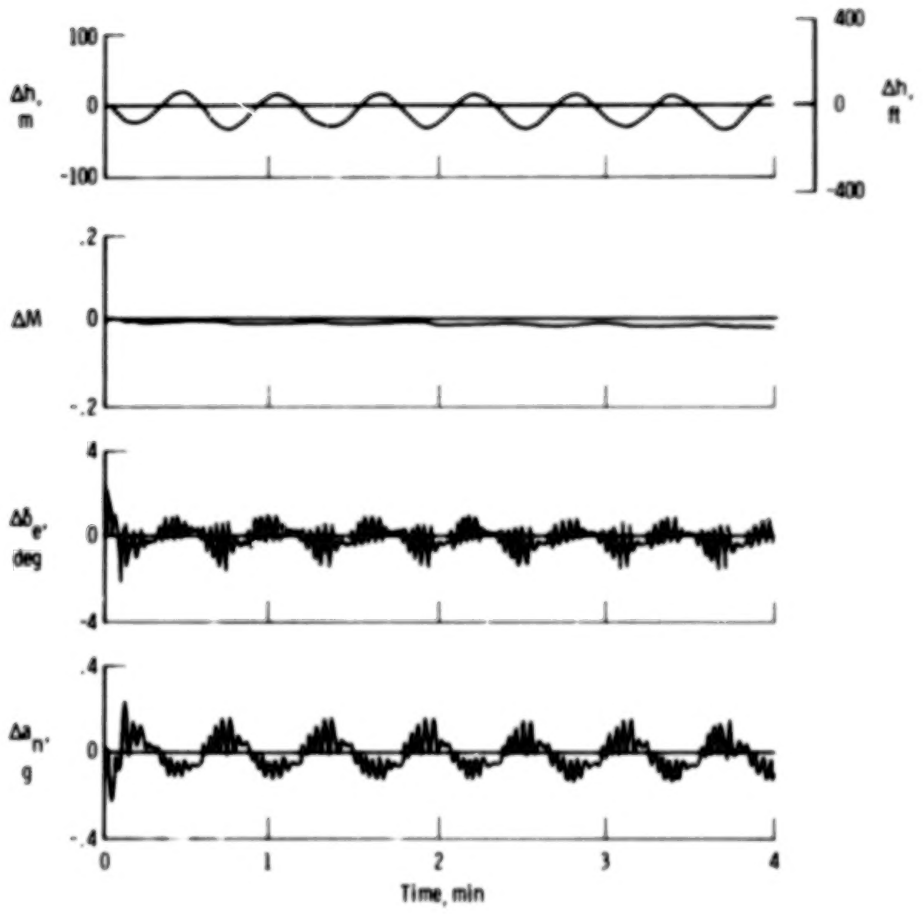

Figure 11. Simulation response of original altitude hold autopilot to a 5-second, 2° elevon step; $p_s(\alpha)$ = 1/2 nominal.

The simulation responses were summarized in terms of first overshoot peak; period of the first oscillation; a damping index parameter, DI, defined in appendix B; and the time required to reach and maintain altitude within ±9.1 meters (±30 feet) of steady state, which is denoted as t_{30}.

The gains investigated were $K_{\theta_{\int h}}$, K_{θ_h}, $K_{\theta_{\dot{h}}}$, K_θ, and K_h (fig. 6). As each gain was varied, the remaining gains were held constant at the values selected for incorporation in the modified autopilot. The final modified gain values in terms of a fraction of nominal were as follows:

$$K_{\theta_{\int h}} = 1/4$$

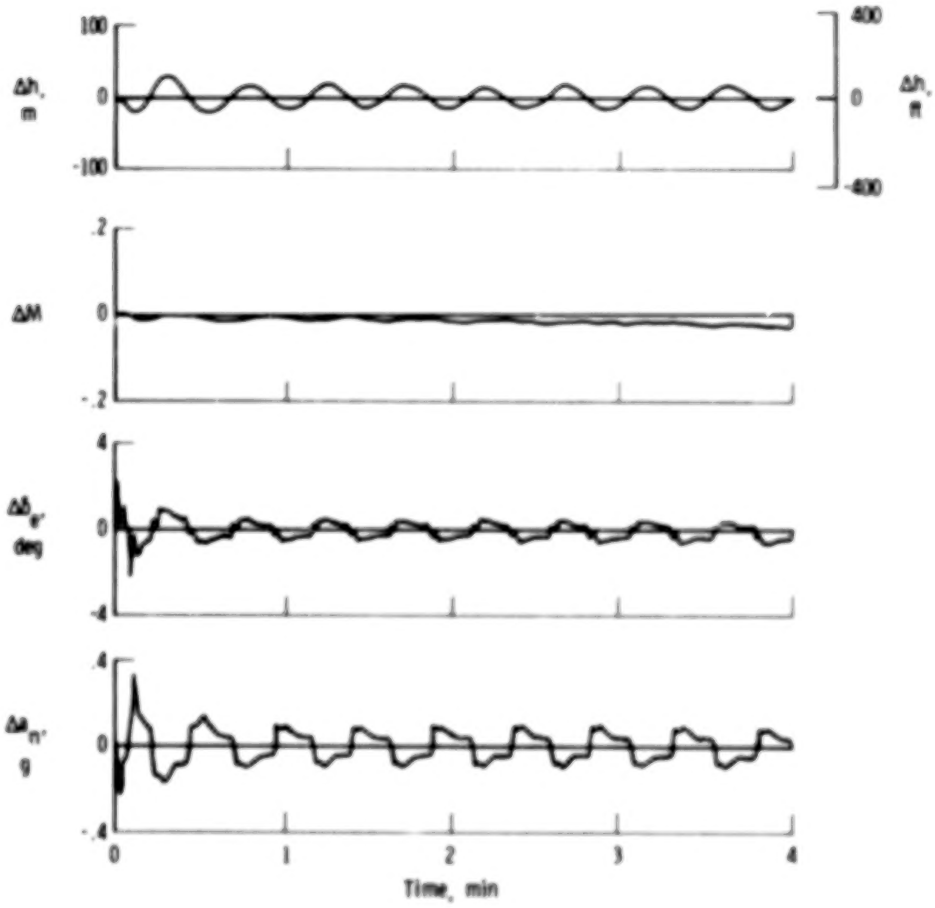

Figure 12. Simulation response of original altitude hold mode to 5-second, 2° elevon step; $p_s(a) = 0$.

$$K_{\theta_h} = 1/2$$

$$K_{\theta_{\dot{h}}} = 1$$

$$K_{\theta} = 1$$

$$K_h = 1$$

The $K_{\theta_{\int h}}$ parametric variation results are presented in figure 14. The first overshoot is a constant 122 meters (400 feet) for all values of $K_{\theta_{\int h}}$. The period

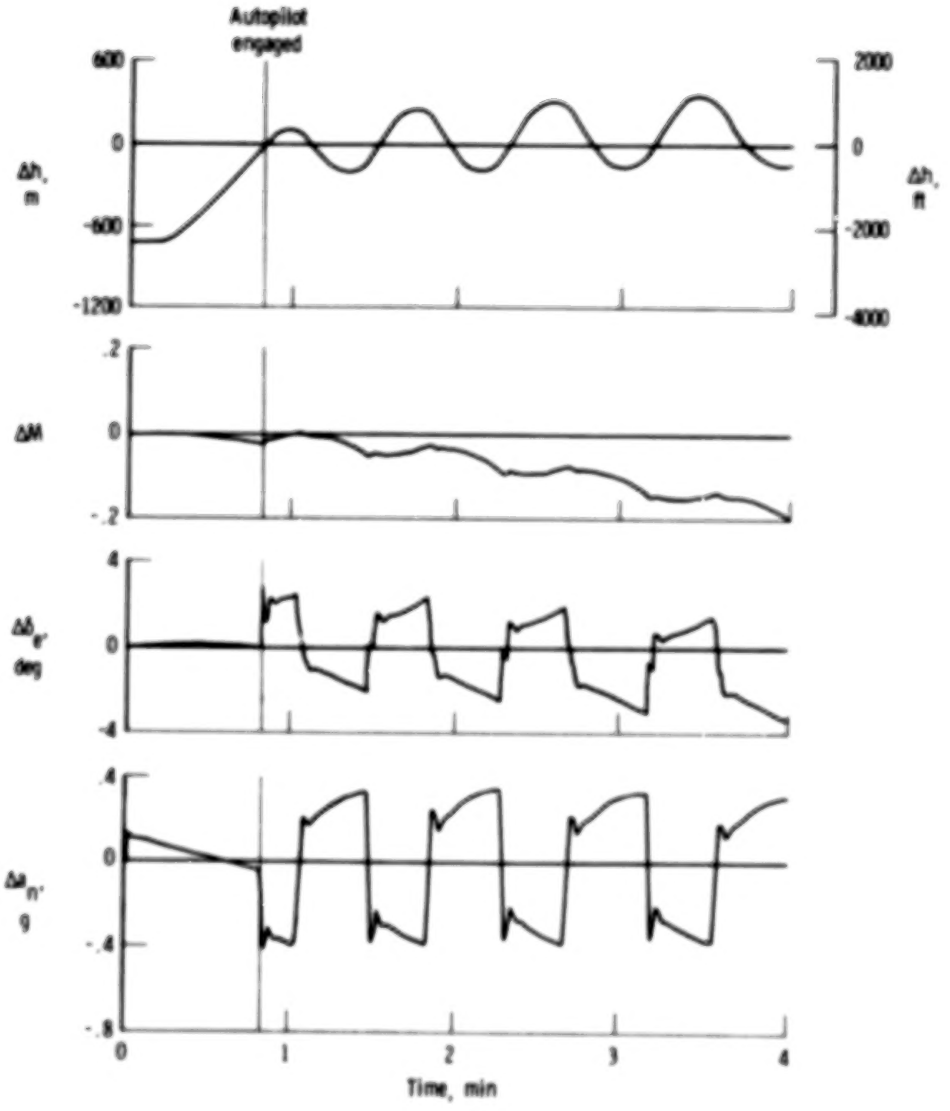

Figure 13. Simulation response of original altitude hold mode to initial rate of climb of approximately 21 m/sec (70 ft/sec): $p_s(a) = 0$.

is a constant 50 seconds for $K_{\theta f_h}$ greater than one-fourth nominal; however, for low values of $K_{\theta f_h}$ the period becomes difficult to define because of the extremely long time required to return to steady state. When $K_{\theta f_h}$ is zero, the altitude does not return to the engage altitude, but converges to a constant bias. Both DI and t_{30}

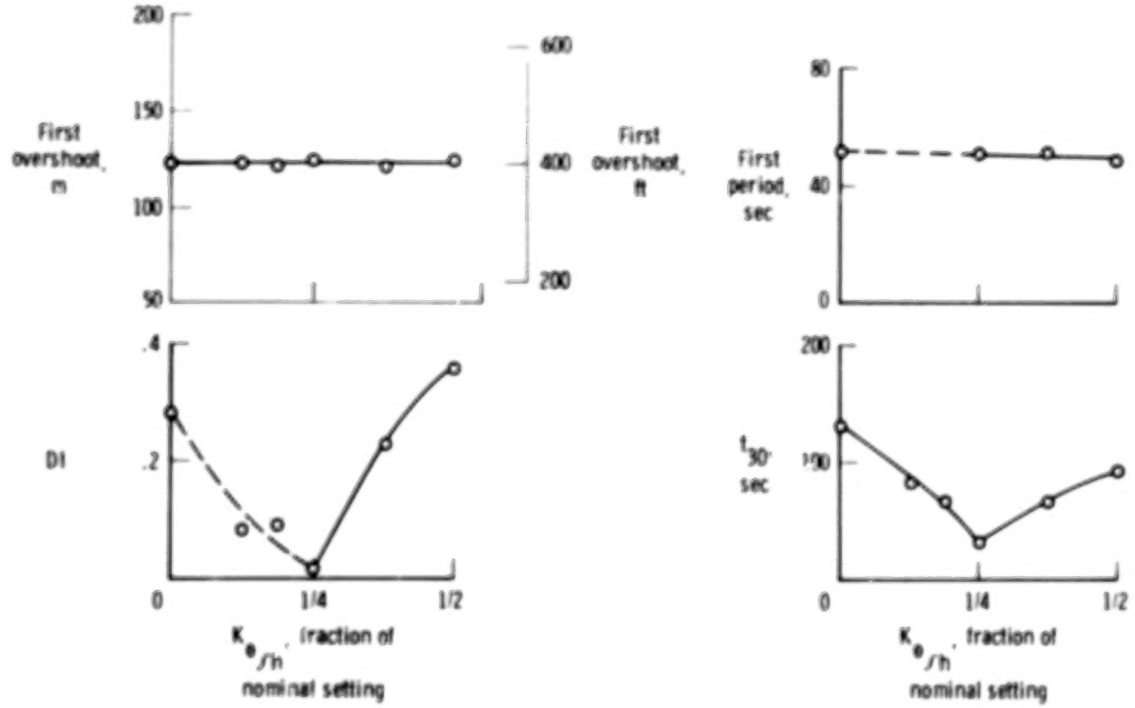

Figure 14. Variation of modified altitude hold mode characteristics with $K_{\theta_{fh}}$. In fractions of nominal settings, $K_{\theta_{\dot{h}}} = 1$, $K_{\theta_h} = 1/2$, $K_{\theta} = 1$, and $K_h = 1$.

reach their minimum values at the final modified gain; however, DI and t_{30} degrade rapidly as $K_{\theta_{fh}}$ is increased or decreased.

The K_{θ_h} parametric variation results are presented in figure 15. The first overshoot is a constant 122 meters (400 feet) for all values of K_{θ_h}; however, the period decreases from 90 seconds to 25 seconds as K_{θ_h} increases from one-fourth nominal to nominal. Both DI and t_{30} reach their minimum values at the final modified gain. Again, DI and t_{30} degrade significantly as K_{θ_h} is either increased or decreased.

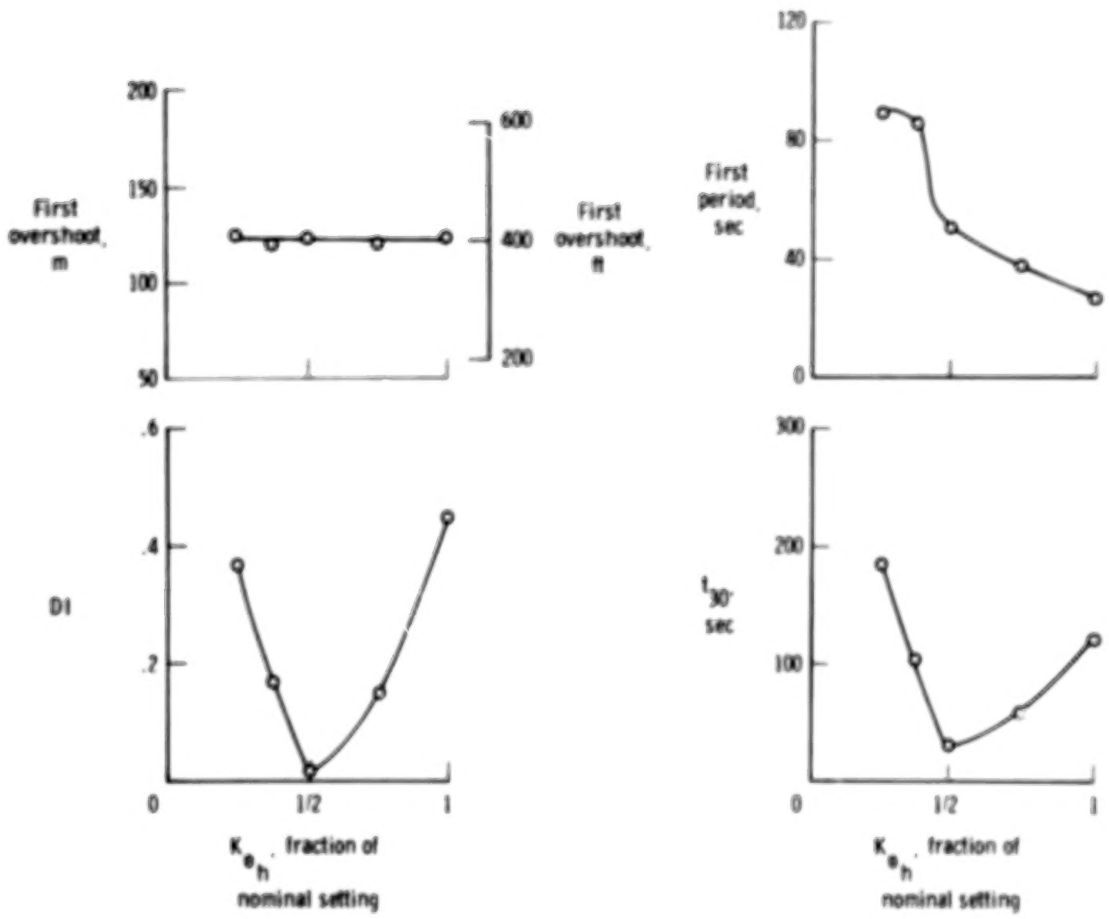

Figure 15. Variation of modified altitude hold mode characteristics with K_{θ_h}. *In fractions of nominal settings,* $K_{\theta_{\dot{h}}} = 1$, $K_{\theta_{\int h}} = 1/4$, $K_{\theta} = 1$, *and* $K_h = 1$.

The $K_{\theta_{\dot{h}}}$ parametric variation results are presented in figure 16. The first overshoot is 122 meters (400 feet) for all values of $K_{\theta_{\dot{h}}}$; however, the period increases from 40 seconds to 115 seconds as $K_{\theta_{\dot{h}}}$ increases from one-half nominal to twice nominal. DI and t_{30} are at or near their minimum values at the nominal gains. However, the degradation in characteristics is not as significant for small increases in $K_{\theta_{\dot{h}}}$ as for the gains previously discussed.

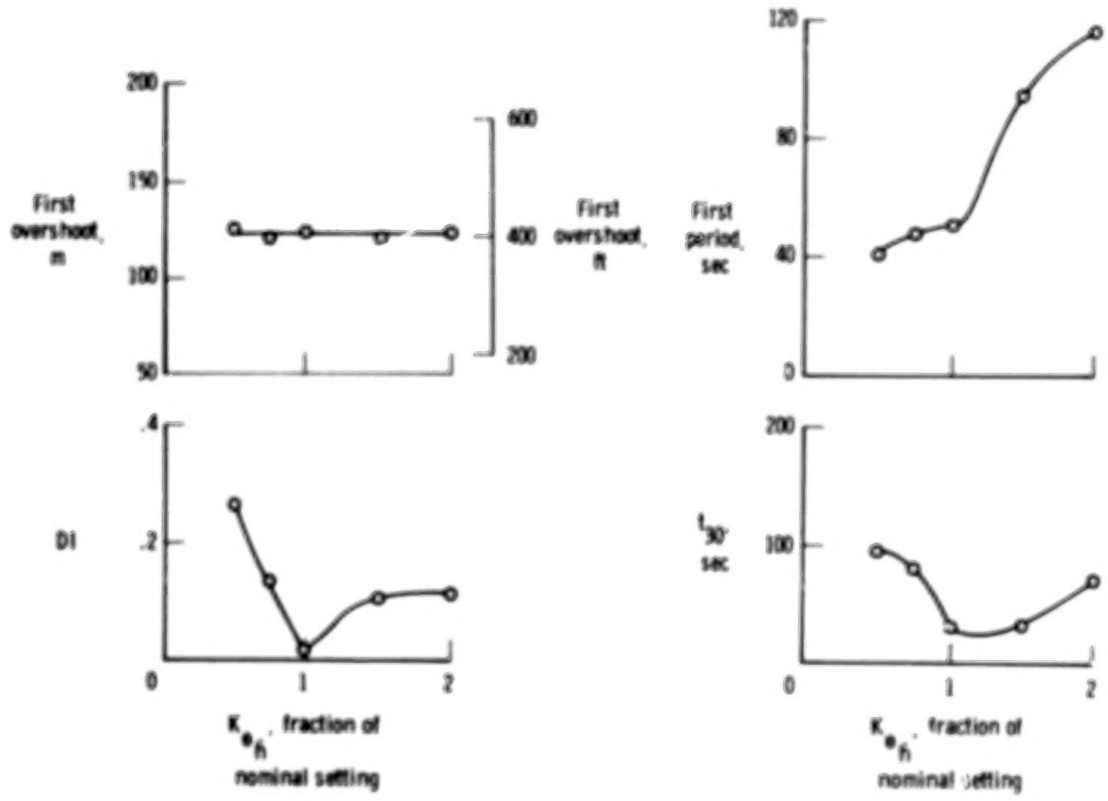

Figure 16. Variation of modified altitude hold mode characteristics with $K_{\theta_{\dot{h}}}$. In fractions of nominal settings, K_{θ_h} = 1/2, $K_{\theta_{\int h}}$ = 1/4, K_θ = 1, and K_h = 1.

The K_θ gain variation in figure 17 illustrates the effect of the attitude loop on altitude hold. The parametric variation of K_θ illustrates that the nominal attitude hold mode is a good inner loop for the modified altitude hold autopilot. The major effect of reducing K_θ is to seriously degrade DI, whereas an increase in K_θ significantly increases t_{30}.

The K_h gain variation shown in figure 18 illustrates the effect of varying the modified $K_{\theta_{\int h}}$, K_{θ_h}, and $K_{\theta_{\dot{h}}}$ gains simultaneously. A reduction of K_h increases the first overshoot, the period, DI, and t_{30}; an increase in K_h increases the period, DI, and t_{30}.

Simulation response time histories of the modified autopilot configuration with $p_s(\alpha)$ equal to zero are presented in figures 19 and 20. Figure 19 is the response

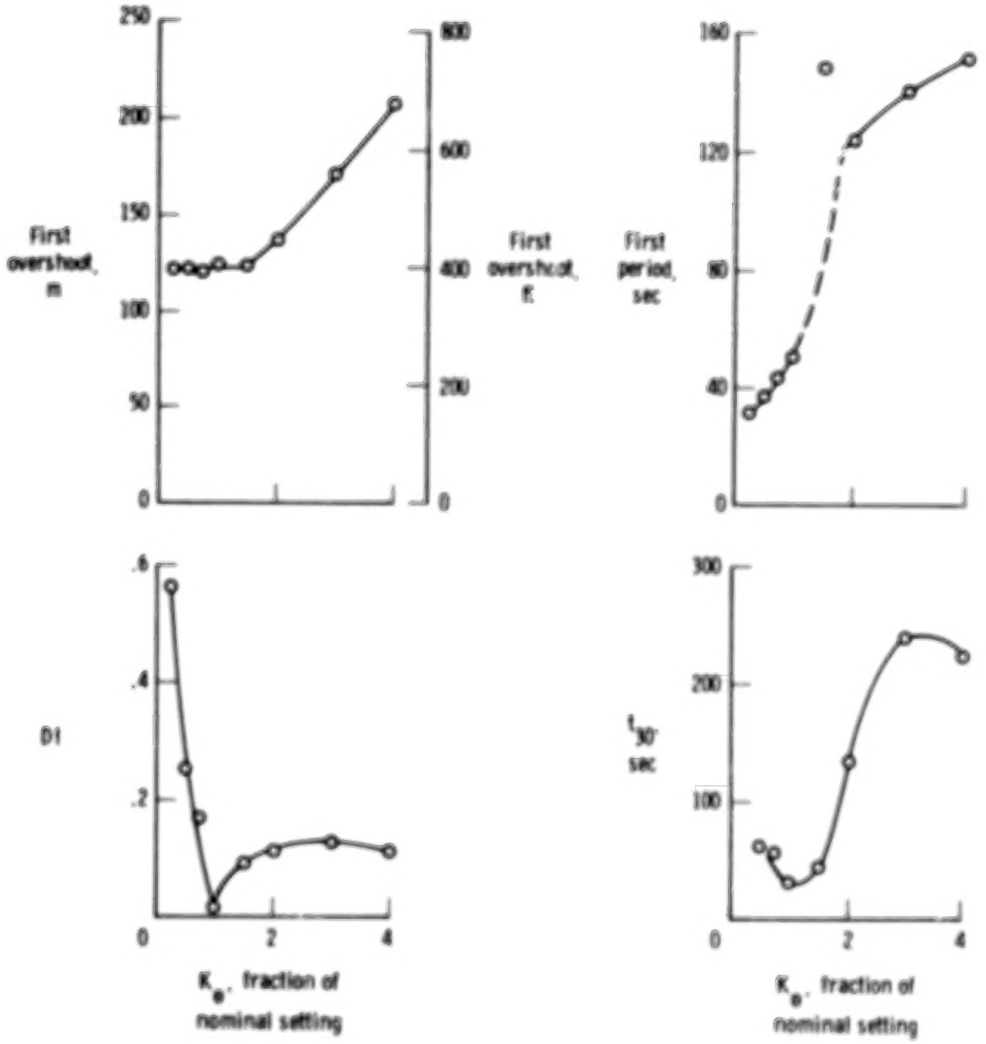

Figure 17. Variation of modified altitude hold mode characteristics with K_θ. *In fractions of nominal settings,* $K_{\theta_{\dot{h}}} = 1$, $K_{\theta_h} = 1/2$, $K_{\theta_{\dot{h}h}} = 1/4$, *and* $K_h = 1$.

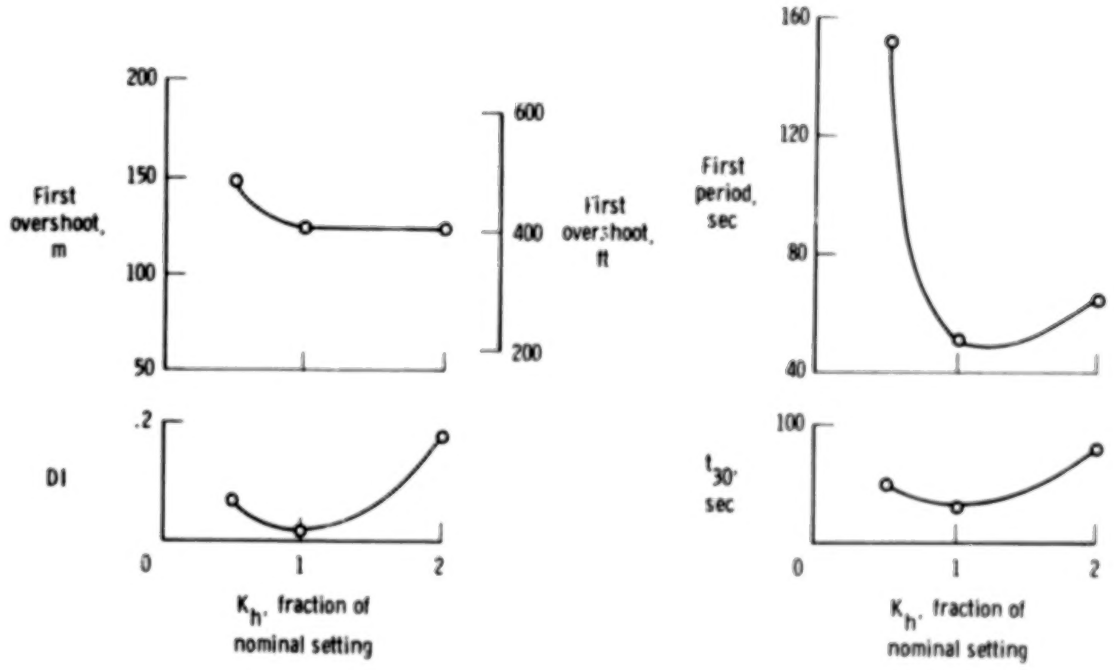

Figure 18. Variation of modified altitude hold mode characteristics with K_h. In fractions of nominal settings, $K_\theta = 1$, $K_{\theta_{\dot{h}}} = 1$, $K_{\theta_h} = 1/2$, and $K_{\theta_{fh}} = 1/4$.

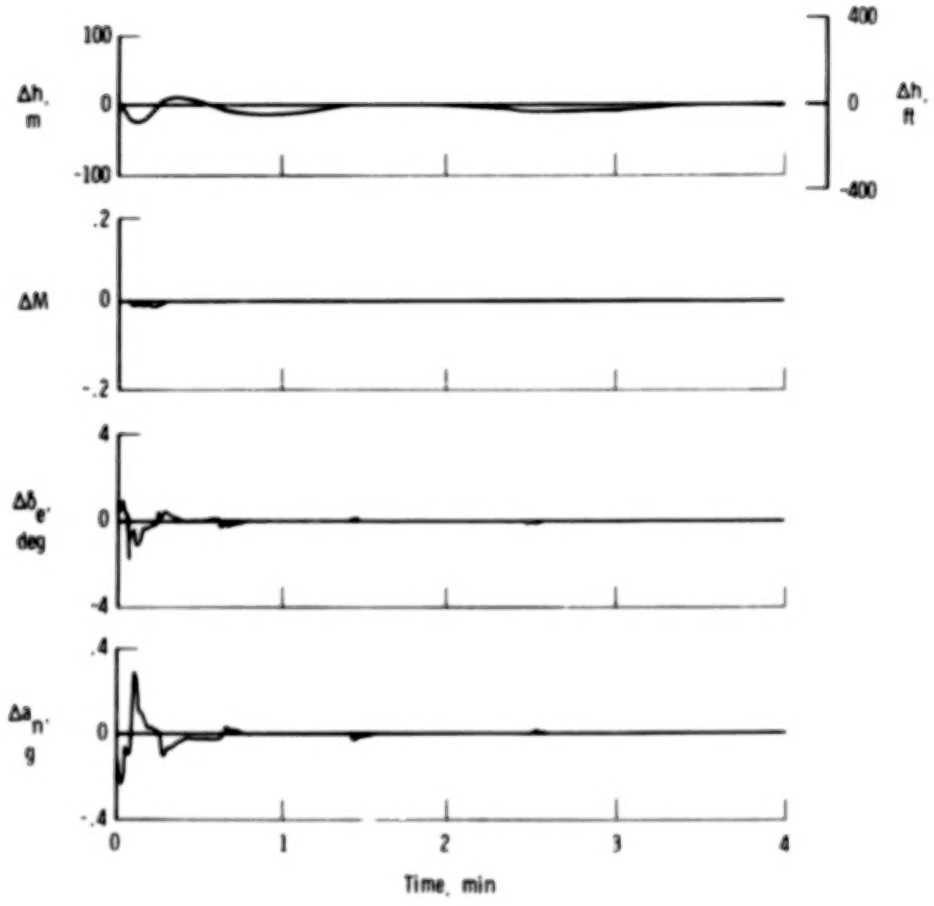

Figure 19. Simulation response of modified altitude hold to 5-second, 2° elevon step; $p_s(\alpha) = 0$.

to a 5-second, 2° elevon step, and figure 20 is an engagement of altitude hold from an initial rate of climb of 21 meters per second (70 feet per second). In both cases, the low frequency mode is well damped, as was indicated in the parametric studies. (The flattening in the Δh trace in figure 20 and in the Δh and ΔM traces in other time histories represents the limit of the recording device.)

Effect of sensitivity of static pressure to angle of attack.—Simulation time histories illustrating the effect of various factors of nominal $p_s(\alpha)$ on the original autopilot are presented in figure 21. The autopilot was engaged from the start and the disturbance was a 5-second, 2° elevon step. As $p_s(\alpha)$ increased from zero to nominal, the short-period mode converged to a large-amplitude limit cycle; as $p_s(\alpha)$ decreased from zero to negative nominal, the long-period mode converged to a large-amplitude limit cycle.

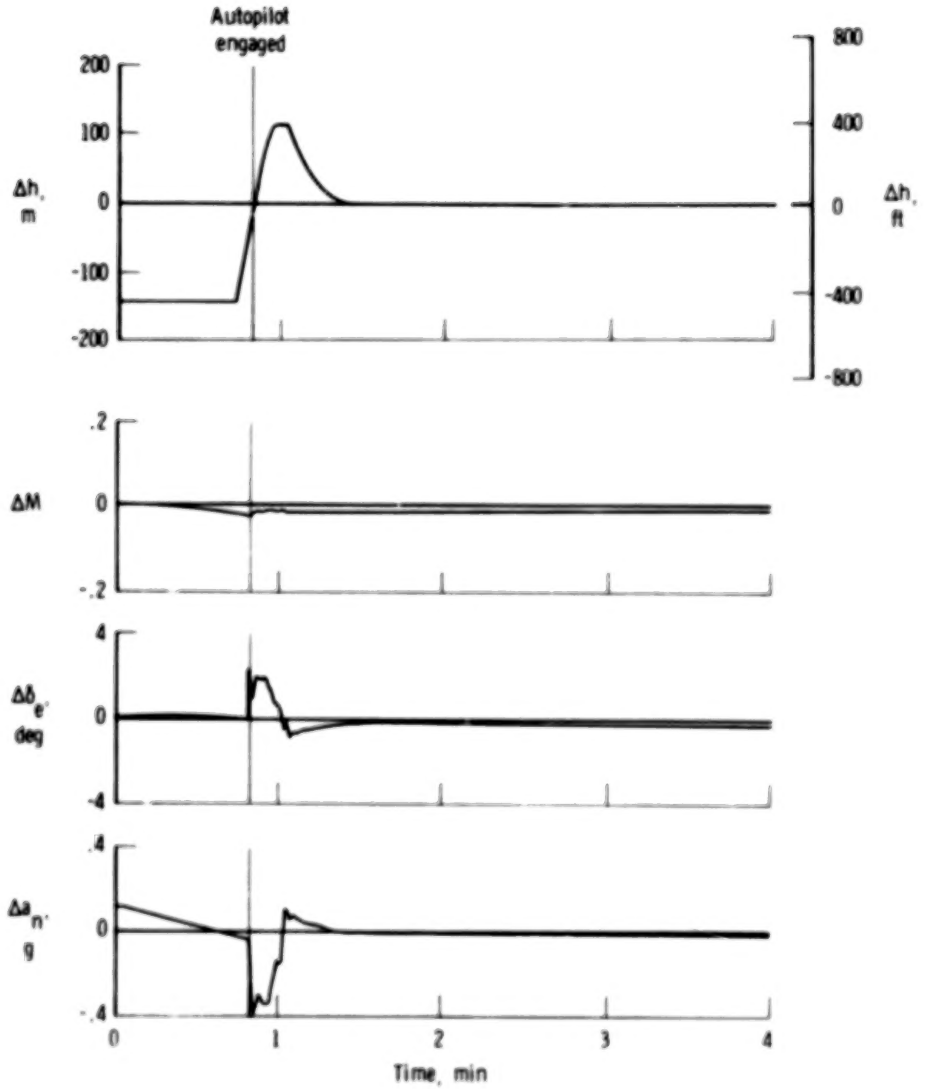

Figure 20. Simulation response of modified altitude hold to initial rate of climb of approximately 21 m/sec (70 ft/sec); $p_s(\alpha) = 0$.

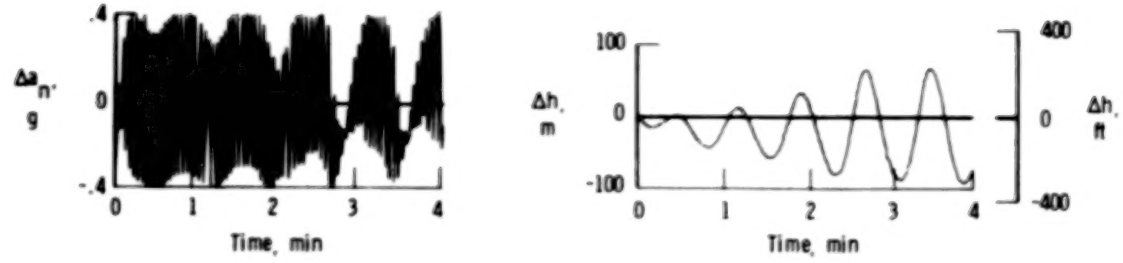

(a) $p_s(\alpha) = 1.$

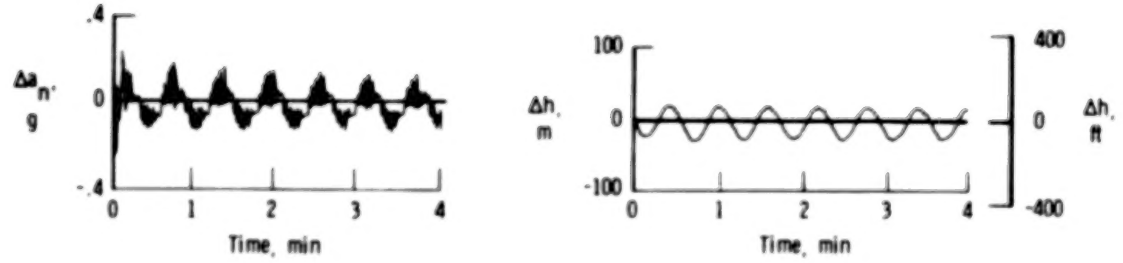

(b) $p_s(\alpha) = 1/2.$

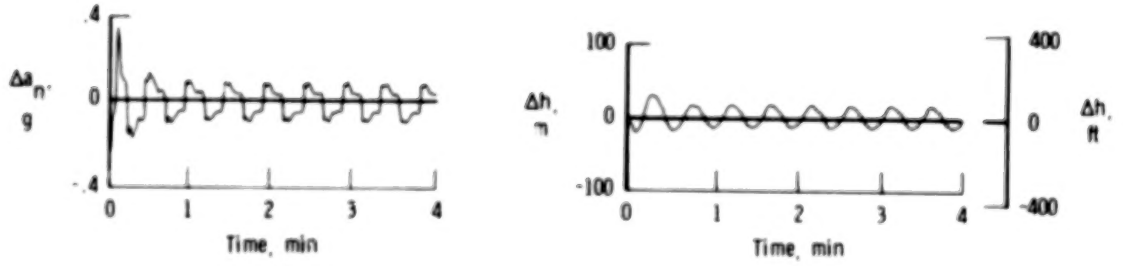

(c) $p_s(\alpha) = 0.$

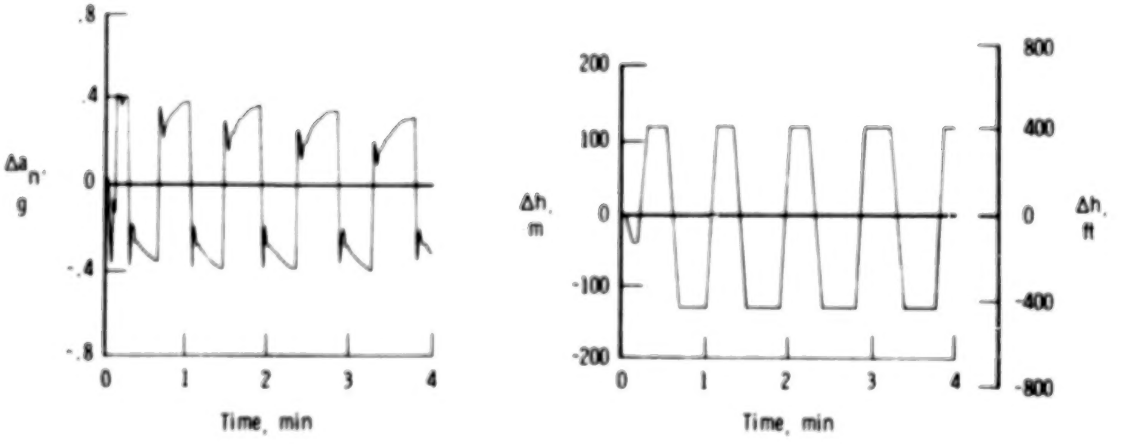

(d) $p_s(\alpha) = -1/2.$

Figure 21. Simulation responses of original altitude hold for various fractions of nominal $p_s(\alpha)$*. Input is 5-second, 2° elevon step.*

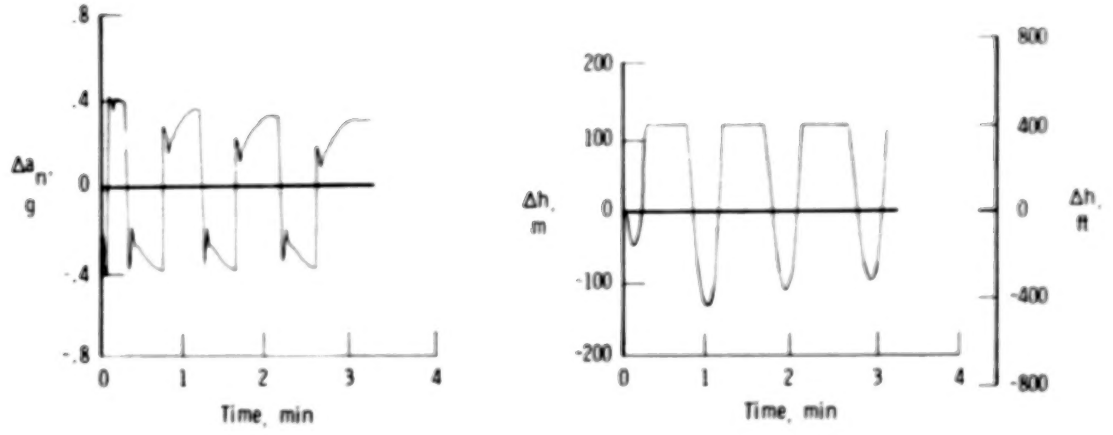

(e) $p_s(\alpha) = -1$.

Figure 21. Concluded.

Simulation responses of the modified autopilot with $p_s(\alpha)$ values of one-half nominal and nominal are presented in figures 22 and 23. The disturbance in both examples was a 5-second, 2° elevon step. The $p_s(\alpha)$ value of one-half nominal (fig. 22) is representative of the majority of flight data; however, larger values of angle of attack (such as in a turn) would tend to drive $p_s(\alpha)$ toward the nominal value (fig. 23). A divergent-convergent low-amplitude oscillation exists for a $p_s(\alpha)$ of one-half nominal and, as $p_s(\alpha)$ approaches the nominal value, the oscillation gradually approaches a steady-state, large-amplitude limit cycle.

Compensation for static pressure angle-of-attack sensitivity.—To compensate for the angle-of-attack sensitivity of static pressure, the high frequency oscillations were damped by feeding back high-passed pitch rate. This method is relatively insensitive to nose boom configuration.

The loop used to damp the high frequency mode consisted primarily of high-passed ($\tau = 2$) pitch rate summed with the attitude hold loop of the autopilot (fig. 24). In addition, the high-passed pitch rate loop included a notch filter for aircraft bending compensation and a cutoff filter ($\tau = 0.02$). The nominal $K_{\dot{\theta}}$ was 1.07 deg θ/(deg/sec $\dot{\theta}$). Figure 25 is a simulation response to a 5-second, 2° elevon step with the modified altitude hold gains and a nominal $p_s(\alpha)$. As shown, the high frequency mode of figure 23 is completely suppressed. The gain, $K_{\dot{\theta}}$, of the high-passed pitch rate loop is one-half nominal in this example. Analytically, larger values are desirable; however, larger values could feed significant system noise to the elevon.

Impact pressure feedback.—At high altitude cruise conditions, the YF-12 airplane has a phugoid mode with a damping range from slightly positive to negative.

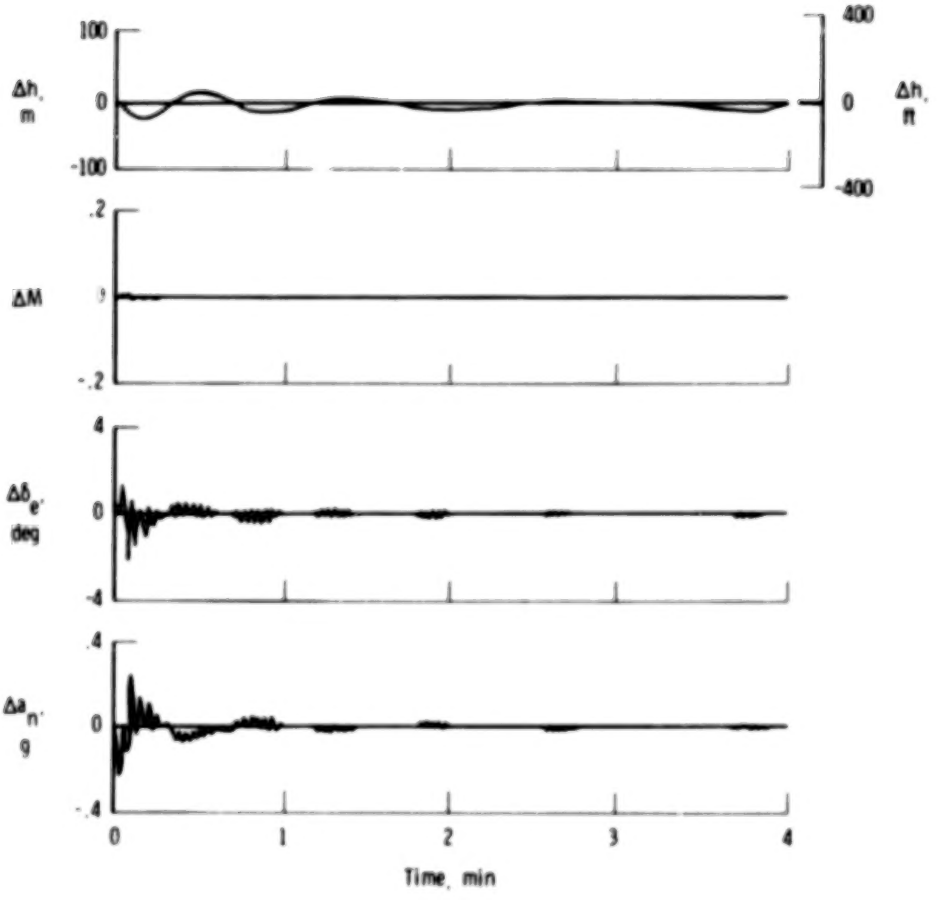

Figure 22. Simulation response of modified altitude hold to 5-second, 2° elevon step; $p_s(\alpha)$ = 1/2 nominal.

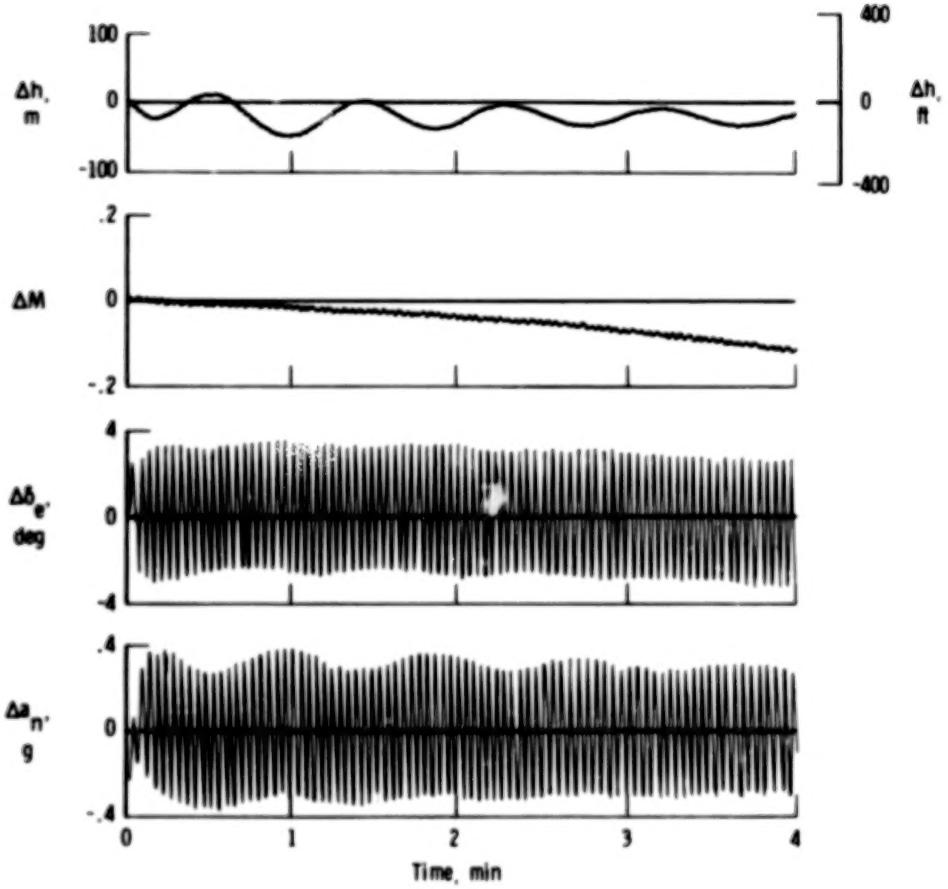

Figure 23. Simulation response of modified altitude hold to 5-second, 2° elevon step; $p_s(\alpha)$ = nominal.

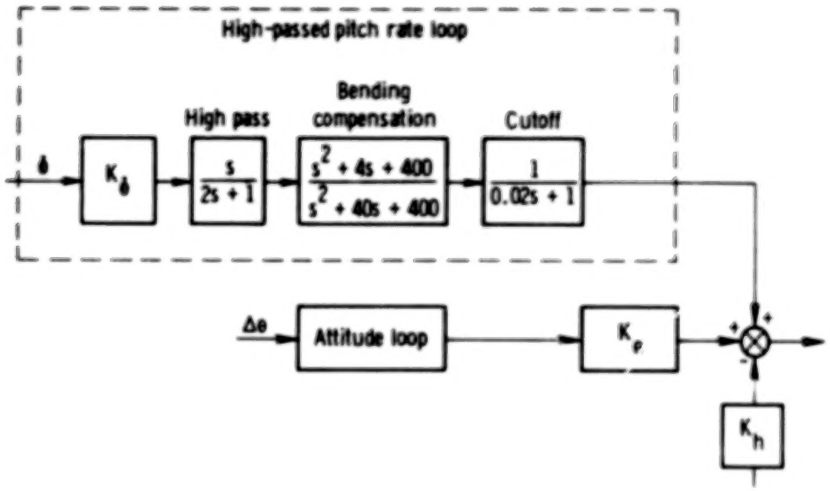

Figure 24. High-passed pitch rate loop used to compensate for static pressure angle-of-attack sensitivity (see fig. 6).

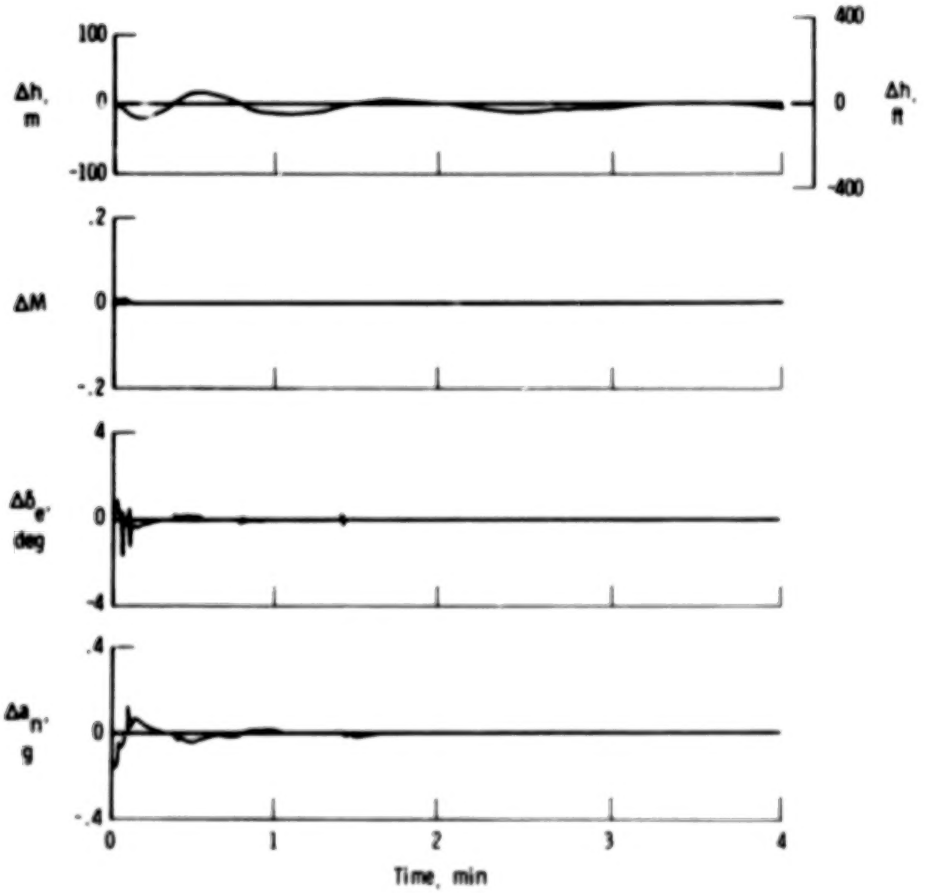

Figure 25. Simulation response of modified altitude hold to 5-second, 2° elevon step. $p_s(\alpha)$ = nominal and $K_{\dot{\theta}}$ = 1/2 nominal.

Because the original altitude hold was generally unsatisfactory, the pilot flew the constant altitude runs manually (SAS on but autopilot off). One control concept to improve SAS-on handling qualities was to significantly increase phugoid damping by feeding back high-passed ($\tau = 5$) impact pressure, q_c. A filter ($\tau = 1$) was included in the q_c feedback loop and the high-pass gain was -9.6 deg δ_e/(N/m^2 q_c) (-0.2 deg δ_e/(lb/ft^2 q_c)). Figure 26 presents a comparison of the basic aircraft phugoid mode and the phugoid mode augmented by q_c feedback. The damping is improved from a nearly neutral to a deadbeat condition.

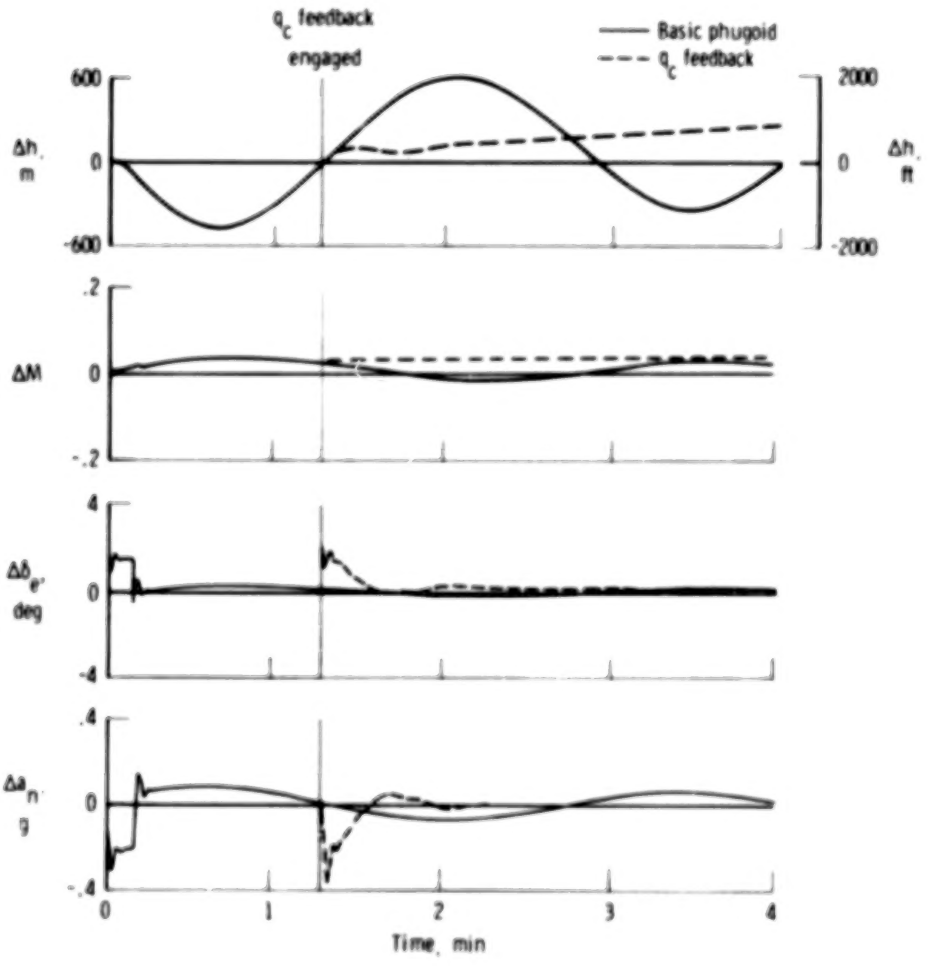

Figure 26. Simulation comparison of basic aircraft phugoid and q_c-augmented phugoid modes for 10-second, 2° elevon step; SAS on.

The effect of adding the q_c loop to the modified altitude hold autopilot was negligible, as shown by a comparison of figure 27 (q_c on) and figure 20 (q_c off).

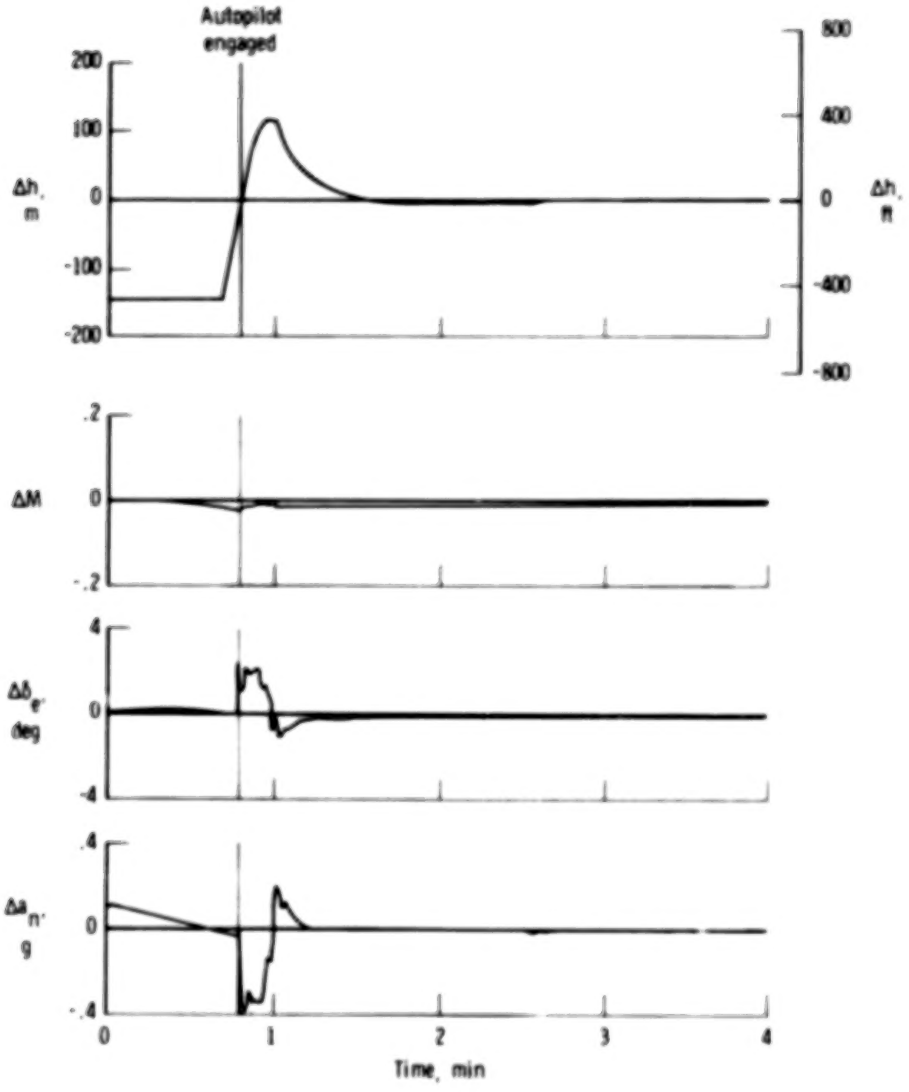

Figure 27. Simulation response of modified altitude hold to initial rate of climb of approximately 21 m/sec (70 ft/sec) with $p_s(a) = 0$ and q_c feedback.

Pitch Flight Control System Hardware Changes

The pitch autopilot changes implemented based on the previous studies are presented in figure 28. The gyro used in the high-passed pitch rate loop was the backup for pitch SAS. An additional ADC was modified to provide $\log_{10} q_c$, which is linear with q_c over the range of interest. In addition to the changes indicated on figure 28, the altitude error and integral altitude gains, K_{θ_h} and $K_{\theta_{\int h}}$, were reduced to one-half and one-fourth of their nominal values. The altitude rate gain, $K_{\theta_{\dot{h}}}$, and $K_{\dot{\theta}}$ were left at their nominal values. The nominal value of K_{q_c}

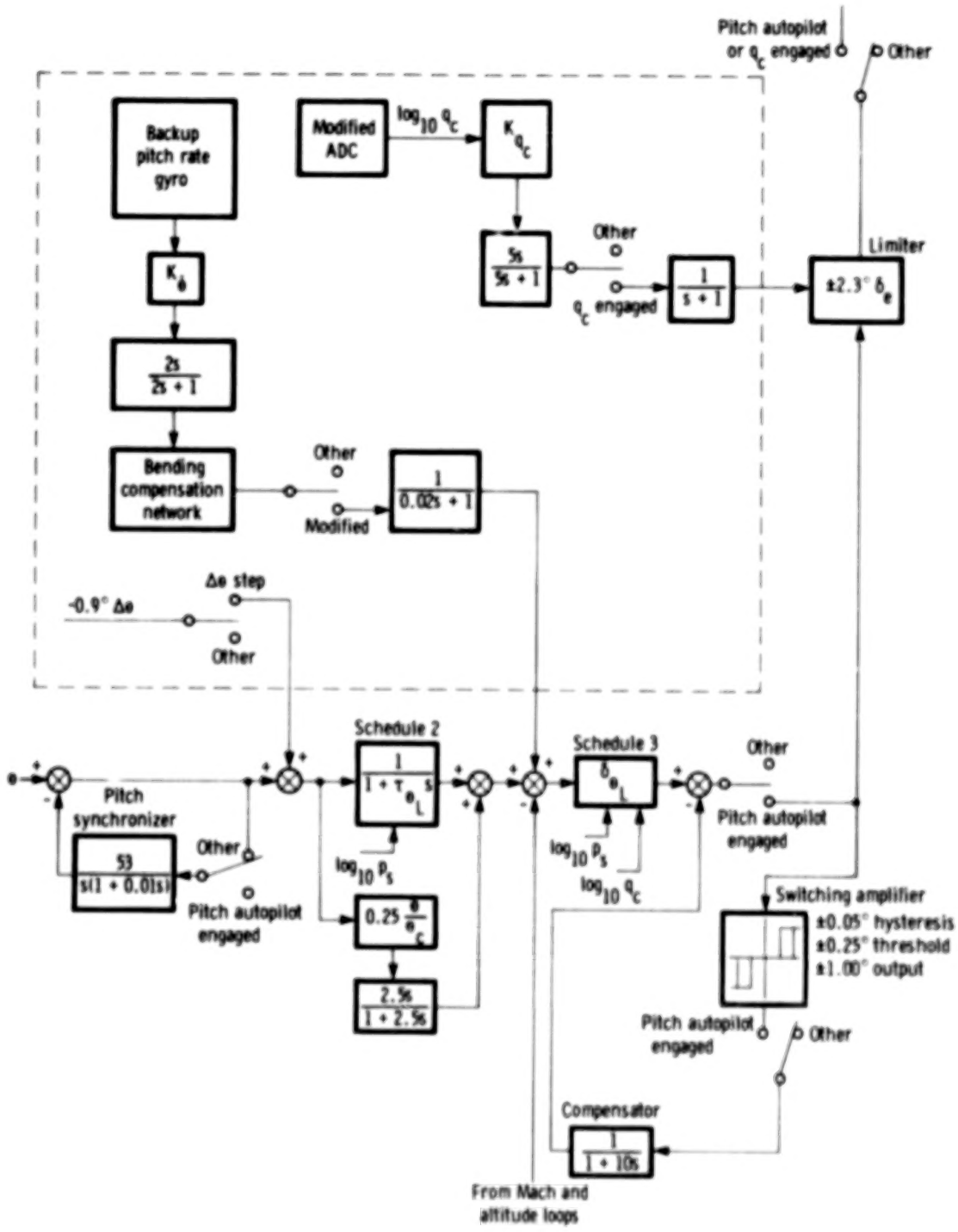

Figure 28. Pitch autopilot modifications (see fig. 6).

was -330 deg $\delta_e/\log_{10} q_c$. System flexibility was obtained by providing a gain variation of at least ±6 decibels from the modified values for $K_{\dot{\theta}}$, K_{q_c}, $K_{\theta_{\dot{h}}}$, K_{θ_h}, and $K_{\theta_{\int h}}$.

The cockpit flight test panel contained the q_c on-off switch, the modified-original altitude hold select switch, and the five variable potentiometers. In the modified altitude hold position, the gains were switched from their original values to the modified values and the high-passed pitch rate loop was included. The $\Delta\theta$ disturbance function switch was also located on the flight test panel and could be engaged in any autopilot mode.

In-Flight Performance of Modified Autopilot

The first engagement of the modified altitude hold mode in flight introduced a hardware system problem that had not been anticipated. When the modified altitude hold mode was engaged, the system went into a limit cycle that produced an elevon output of ±1° at a frequency of 1 hertz (fig. 29). The resultant normal accelerations of ±0.03g at the cockpit were evident to the crew. (Note that this is the only figure with cockpit acceleration; all other accelerations were measured at the center of gravity.)

Although the altitude was maintained accurately, the system performance was clearly undesirable. After approximately 2 minutes of the run, the pilot reduced the high-passed pitch rate gain, $K_{\dot{\theta}}$, from 1.07 to 0.65. An elevon limit cycle of ±0.3° still persisted, but the crew could no longer distinguish the accelerations from the nominal level of aircraft vibration. $K_{\dot{\theta}}$ was subsequently reduced to 0.50 on this flight. Further attempts to reduce $K_{\dot{\theta}}$ produced the following gain schedule as a function of Mach number:

	$K_{\dot{\theta}}$
$M \leq 1.4$	0.18
$1.4 < M \leq 2.75$	0.35
$M > 2.75$	0.50

When the gain was reduced below the above values, the effects of the angle-of-attack sensitivity of static pressure became apparent.

Appendix C analyzes the problem caused by the negative deficiency characteristic (ref. 10) of the backup pitch rate gyro. Briefly, the nonlinear gyro output around zero caused the rate signal to bounce from positive to negative in this region and effectively produced large gains at low input levels. Subsequent

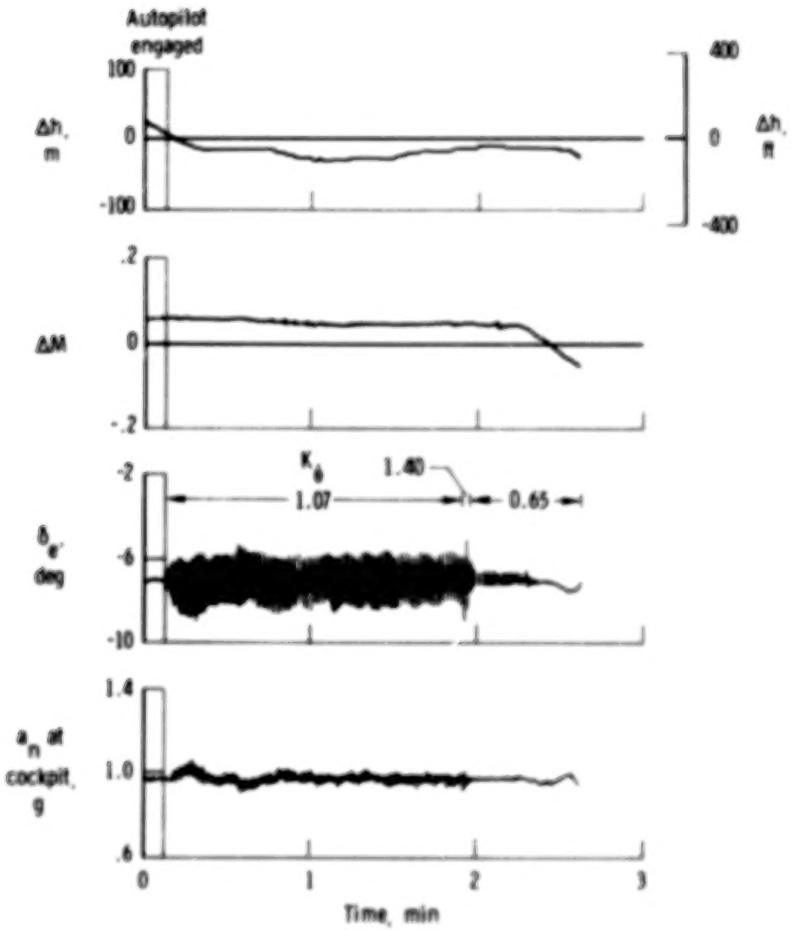

Figure 29. Effect of pitch gyro nonlinearity (negative deficiency) in the high-passed pitch rate feedback loop.

research showed that the gyro was noted for reliability rather than precision. It was decided that by using the $K_{\dot{\theta}}$ gain schedule given previously, the crew would not be able to discern the limit cycle. Because of this and because the gyro did not affect overall autopilot performance, no attempt was made to improve or change the gyro.

The following sections discuss the in-flight performance of the modified altitude hold autopilot, including the results of some limited changes in the modified control system.

Modified altitude hold.—Typical flight test data obtained with the modified altitude hold autopilot are shown in figure 30. After engagement, the autopilot maintained altitude within ±8 meters (±25 feet) for the 4-minute duration of the run. The long-period (approximately 35-second), low-amplitude oscillation is due to the threshold of the air data computer. After 2 1/2 minutes of the run, the pilot

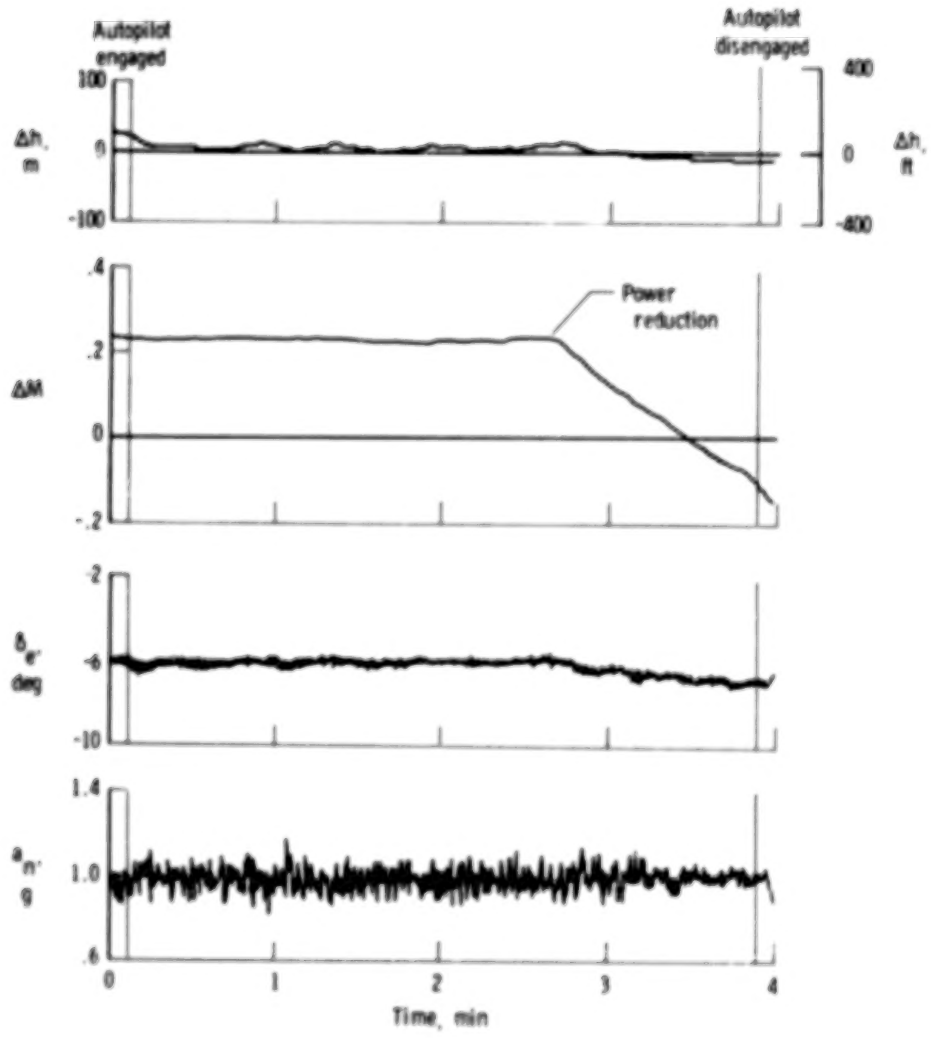

Figure 30. Performance of modified autopilot.

began a deceleration. As illustrated, there was no degradation of altitude hold, even though Mach number was decreased by 0.4. The high frequency (1-hertz), low-amplitude (±0.02°) oscillation of the elevon is the short-period limit cycle described previously (fig. 29).

A typical YF-12 experimental flight for purposes other than control system research consists of 1-minute periods of flight at stabilized Mach number and altitude conditions for as many conditions as can be scheduled in the flight plan. For these flights, pilots have found the modified autopilot valuable for rapidly attaining and maintaining altitude. Figure 31 illustrates a typical engagement of the modified autopilot with an initial rate of descent of approximately 400 meters per minute (1300 feet per minute).

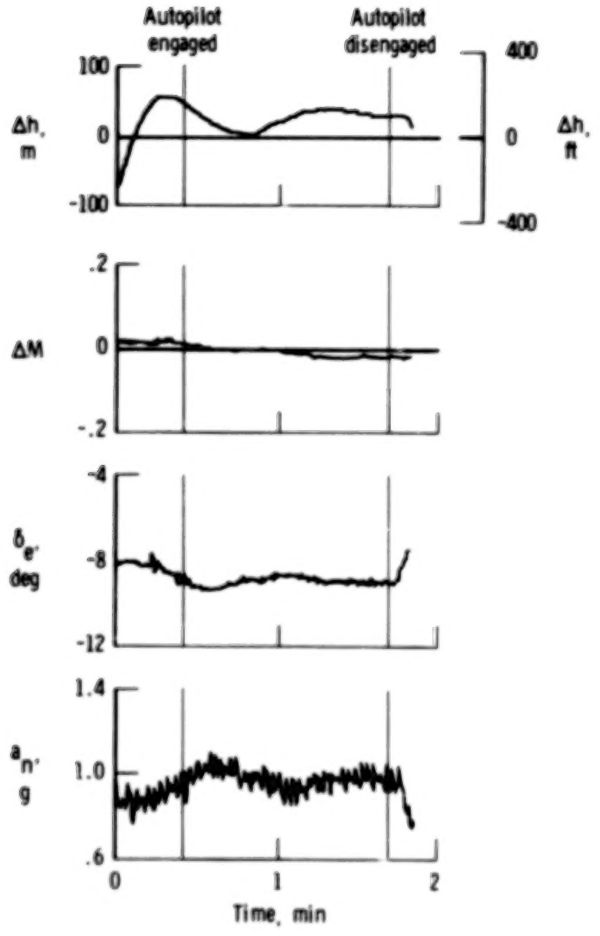

Figure 31. Performance of modified autopilot with initial rate of descent.

The pilots described the atmosphere as stable for both modified autopilot runs; however, any latent aircraft-control system instabilities would probably have been excited by the deceleration in figure 30 or the initial rate of descent condition in figure 31.

A more exacting task for the modified autopilot is operation in turning flight, particularly the transition between wings level and steady-state turning flight. An example of a high speed turn with modified altitude hold is presented in figure 32. The autopilot was engaged with wings level and, after 1 minute, a 35° bank turn was entered. Overall, altitude control was within a 30-meter (100-foot) band.

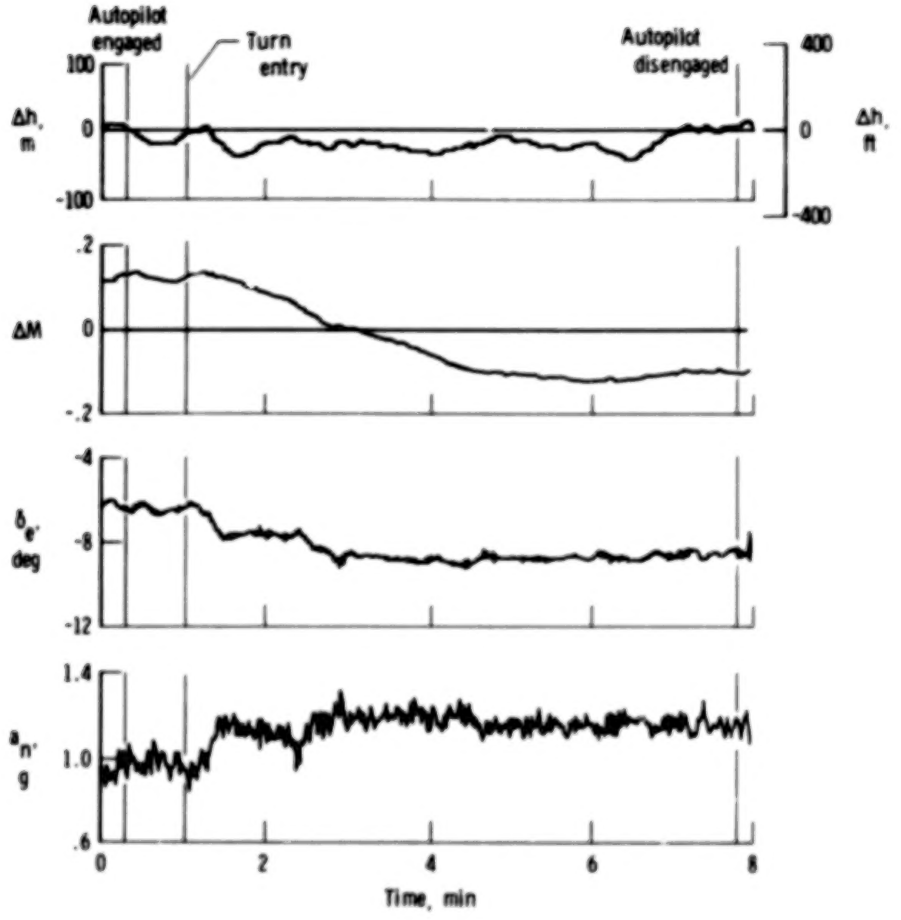

Figure 32. Modified altitude hold performance with turn entry. 35° bank angle.

Figure 33 is a time history of wings level, turn entry, and steady-state turning flight. This figure illustrates a number of problem areas that are peculiar to the present YF-12 control system but must be considered in the design of any altitude hold autopilot.

The altitude hold during the wings level portion was fairly good; however, the rapid turn entry excited a high frequency oscillation, which is caused by the static pressure angle-of-attack sensitivity. In this instance, the $K_{\dot{\theta}}$ of 0.35 was lower than the $K_{\dot{\theta}}$ of 0.50 that was recommended for use at this Mach number. The autotrim also reached its limit during this time period, thus directing the entire autopilot command to the pitch series servos through the ±2.3° limiter (fig. 6). Because the low frequency autopilot command was not removed by the autotrim, the 2.3° autopilot authority limit was reached (after 6 1/2 minutes of the time history) and, at

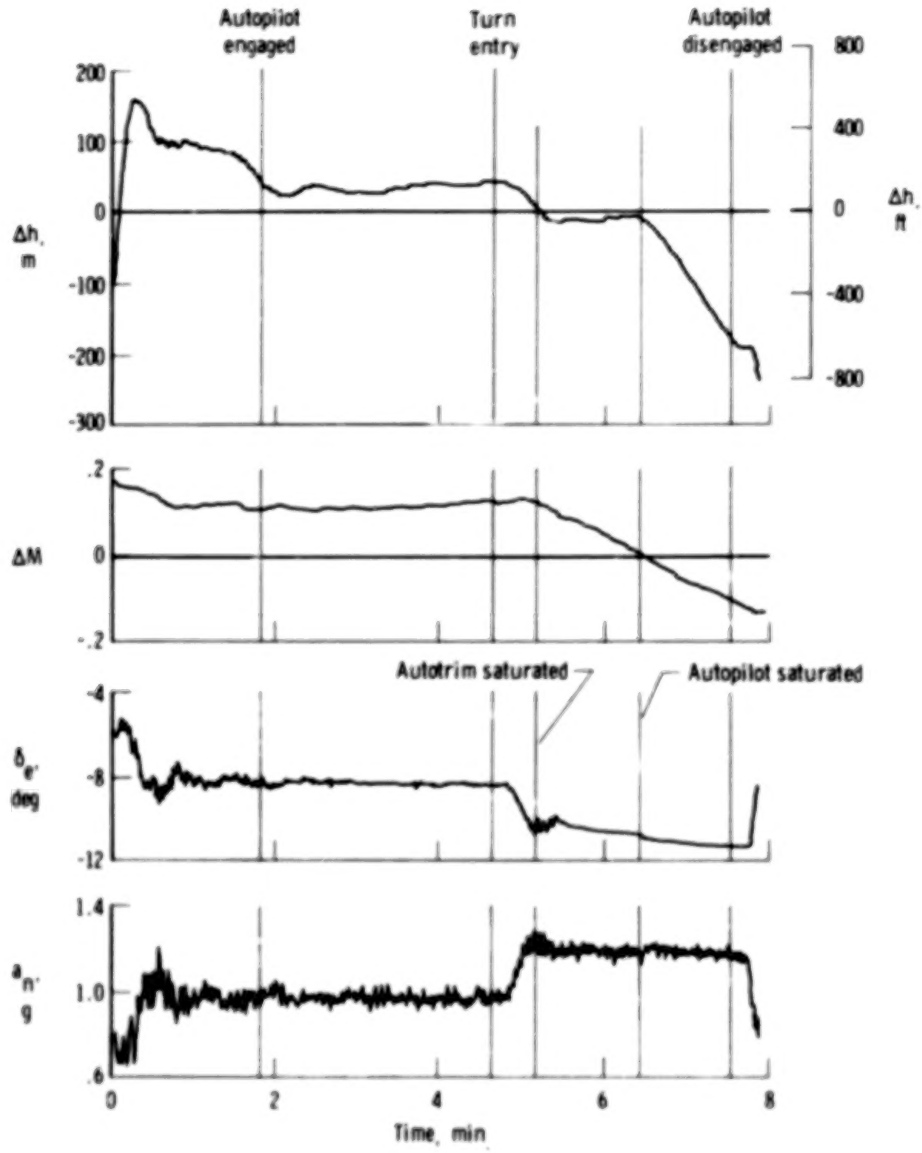

Figure 33. Modified altitude hold performance with turn entry. Autopilot and autotrim saturation; 38° bank angle; $K_{\dot{\theta}} = 0.35$.

that point, altitude could no longer be maintained. An increase in autotrim authority would eliminate this problem.

The effectiveness of the high-passed pitch rate feedback loop in suppressing the angle-of-attack sensitivity effect is illustrated in figure 34. In this example, modified altitude hold was engaged, $K_{\dot{\theta}}$ was set at the desired value, and a $\Delta\theta$ step disturbance was used to excite the aircraft-autopilot system. This test, which was conducted for $K_{\dot{\theta}}$ values of 0.35, 0.18, and 0, clearly showed the increased effectiveness of the high-passed pitch rate feedback with increased values of $K_{\dot{\theta}}$.

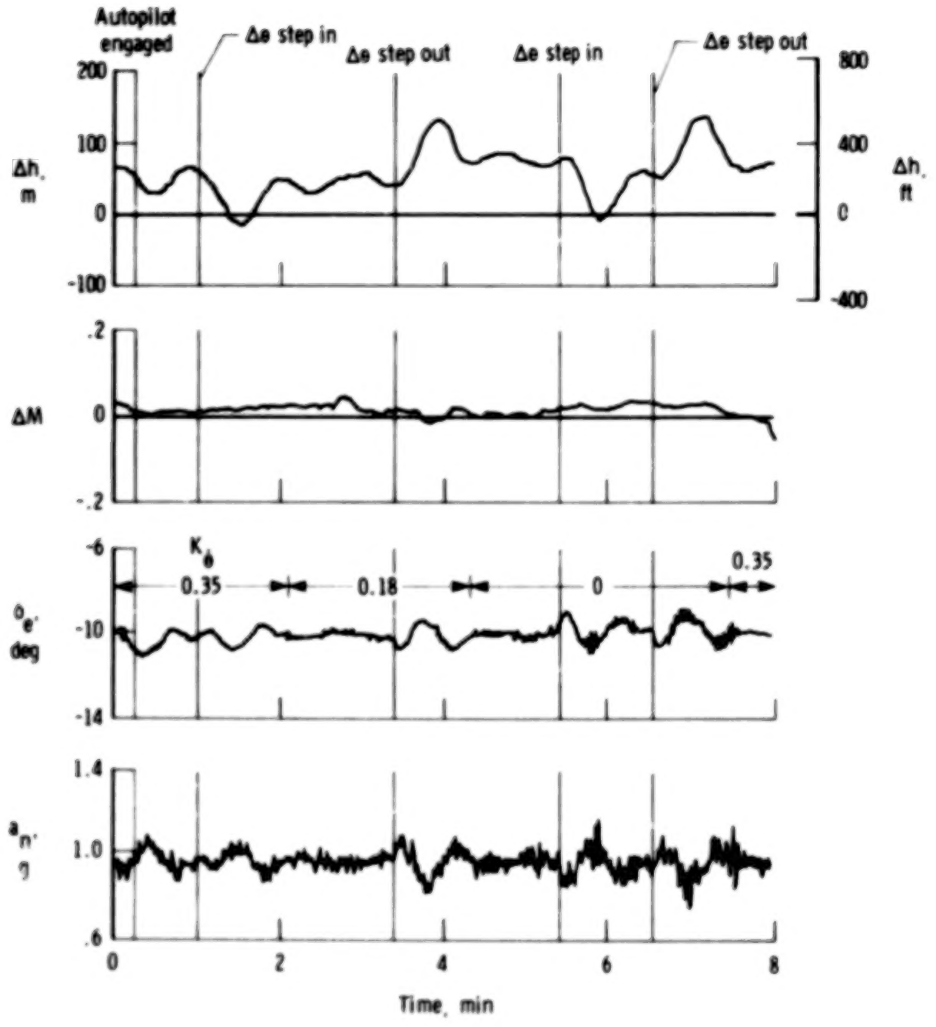

Figure 34. Modified altitude hold performance for various values of $K_{\dot{\theta}}$; response to Δθ disturbance function.

Effect of $K_{\theta_{\int h}}$ on modified altitude hold.—In the first few flights of modified altitude hold operation it was observed that the integrator path of the control system had a significant deadband, which occasionally was offset from zero. The deadband was a result of the integrator, which is mechanical, and had a significant breakout voltage, which in turn was aggravated by the $K_{\theta_{\int h}}$ reduction being made upstream of the integrator. As a result, the original breakout voltage, which was equivalent to an altitude error of ±5 to ±8 meters (±15 to ±25 feet), was changed to an equivalent altitude error of ±18 to ±30 meters (±60 to ±100 feet) for a $K_{\theta_{\int h}}$ of one-fourth the nominal value.

The initial attempt to reduce the breakout level was to increase $K_{\theta \int h}$. Although an increase in $K_{\theta \int h}$ also decreases the damping, it was desirable to observe the tradeoff. Figure 35 presents the results of doubling the gain from the modified

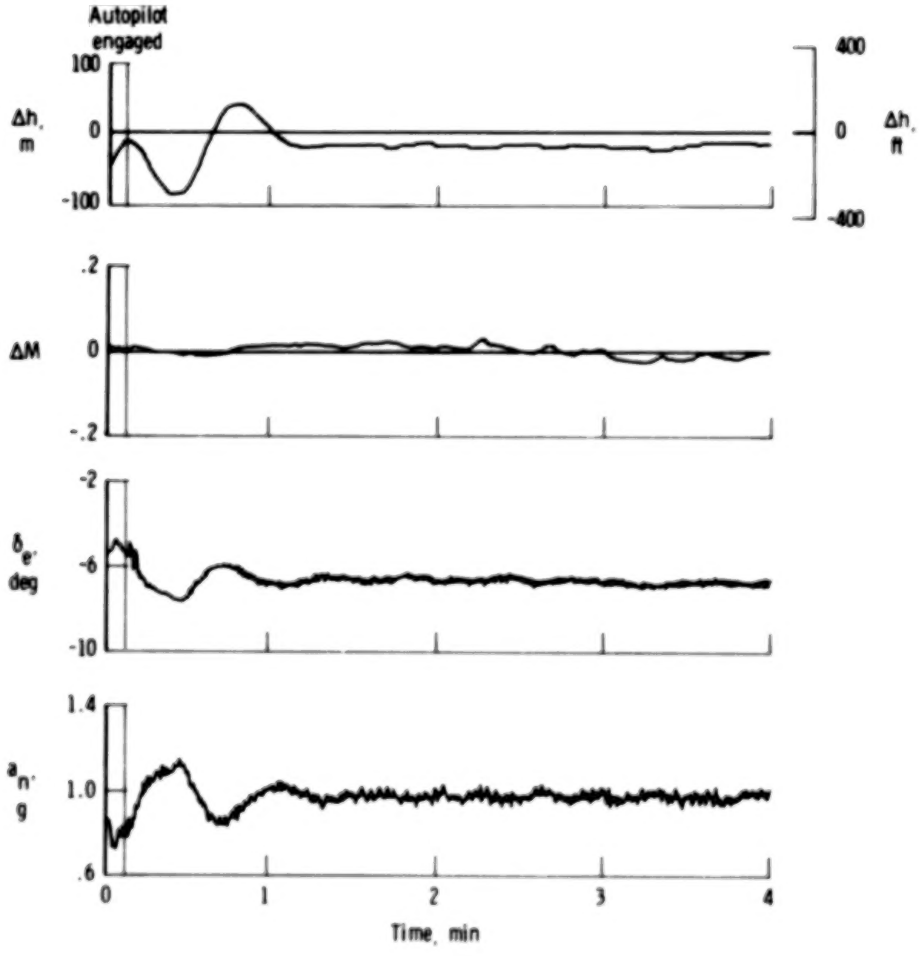

Figure 35. Modified altitude hold; $K_{\theta \int h}$ = 1/2 nominal.

value to a $K_{\theta \int h}$ of one-half the nominal value, which also effectively halves the integrator breakout level. The steady-state altitude hold is very good; however, the apparent low damping associated with the large overshoot after the first minimum is undesirable and objectionable to the pilots. Basically, the pilots feel that the sign of the altitude error should not reverse during the initial capture period. This configuration was clearly less satisfactory than the first autopilot modification; therefore, $K_{\theta \int h}$ was reset to one-fourth the nominal value.

On subsequent flights, the integrator operation became erratic due to the integration of stray voltages, thus making altitude control impossible. To salvage altitude control capability quickly, the integrator was grounded, which is equivalent to setting $K_{\theta \int h}$ to zero. Previous simulator studies indicated that the damping characteristics would be good but that any initial altitude rate at the time of engagement would prevent the steady-state altitude from returning to the original engage altitude. A typical example of modified altitude hold with $K_{\theta \int h}$ set to zero (fig. 36) shows that the initial rate of climb at the time of engagement resulted in a steady-state altitude error of 61 meters (200 feet).

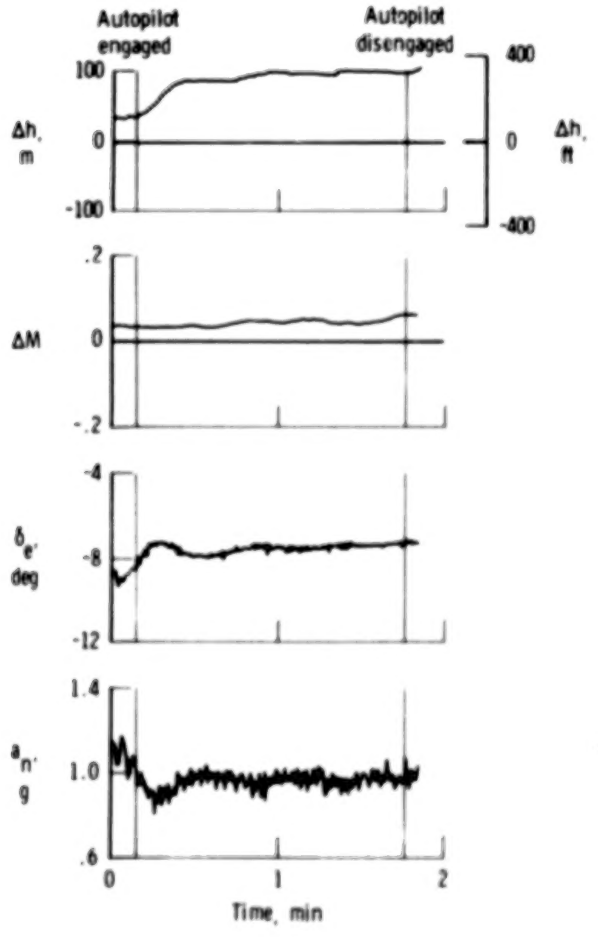

Figure 36. Modified altitude hold; $K_{\theta \int h} = 0$.

Integrator loop improvement.—When the integrator was repaired, $K_{\theta \int h}$ was repositioned downstream of the integrator. In this position, the value of $K_{\theta \int h}$ had no effect on the threshold of the integrator, which remained fixed between ±5 and ±8 meters (±15 and ±25 feet). Flight evaluation of the system with the improved integrator loop showed good performance. The time history shown in figure 37 was obtained with the improved integrator loop and a $K_{\theta \int h}$ of one-fourth nominal. The altitude was quickly returned to its engage condition without an overshoot.

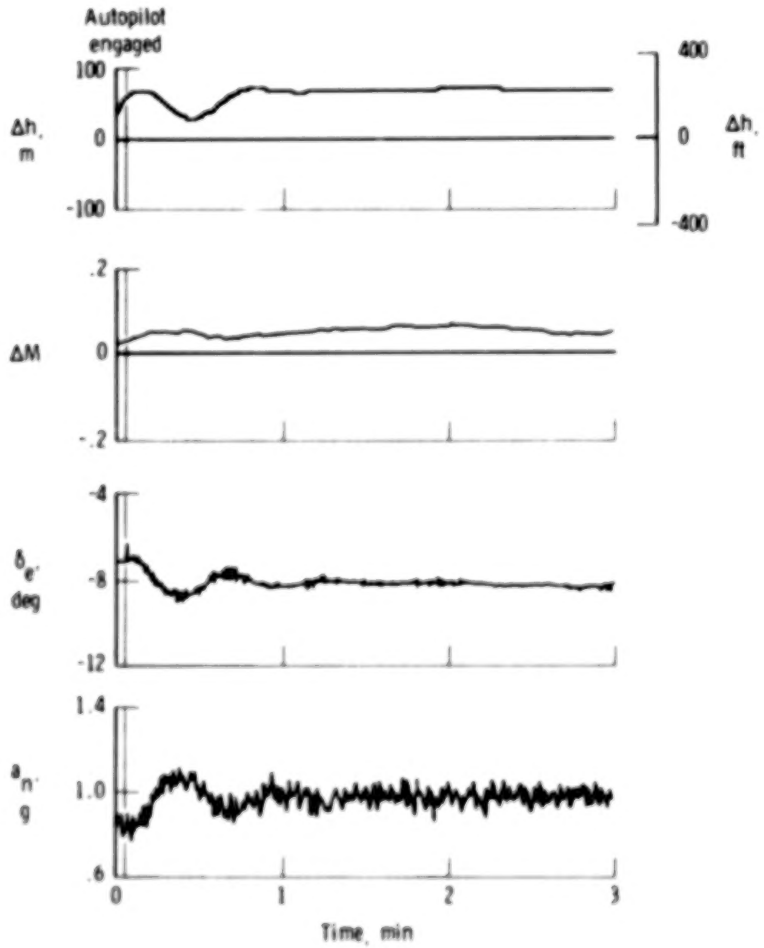

Figure 37. Modified altitude hold with improved integrator resolution; $K_{\theta \int h}$ = 1/4 nominal.

Altitude hold performance with alternate static pressure source.—The modified altitude hold autopilot was also evaluated with the air data computer connected to the angle-of-attack-insensitive static pressure source, p_{s_3}. With this arrangement, the high-passed pitch rate loop was not required; therefore, $K_{\dot{\theta}}$ was set to zero. These tests were also conducted during the period when the integrator was inoperable and, therefore, $K_{\theta_{\int h}}$ was zero.

Figure 38 presents a typical example of altitude hold in this configuration and, as would be expected, the performance is similar to that shown in figure 36 where the air data computer is connected to p_{s_2} and $K_{\theta_{\int h}}$ is zero.

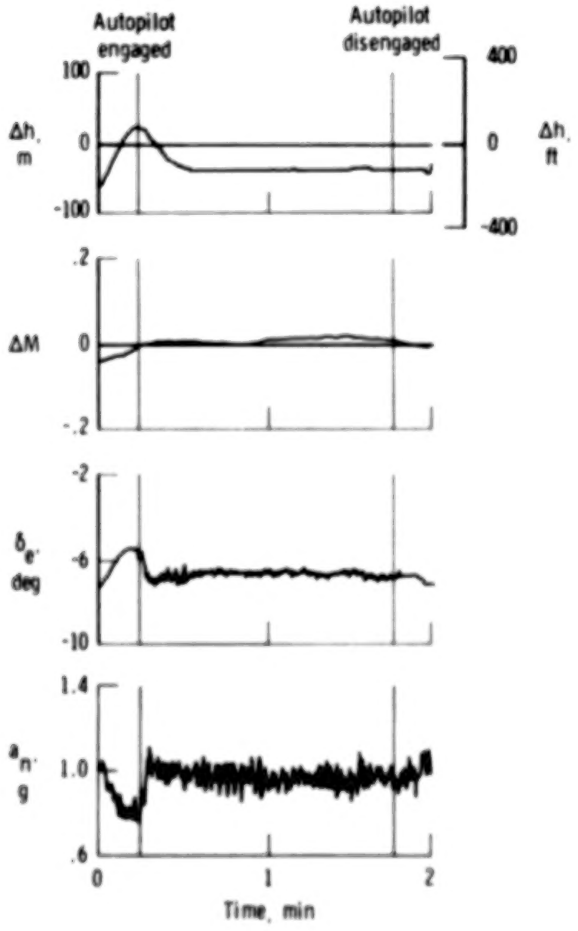

Figure 38. Modified altitude hold with $K_{\theta_{\int h}}$ set to zero and ADC connected to p_{s_3}; $K_{\dot{\theta}} = 0$.

Effects of pressure altitude fluctuations on altitude hold.—One disadvantage of an altitude hold autopilot that uses air data as its only source of altitude information is that the control system chases pressure changes. An example of altitude hold in a fluctuating atmosphere is shown in figure 39. The pressure altitude fluctuations

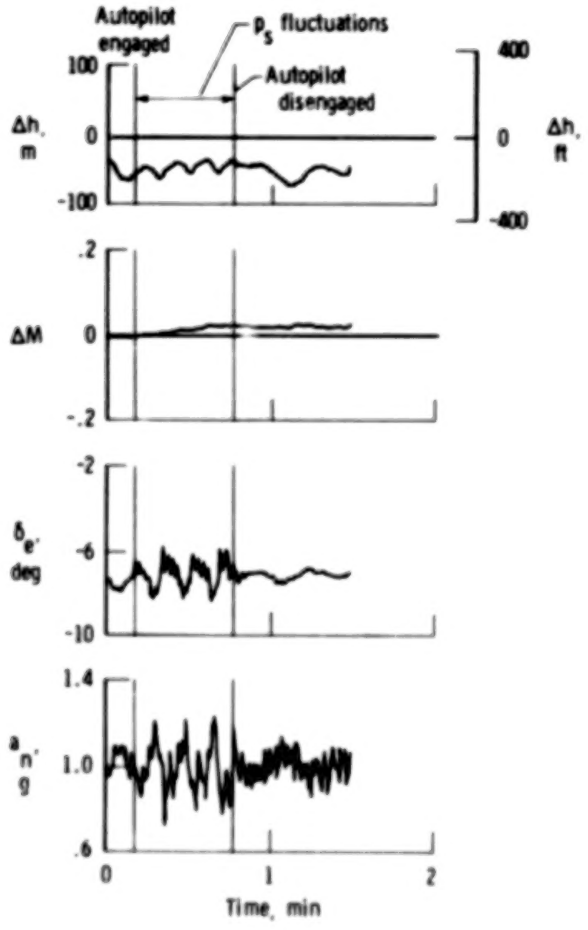

Figure 39. Modified altitude hold response to indicated pressure altitude fluctuations. $K_{\theta_{\int h}} = 0$; *ADC connected to* p_{s_3}; $K_{\dot{\theta}} = 0$.

are equivalent to ±9 meters (±30 feet) with a period of 23 seconds. The ride produced under these circumstances was unacceptable ($a_n = \pm 0.25g$) and as a result the system was disengaged. The large acceleration excursions are due to the large indicated altitude rate signal, $\overline{\dot{ln}\, p_s}$, provided to the autopilot by the ADC in conjunction with the relatively large $K_{\theta_{\dot{h}}}$ on this signal.

Pressure fluctuations can create a severe problem when altitude hold control is used, as illustrated in figure 39. Although such occurrences are infrequent, the example illustrates problems that can be encountered and should be considered in the design stage. One way to minimize the problem would be to provide inertial information to the autopilot. A blended scheme could then use inertial information to control the high frequency component and air data information to control the low frequency component of autopilot control.

Evaluation of impact pressure feedback.—Simulation studies showed that with SAS on, q_c feedback effectively damped the phugoid mode; however, with altitude hold on, the effect of the q_c feedback was negligible.

The in-flight effectiveness of q_c feedback in damping the phugoid mode is illustrated in figure 40. In this example, a 15-second thrust reduction was used

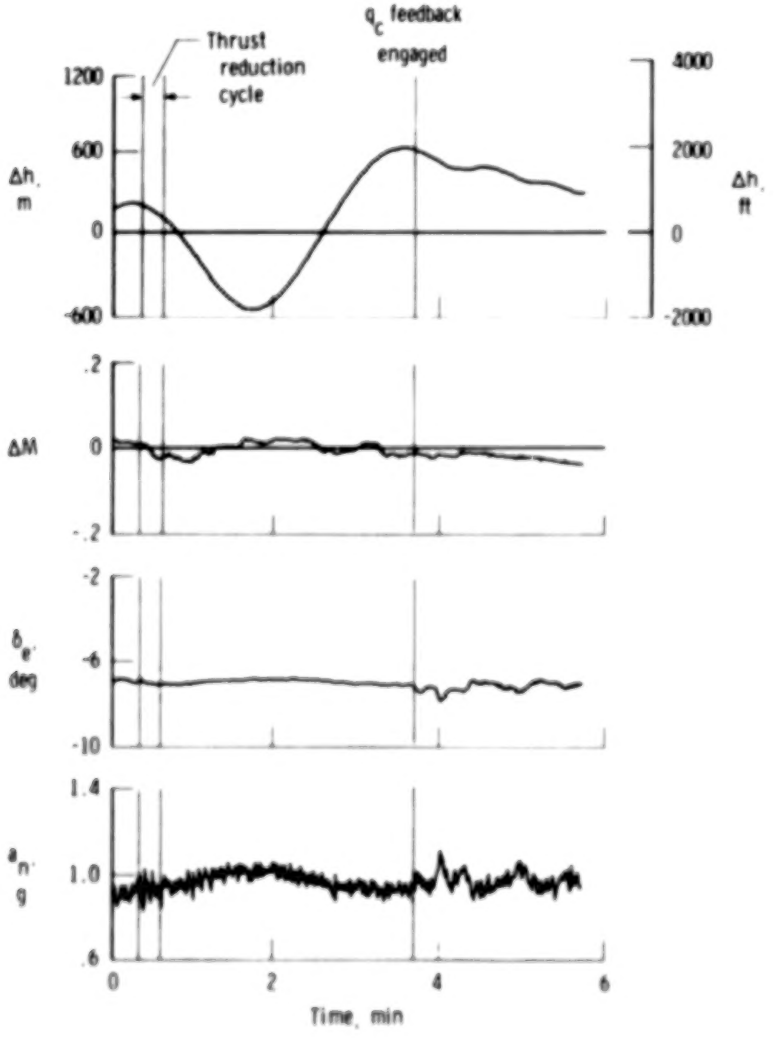

Figure 40. Effect of q_c feedback on phugoid mode. SAS on, autopilot off.

to excite the phugoid mode. The engagement of q_c was effective in damping the phugoid oscillation, which had a peak-to-peak altitude variation of nearly 1220 meters (4000 feet).

Figures 41 and 42 present a comparison of altitude hold with and without the q_c feedback loop engaged. In both examples, the $\Delta\theta$ disturbance function was put in and then taken out approximately 1 1/2 to 2 minutes later. Altitude hold is more sluggish with q_c engaged and has a slight tendency to overshoot. A rougher ride is also produced by the q_c feedback. The rougher ride could be due to atmospheric temperature variations, which result in continual q_c variations.

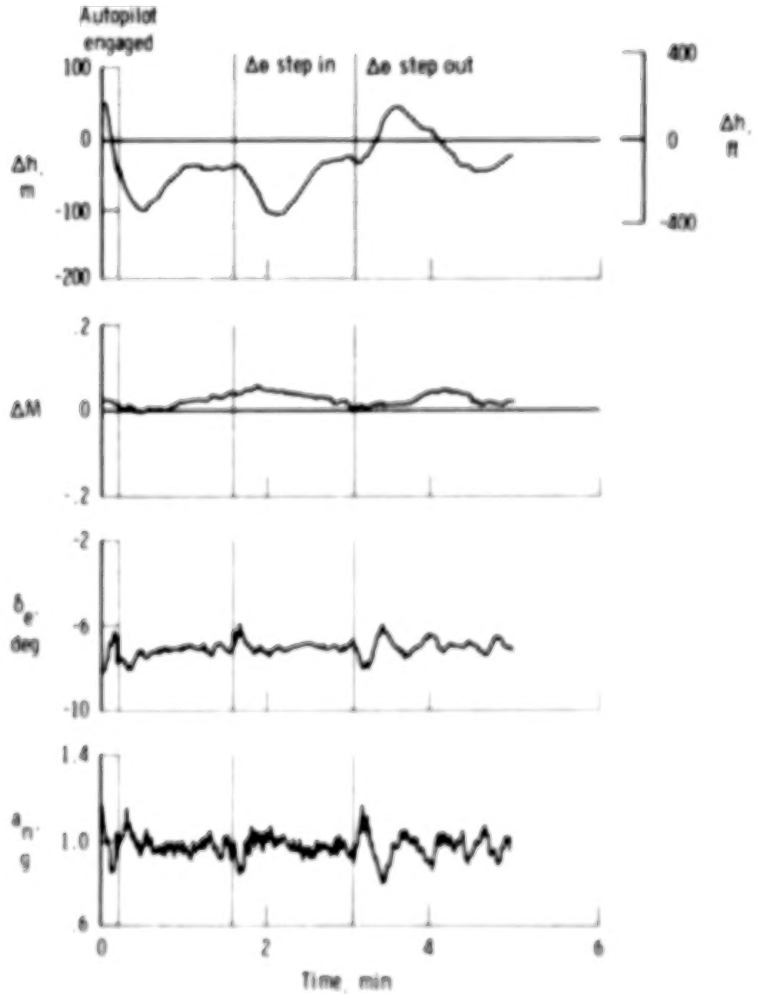

Figure 41. Modified altitude hold with q_c feedback engaged; response to $\Delta\theta$ disturbance function.

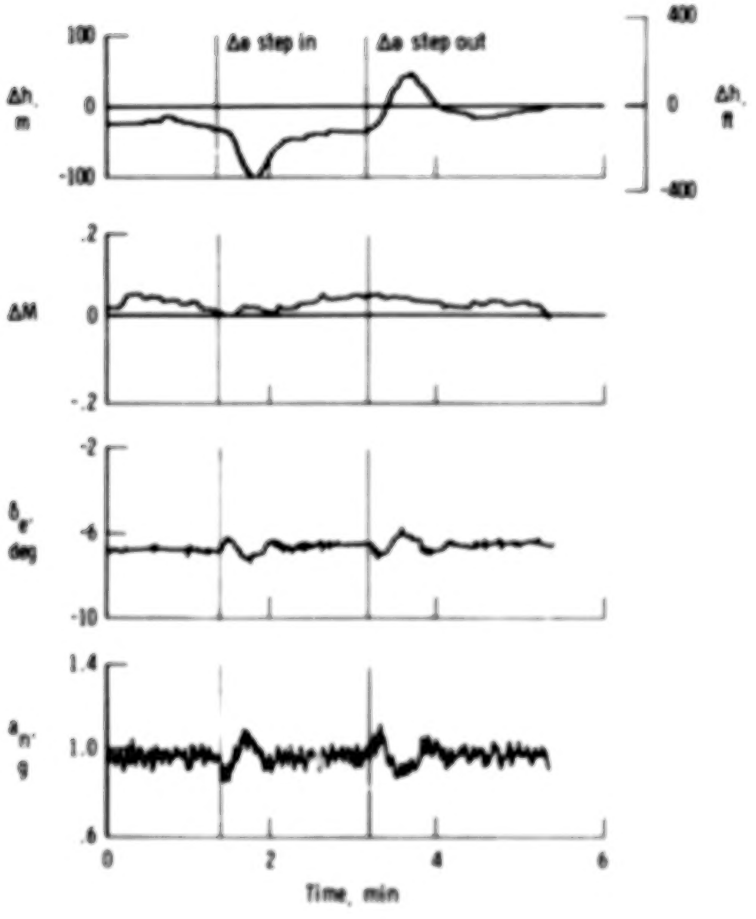

Figure 42. Modified altitude hold without q_c feedback; response to Δθ disturbance function.

Pilots' impressions of autopilot modifications.—The pilots' impressions of the modified altitude hold autopilot configurations ranged from very pleased to quite disappointed, depending on the control system configuration. The configuration most preferred by the pilots, based on all the autopilot experience, was the one that required the least amount of maneuvering from the engage point to steady state. If the altitude hold mode were engaged with the aircraft perfectly trimmed, nearly all the configurations would produce equivalent results. However, based on YF-12 flight experience, nearly all altitude hold engagements are from untrimmed conditions and have rates of climb. This initial rate of climb and the manner in which the control system reacts to it affect the pilot's opinion of the autopilot.

The configuration most preferred by the pilots was that with the altitude integral gain set to zero (figs. 36 and 38). An altitude error always exists when $K_{\theta_{\int h}}$ is

zero and the system is engaged with a rate of climb. To the pilots, however, an altitude error is inconsequential as compared with extra maneuvering; when flying without the aid of the autopilot, the pilot accepts the altitude at which he initially stabilizes if it is within approximately 100 meters (300 feet) of the desired flight condition. Valuable time is wasted if a precise altitude is required. An altitude capture mode that would smoothly converge on a designated altitude would be desirable.

The pilots' comments were favorable with the large integrator threshold, which resulted in well-damped control. The larger the threshold the better the pilots liked the system.

Improving the integrator threshold (making it smaller) by moving the gain $K_{\theta \int h}$ downstream (fig. 37) caused a degradation of pilot opinion and, in the case where $K_{\theta \int h}$ was increased, pilot comments were negative due to the low damping characteristics (fig. 35).

Because the modified configuration with the improved integral loop threshold did not receive the most favorable pilot comments, $K_{\theta \int h}$ was lowered to 0.15 of the nominal value, at which point pilot comments indicated a definite improvement.

The pilots were impressed with the ability of the q_c feedback in damping the phugoid mode, although they detected no benefit in having q_c feedback when altitude hold was engaged.

Extensive handling qualities investigations were also made with and without q_c feedback for manual flightpath control (SAS on) and pitch autopilot control (SAS on). The effect of q_c feedback on handling qualities was negligible in all the configurations tested.

With the altitude hold mode engaged and steady-state control established, the pilot's Mach hold task was easy as compared with simultaneous manual altitude and Mach control.

Mach Hold Autopilot

This section presents the results of the Mach hold autopilot investigation. The discussion covers the original Mach hold performance, the results of simulation studies with parametric variations, and the in-flight performance evaluation of the Mach hold mode with the ADC connected to the angle-of-attack-insensitive static pressure source.

Original Mach Hold Operation

The Mach hold mode of the YF-12A autopilot was designed to operate over the entire Mach number range of the airplane; however, experience revealed long-period, large amplitude divergent characteristics. Figure 43 presents a typical

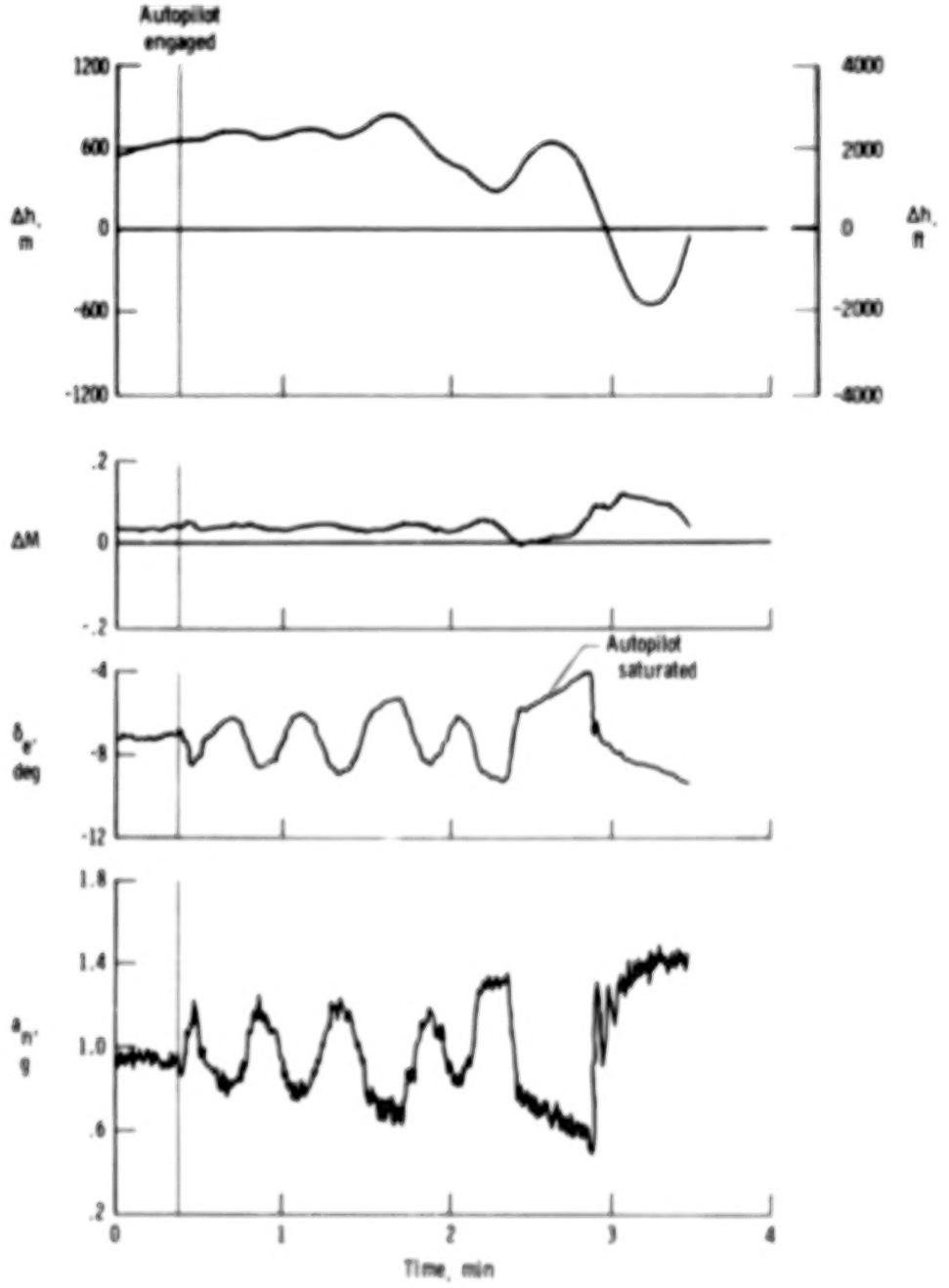

Figure 43. Original Mach hold.

time history of a Mach hold engagement at approximately Mach 3.0 and an altitude of 23,600 meters (77,500 feet) with the air data computer connected to the angle-of-attack-sensitive static ports, p_{s_2}. Control of Mach number is good at first, with a period of 30 seconds and elevon inputs of ±1.5° commanding a normal acceleration of ±0.2g. Two minutes after engagement the oscillation has diverged sufficiently to saturate the autopilot output ($\Delta\delta_e = \pm 2.3°$), as evidenced by the ramp type of elevon control which is due to the autotrim function of the autopilot. The autotrim function begins to destabilize when the autopilot output saturates. In this configuration, a steady-state autopilot limit cycle develops from which the autopilot cannot recover with Mach hold engaged. The peak-to-peak altitude change was 1370 meters (4500 feet) and the peak accelerations were greater than ±0.4g. There were no pilot inputs or obvious atmospheric disturbances to contribute to the problem.

Simulation Studies

The Mach hold autopilot problem was investigated briefly on the simulator. The areas of investigation were static pressure angle-of-attack sensitivity and outer-loop gain effectiveness. The primary means of disturbing the simulation was a drag pulse, which consisted of a deceleration of 3.048 m/sec^2 (10 ft/sec^2) for a duration of 1 to 5 seconds and resulted in approximate Mach number losses of 0.01 to 0.04. A drag pulse is a controlled disturbance that can be duplicated on the aircraft by a thrust reduction and is also representative of a step temperature change.

The Mach hold capability of the present control system is sensitive to variations of $p_s(\alpha)$, as shown in figure 44. For a 5-second drag pulse, which causes an initial

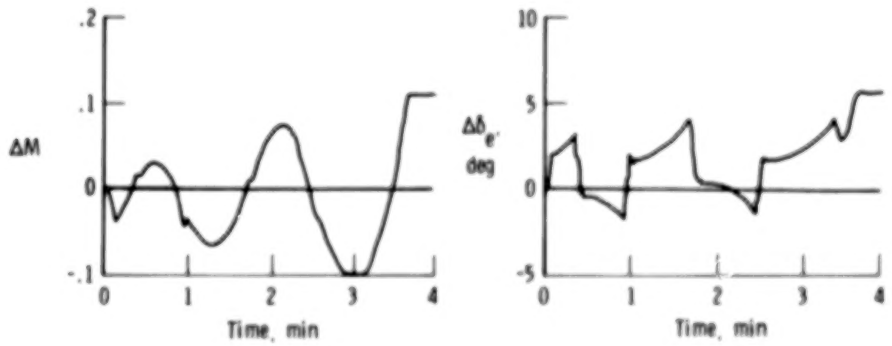

(a) $p_s(\alpha) = 1$.

Figure 44. Simulation responses of original Mach hold for various fractions of nominal $p_s(\alpha)$. Input is a deceleration of 3.048 m/sec^2 (10 ft/sec^2) for 5 seconds; K_{θ_M} and $K_{\theta\int M}$ are nominal.

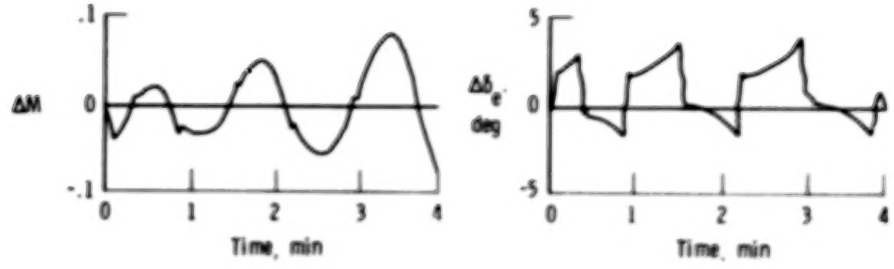

(b) $p_s(\alpha) = 3/4$.

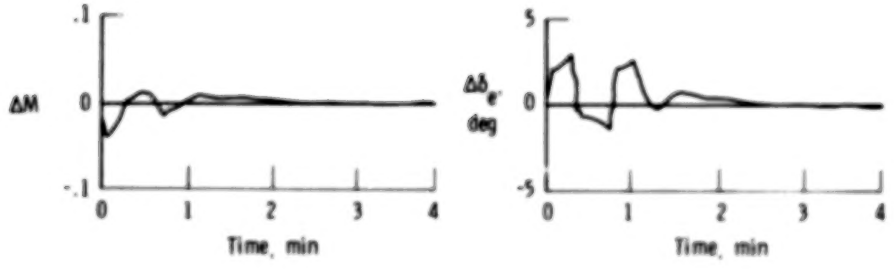

(c) $p_s(\alpha) = 1/2$.

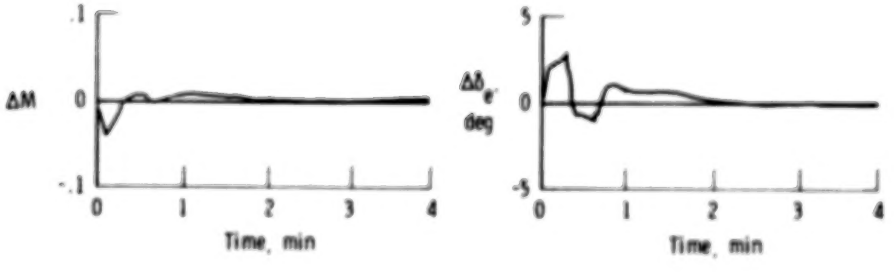

(d) $p_s(\alpha) = 1/4$.

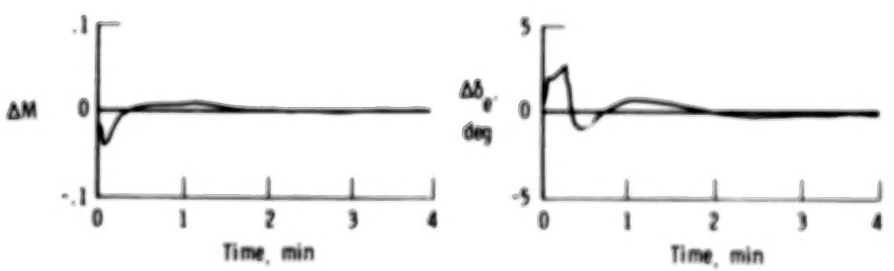

(e) $p_s(\alpha) = 0$.

Figure 44. Concluded.

Mach loss of 0.04, the system is unstable for a $p_s(\alpha)$ from three-fourths nominal to nominal. As stated previously, the actual effective flight value of $p_s(\alpha)$ ranges from one-half nominal to nominal depending on angle of attack and attenuation at the higher frequencies. Elimination of $p_s(\alpha)$ is obviously desirable.

In addition, the autopilot-aircraft nonlinearities make Mach hold stability sensitive to the disturbance magnitude. As shown in figure 45, the Mach hold control system with a nominal $p_s(\alpha)$ is stable for drag pulses of short duration. However, for drag pulse durations of 4 seconds and longer, which result in Mach errors of 0.03 and greater, the system diverges.

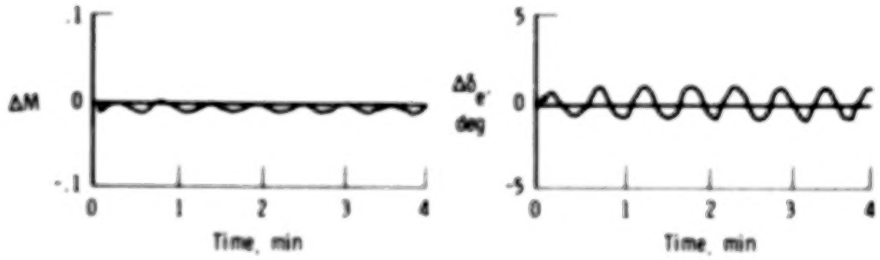

(a) Drag duration = 1 second.

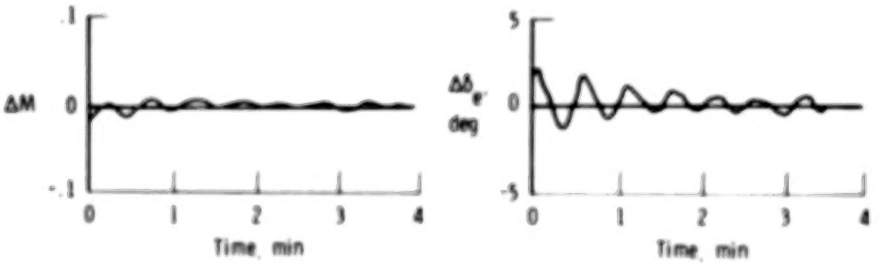

(b) Drag duration = 2 seconds.

Figure 45. Simulation responses of original Mach hold drag pulses of various lengths. $p_s(\alpha)$ = nominal; deceleration = 3.048 m/sec^2 (10 ft/sec^2); K_{θ_M} and $K_{\theta \int M}$ are nominal.

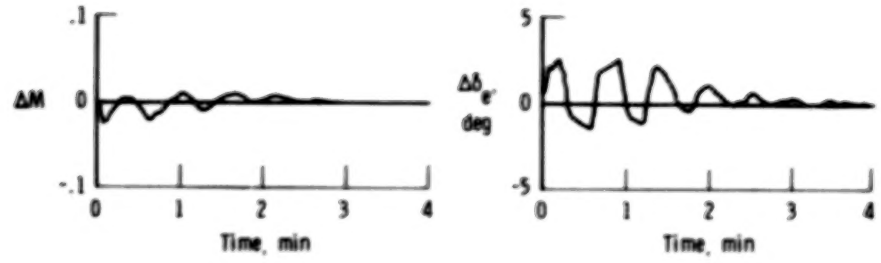

(c) Drag duration = 3 seconds.

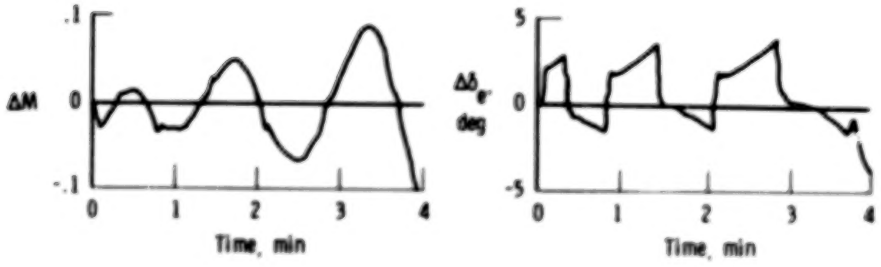

(d) Drag duration = 4 seconds.

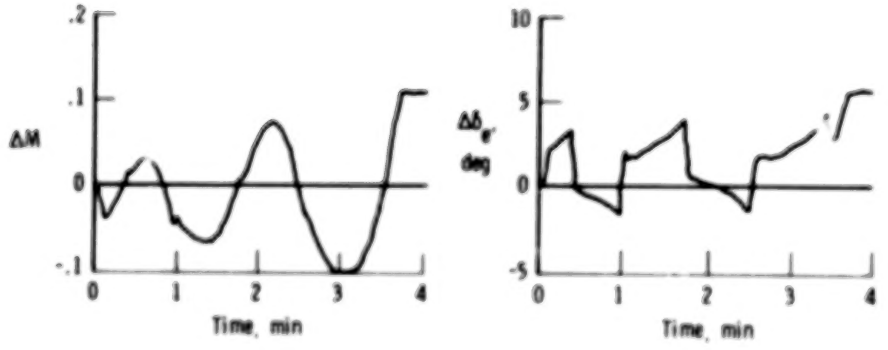

(e) Drag duration = 5 seconds.

Figure 45. Concluded.

Simulation time histories for parametric variations of the outer-loop gains, K_{θ_M} and $K_{\theta \int_M}$, are presented in figure 46. For this study, $p_s(\alpha)$ was set to one-half nominal to prevent the angle-of-attack sensitivity from obscuring the effects of the gain variations; the disturbance was a 5-second drag pulse. As shown, a reduction in $K_{\theta \int_M}$ to one-half its nominal value minimizes autopilot saturation, thereby improving Mach control. As expected, an increase in $K_{\theta \int_M}$

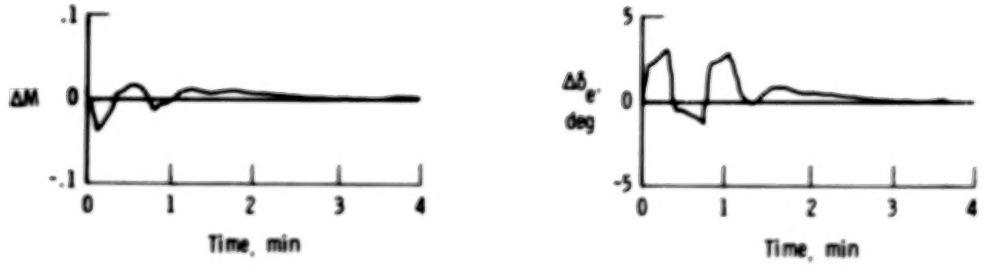

(a) K_{θ_M} = nominal, $K_{\theta \int_M}$ = nominal.

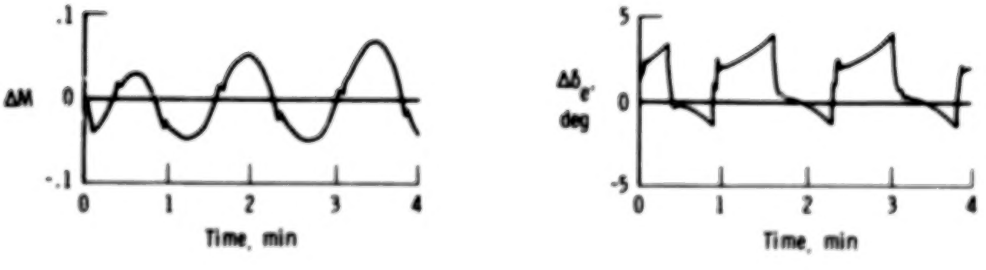

(b) K_{θ_M} = nominal, $K_{\theta \int_M}$ = 1 1/2 nominal.

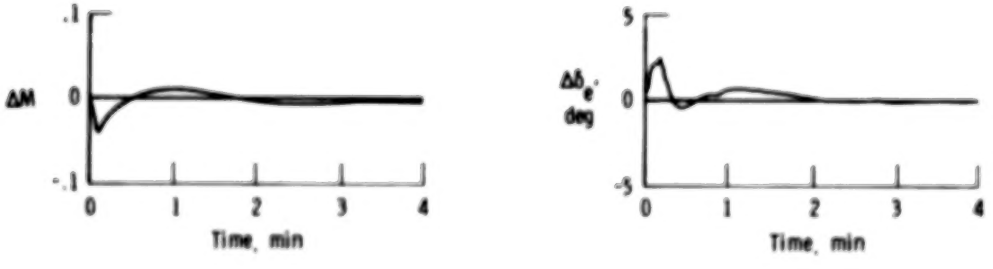

(c) K_{θ_M} = nominal, $K_{\theta \int_M}$ = 1/2 nominal.

Figure 46. Simulation responses of original Mach hold for various outer-loop gain values. p_s(a) = 1/2 nominal; input is a deceleration of 3.048 m/sec^2 (10 ft/sec^2) for 5 seconds.

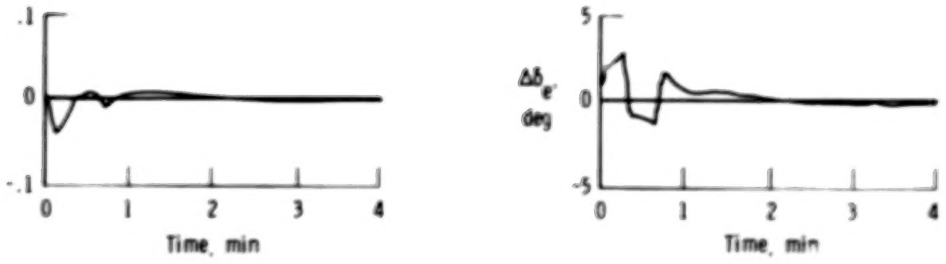

(d) K_{θ_M} *= 1 1/2 nominal,* $K_{\theta\int_M}$ *= nominal.*

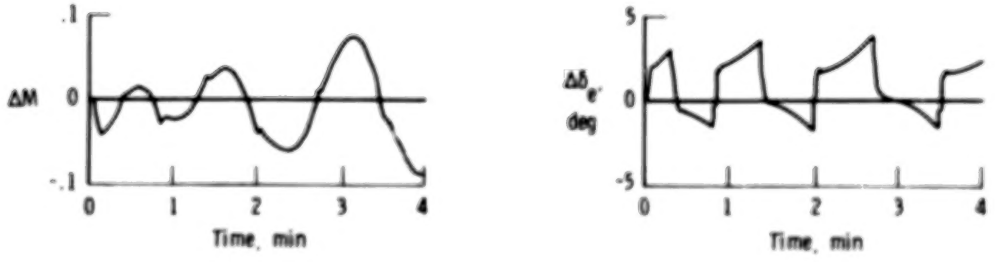

(e) K_{θ_M} *= 1/2 nominal,* $K_{\theta\int_M}$ *= nominal.*

Figure 46. Concluded.

increases the divergence of the system. In addition, some increase in K_{θ_M} appears to improve the stability of the system, whereas a decrease in K_{θ_M} causes the system to diverge and saturate.

A review of the simulation results emphasizes that at high speeds a conventional Mach hold autopilot with elevator control is sensitive to small Mach number changes, and that even normal atmospheric variations will cause a wavy ride, because Mach number is controlled through changes in altitude.

Mach Hold Flight Results With ADC Connected to p_{s_3}

As stated previously, the ADC was connected to the static pressure angle-of-attack-insensitive source, p_{s_3}, to eliminate the high frequency oscillations experienced in the original altitude hold autopilot. Therefore, the influence of the p_{s_3} hookup on Mach hold was also investigated, although improvement in Mach hold was not a formal objective of the present study.

With the p_{s_3} hookup, the Mach hold mode was stable, as shown in figure 47, and Mach number was held within ±0.02. However, to maintain Mach number, the

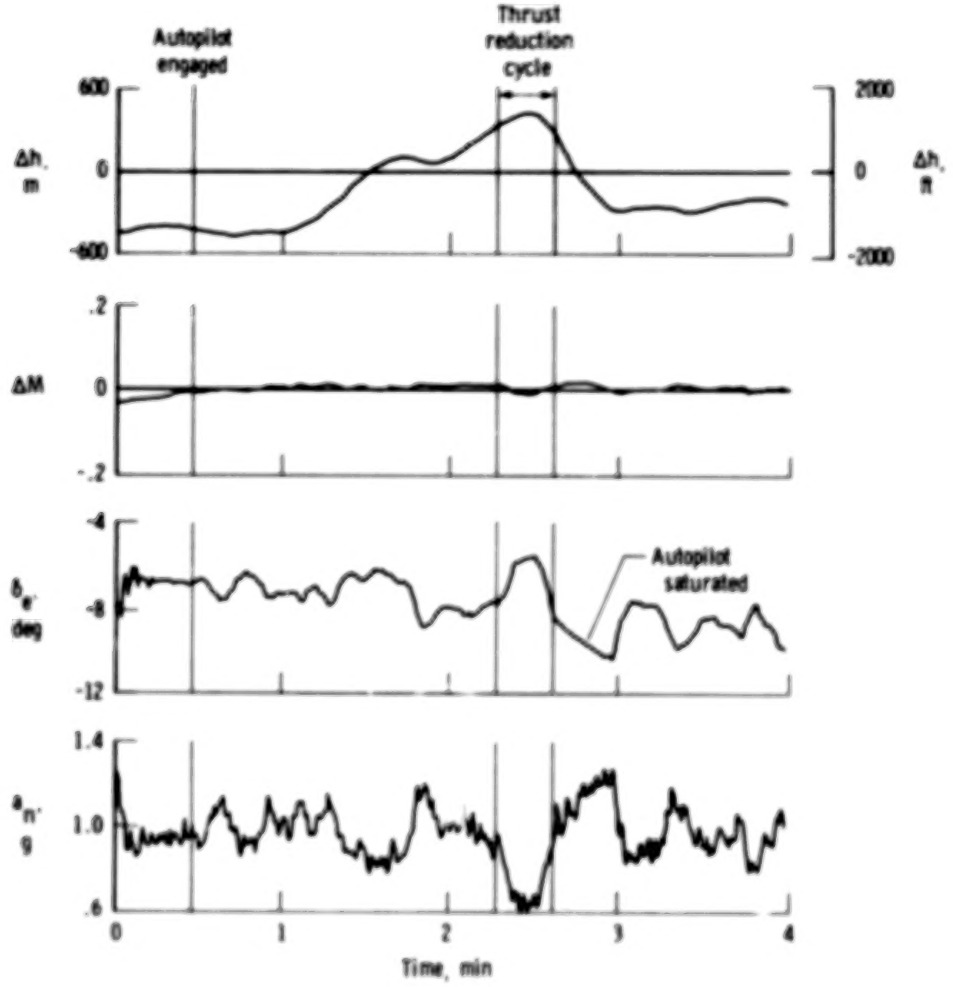

Figure 47. Mach hold operation with angle-of-attack-insensitive static pressure, p_{s_3}.

aircraft was put into a climb (the power levers were not moved) because of the slight initial acceleration at the point of engagement. Approximately 2 minutes after Mach hold engagement, the pilot reduced thrust to produce a controlled deceleration disturbance function to demonstrate the Mach hold control system's capabilities. As shown, the Mach number loss was minimal; however, a large altitude loss was necessary to compensate for the loss of thrust. In general, altitude changes required to control Mach number result in poor ride qualities.

The autopilot signal was saturated for approximately 20 seconds during the recovery of Mach number, but the autopilot recovered and there was no evidence of long-period instabilities.

The gradual increase of altitude in the Mach hold example (fig. 47) emphasizes that a single controller does not permit simultaneous altitude and Mach control. Studies are underway for the implementation of an autothrottle Mach controller, which would permit the independent control of Mach number and altitude.

CONCLUDING REMARKS

An autopilot improvement program was undertaken to improve the poor altitude hold and Mach hold control system characteristics at high altitude, high speed flight conditions.

Static pressure source sensitivity to angle of attack was found to have a significantly adverse effect on the altitude hold and Mach hold autopilot modes.

Good altitude hold was demonstrated at high altitude using existing autopilot concepts and hardware with only minor modifications. These modifications consisted of adding a high-passed pitch rate feedback to compensate for the effects of angle-of-attack sensitivity on altitude measurements and reducing the altitude error gain and altitude integral gain.

Reducing the integrator threshold and increasing the altitude integral gain improved the altitude tracking performance; however, these changes also caused unfavorable pilot comments due to an apparent sensed decrease in stability.

Good Mach hold using elevator control was demonstrated at high Mach numbers with an angle-of-attack-insensitive static pressure hookup. However, large altitude changes were necessary to compensate for small Mach number changes, which resulted in poor ride qualities.

Dryden Flight Research Center
National Aeronautics and Space Administration
Edwards, Calif., November 22, 1976

APPENDIX A.—DETAILED DESCRIPTION OF FLIGHT CONTROL SYSTEM ELEMENTS

Nose Boom

The air data information was obtained from a compensated nose boom as shown in figure 4. The nose boom installation is described in detail in reference 7. The p_{s_2} ports were connected to the air data computer and provided the primary altitude information to the pilot and the autopilot. The p_{s_1} ports provided pilot backup information. The p_{s_2} and p_{s_1} ports were located on the compensated portion of the nose boom to minimize the transonic static pressure position error correction. However, these compensated ports become sensitive to angle of attack as Mach number increases (ref. 11). The Mach error, ΔM, can be converted to a static pressure error, Δp_s, by the expression

$$\Delta p_s = F(p_s/M)\Delta M$$

where F is a function of Mach number as illustrated in figure 48. The p_{s_3} ports were identical in location and configuration to the static ports on the standard NASA

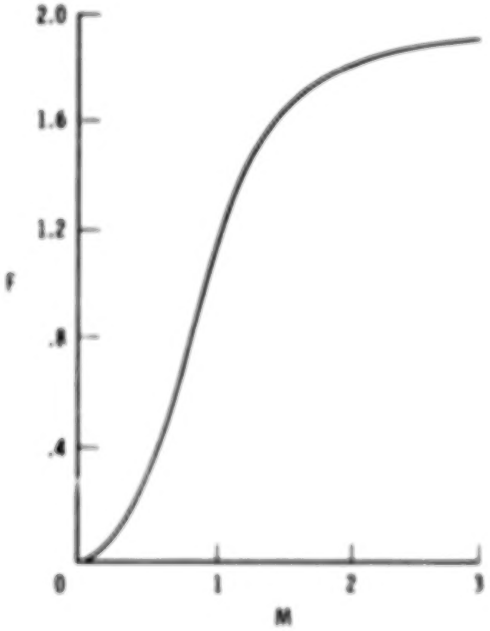

Figure 48. Variation of $\frac{\Delta p_s/p_s}{\Delta M/M}$, F, *with Mach number.*

pitot-static nose boom probe, which is described in detail in reference 12. Wind tunnel and flight data confirmed that the static pressure error due to angle of attack was negligible. A flight calibration of this probe position is presented in reference 11 and, as would be expected, the transonic position correction for the p_{s_3} ports is much larger than that for the compensated ports, p_{s_1} and p_{s_2}.

The air data computer is approximately 6 meters (20 feet) aft of the total and static pressure ports and, therefore, a significant amount of lag is present in the indicated p_{t_2} and p_s measurements. Ground calibrations of the p_{t_2} system gave a sea level lag constant, $\tau_{sl_{p_{t_2}}}$, of 0.27 second, which can be converted to a time constant at a given Mach number and altitude by the expression

$$\tau_{p_{t_2}} = \tau_{sl_{p_{t_2}}} (p_{sl}/p_{t_2})$$

An in-flight determination of the p_{s_2} system lag constant was performed at the aircraft short-period frequency. The sea level lag constant, $\tau_{sl_{p_{s_2}}}$, was 0.056 second, which converts to a time constant at the altitude of interest by the expression

$$\tau_{p_{s_2}} = \tau_{sl_{p_{s_2}}} (p_{sl}/p_{s_2})$$

Air Data Computer

The air data computer receives total and static pressure data from the compensated nose boom installation and computes Mach number and altitude information for pilot display and autopilot information. The ADC is an electromechanical device that uses two force-rebalancing pressure sensor servo loops. Figure 49 illustrates the operation of the static pressure, p_s, and impact pressure, q_c, servo loops, which are similar. A change of pressure within the transducer causes the evacuated bellows to exert a torque about a torsion bar, which, in turn, causes a servo loop to exert a rebalancing torque about the opposite end of the torsion bar. The twisting of the torsion bar is proportional to the pressure. The mechanism measures pressures with only minute bellows displacements, minimizing the adverse effects of nonlinear bellows spring rates and bellows hysteresis. In both loops, the pressure rates, $\dot{p}_s$ and $\dot{q}_c$, are measured by the velocity generator, which measures the rate of the motor displacement. Mach number, altitude, and associated rate information are determined by the use of cams.

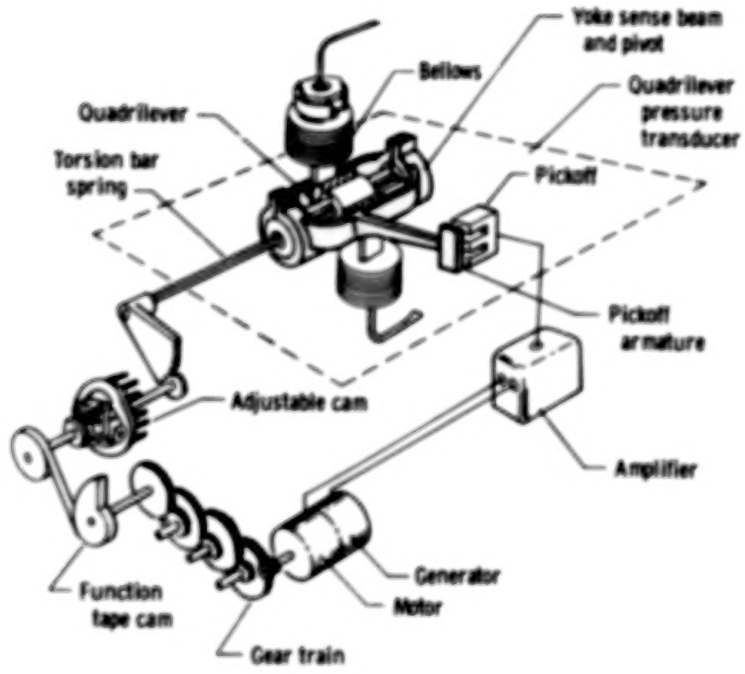

Figure 49. Diagram of pressure computing servo loop.

Flight data input and output characteristics of the ADC static pressure servo loop at Mach 3.0 and an altitude of 23,600 meters (77,500 feet) are presented in figure 50. These data are the result of a control system-induced limit cycle. The actual pressure variation input to the ADC is presented in figure 50(a). The ADC output signals are voltages proportional to the altitude change from the engage point and to the altitude rate (fig. 50(b)). The threshold is then determined by comparing the constant portions of either the altitude or altitude rate trace (fig. 50(b)) with the actual pressure altitude variation (fig. 50(a)). At an altitude of 23,600 meters (77,500 feet), the threshold is approximately 3.7 meters (12 feet).

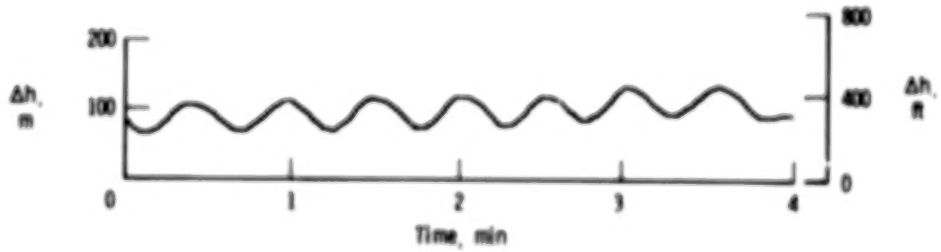

(a) Air data computer input.

Figure 50. Air data computer input and output characteristics. $M \approx 3.0$, $h \approx 23,600$ meters (77,500 feet).

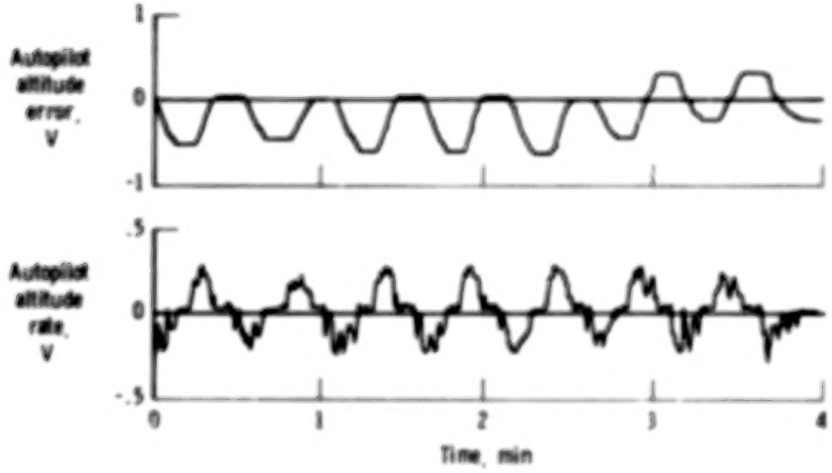

(b) Air data computer outputs.

Figure 50. Concluded.

The frequency response characteristics of the ADC were determined in the lab and are presented in figure 51. The frequency response tests were perturbations

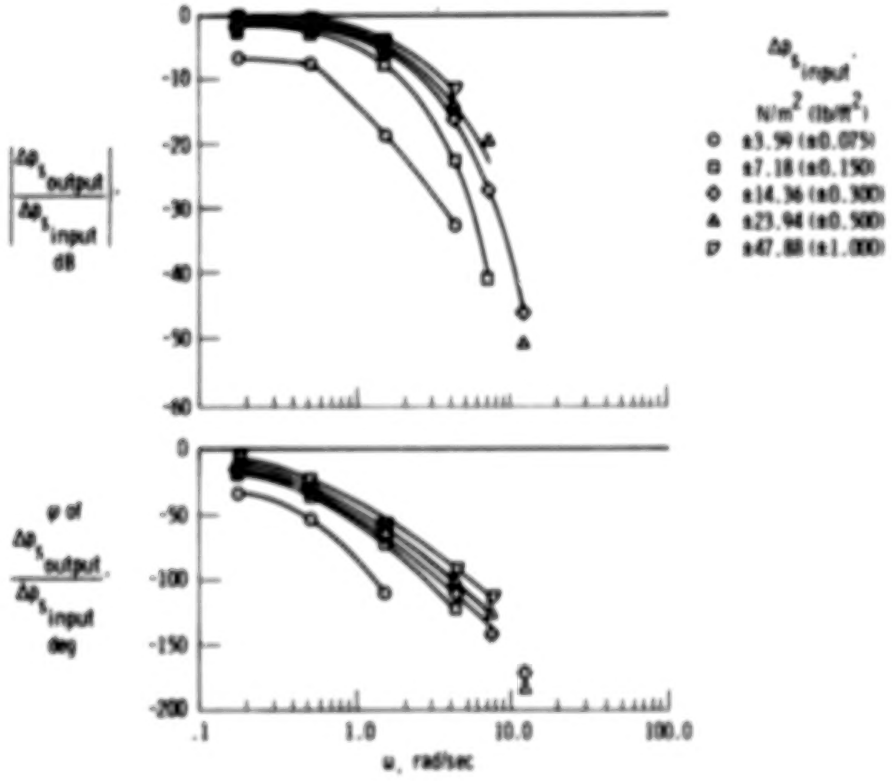

Figure 51. Frequency response of air data computer for various input levels.

about the nominal flight condition of Mach 3.0 and an altitude of 23,600 meters (77,500 feet). A minimum amount of tubing was used to connect the pressure oscillator to the ADC. The frequency response is constant to approximately 0.5 radian per second; however, the lower amplitude pressure variations are significantly attenuated by the threshold.

Original Altitude and Mach Hold Control Systems

The YF-12 pitch-axis vehicle control system is shown in figure 6. The time constant and gains, which are scheduled as functions of flight condition, are presented in figure 52.

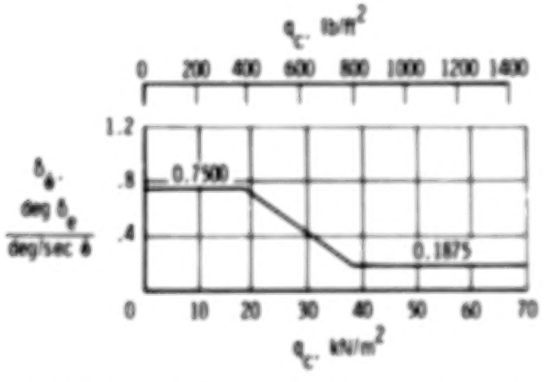

(a) Schedule 1: pitch rate-to-elevon gain schedule.

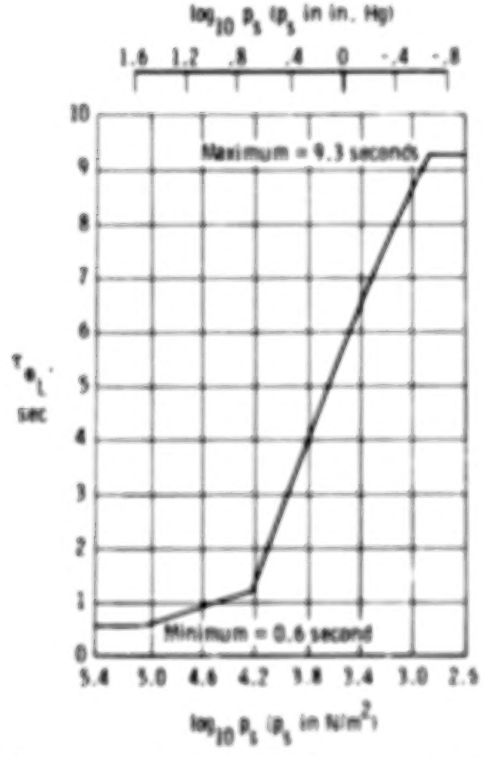

(b) Schedule 2: pitch attitude low-pass time constant.

Figure 52. Autopilot schedules.

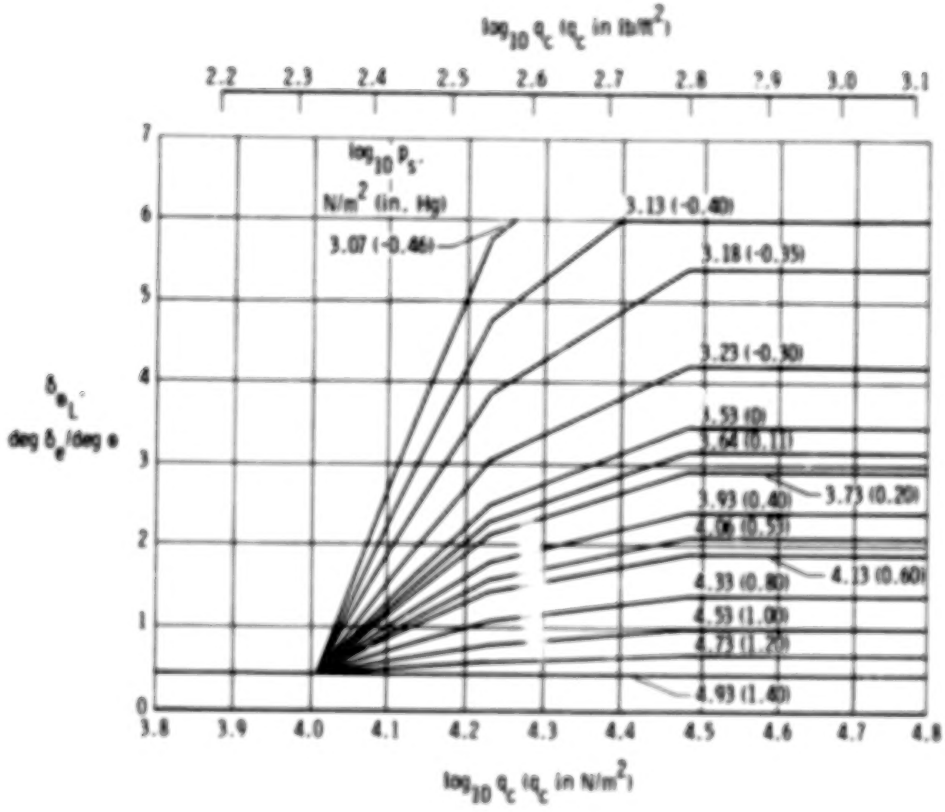

(c) Schedule 3: pitch attitude gain schedule.

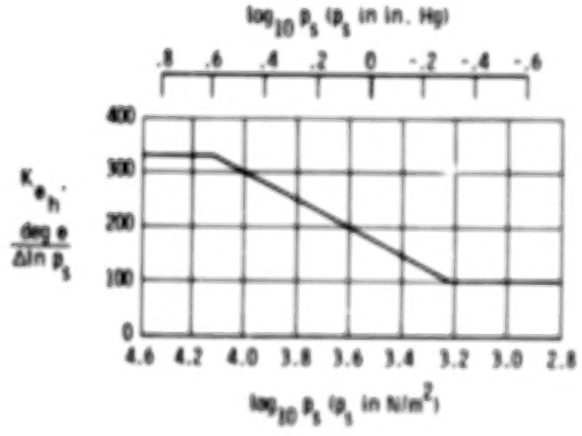

(d) Schedule 4: altitude displacement gain schedule.

Figure 52. Continued.

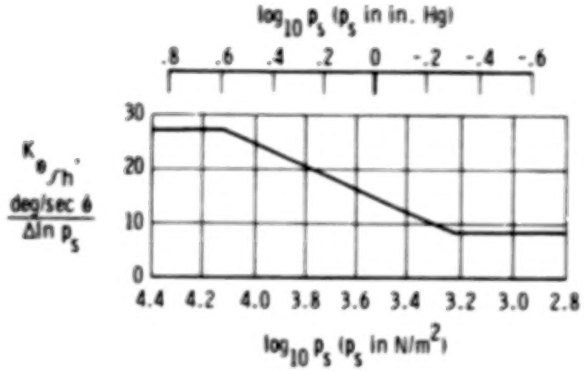

(e) Schedule 5: altitude integral gain schedule.

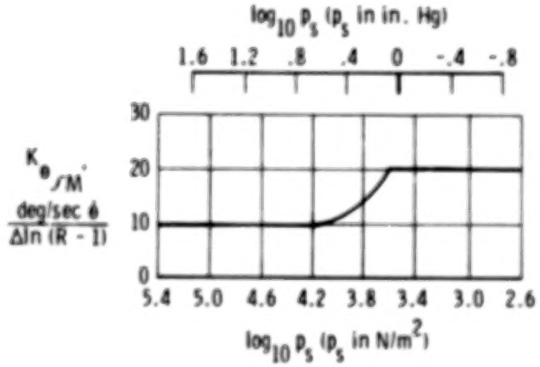

(f) Schedule 6: Mach integral gain schedule.

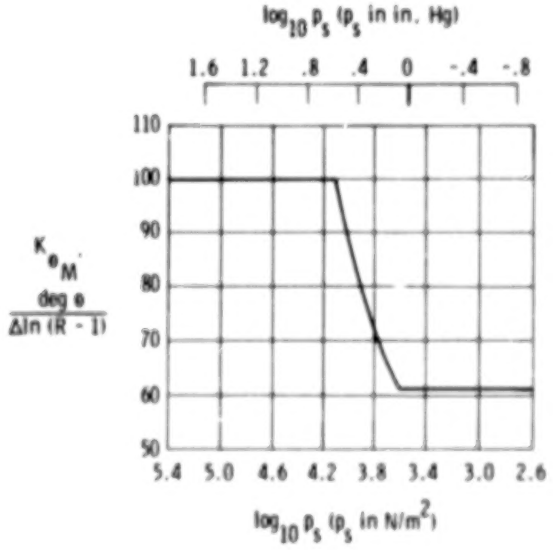

(g) Schedule 7: Mach displacement gain schedule.

Figure 52. Continued.

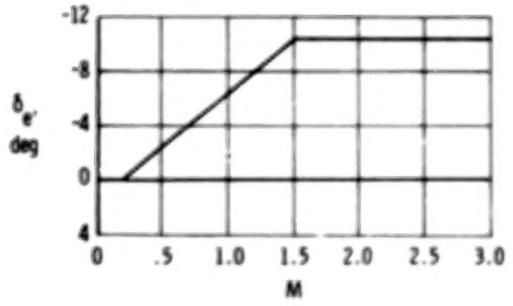

(h) Schedule 8: Mach trim system compensation.

Figure 52. Concluded.

Pitch SAS is used full time on the aircraft and consists of proportional pitch rate feedback for short-period damping augmentation. At altitudes above 15,200 meters (50,000 feet), lagged pitch rate is added to increase the aircraft's effective static stability. In the SAS mode, speed stability augmentation is provided from Mach 0.2 to Mach 1.5.

The primary autopilot mode is attitude hold; the altitude and Mach hold modes are outer loops of the attitude hold mode. Attitude hold consists of lagged pitch attitude and high-passed pitch attitude, which are summed. The signal is multiplied by a scheduled gain and then simultaneously sent to the pitch series servo and the autotrim and its compensator. There is an elevon limit of ±2.3° on the SAS servo input. The threshold of the autotrim is 0.1 degree per second. The pilot can command pitch attitude changes through a pitch attitude trim wheel.

The altitude hold mode receives altitude and altitude rate information from the ADC in terms of $\Delta ln\ p_s$ and $\dot{\overline{ln\ p_s}}$ respectively. The quantity $\Delta ln\ p_s$ is a perturbation around the flight condition that exists at the time of engagement. This perturbation is obtained by means of a clutch system within the ADC. The range of $\Delta ln\ p_s$ is equivalent to approximately ±155 meters (±507 feet). At an altitude of 23,600 meters (77,500 feet), the natural log quantities given above are related to altitude by the following expressions. In SI Units,

$$\Delta h = (-6490)\Delta ln\ p_s$$

$$\dot{h} = (-6490)\dot{\overline{ln\ p_s}}$$

In U.S. Customary Units,

$$\Delta h = (-21,300)\Delta ln\ p_s$$

$$\dot{h} = (-21,300)\dot{\overline{ln\ p_s}}$$

Altitude rate, altitude error, and integral altitude are then summed and added to the attitude loop.

The Mach hold mode receives Mach information from the ADC in terms of $\Delta ln\ (R - 1)$, which is a perturbation around the flight condition at the time of engagement and a clutched function of the ADC. The range of the $\Delta ln\ (R - 1)$ is approximately equivalent to ±0.25 Mach number at Mach 3.0. At Mach 3.0, $\Delta ln\ (R - 1)$ is related to ΔM by the expression

$$\Delta M = (1.43)\Delta ln\ (R - 1)$$

Mach error and integral Mach error are then summed and added to the attitude loop. Mach rate feedback was originally designed into the system, but the signal was found to have excessive noise and did not contribute to Mach stability.

APPENDIX B.—DEFINITION OF DAMPING INDEX AND RELATIONSHIP WITH SECOND-ORDER SYSTEM SUBSIDENCE RATIO

The subsidence ratio for a second-order system is defined as $\frac{|X_m|}{|X_0|}$, based on the following sketch (ref. 13).

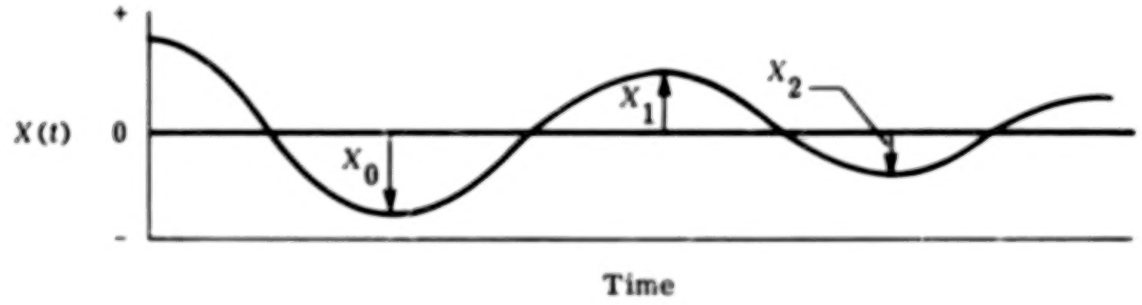

The quantity $X(t)$ can be expressed as

$$X(t) = A\left(e^{-\zeta\omega_n t}\right)\cos\left(\omega_d t\right)$$

where A is an arbitrary amplitude. The time, t, at the peaks of the oscillation is expressed as

$$t = \frac{1}{\omega_d}\left(\frac{\pi}{2} + \pi m\right)$$

Evaluating $X(t)$ at peak values of the oscillation yields the following subsidence ratio definition:

$$\frac{|X_m|}{|X_0|} = e^{\delta\pi m}$$

where $\delta = -\zeta/\sqrt{1 - \zeta^2}$.

The subsidence ratio definition assumes that the parameter measured is linear and oscillating about zero or some known bias, which must be removed prior to evaluation. The simulation used in the autopilot studies was nonlinear and greater than second order; therefore, a given parameter did not oscillate about a known bias. However, much of the basic response information approximated second-order data superimposed on an exponential curve.

Based on the following sketch, a damping parameter similar to the subsidence ratio was defined. This damping parameter, referred to herein as the damping index, *DI*, is given by the following expression:

$$DI = \frac{X_2 - X_1}{X_0 - X_1}$$

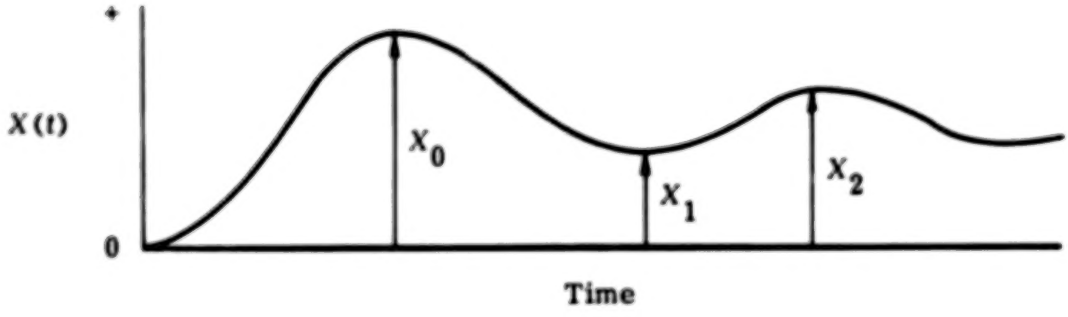

When this formula is applied to a second-order system,

$$DI = e^{\delta\pi}$$

which is identical to the subsidence ratio definition when m equals 1.

APPENDIX C.—ANALYSIS OF MODIFIED AUTOPILOT

HIGH FREQUENCY OSCILLATION

Experimental studies showed that measured static pressure was sensitive to angle of attack and that this sensitivity tended to reduce the short-period stability with the outer loops engaged. To partially compensate for this destabilizing effect, high-passed pitch rate was implemented in the modified altitude hold autopilot as an additional feedback loop.

Figure 53 is a block diagram of the attitude portion of the modified system. Pitch rate is sensed by a backup SAS gyro, which is forward of the center of gravity; high-passed through the filter $\frac{50s}{(s + 0.5)(s + 50)}$; and then summed with the autopilot outer-loop signals at the gain schedule 3 input summer (fig. 28).

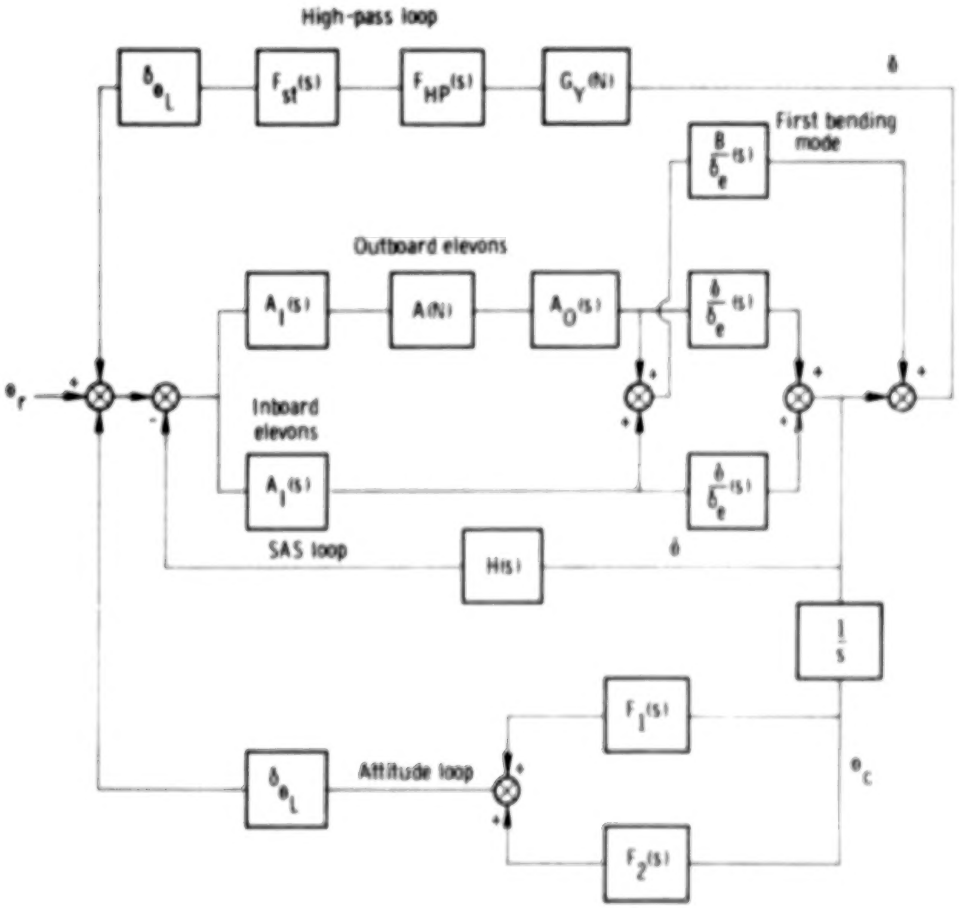

Figure 53. Block diagram of modified autopilot attitude hold mode.

On the first flight after implementation of the modified autopilot, with the high-passed pitch rate feedback loop engaged and set at a gain of 1.07, the aircraft developed an undesirable residual oscillation. The oscillation, which had a frequency of approximately 3 hertz, was bounded at a peak-to-peak pitch rate of less than 0.6 degree per second.

The transfer functions that describe the pertinent elements of the system modeled (fig. 53) are as follows:

$$\frac{B}{\delta_e}(s) = \frac{K_B s \omega_B^2}{s^2 + 2\zeta_B \omega_B + \omega_B^2}$$

where $15.7 \leq \omega_B \leq 20.6$, $K_B = 0.016$, and $\zeta_B = 0.05$; and

$$\frac{\dot{\theta}}{\delta_e}(s) = \frac{0.575s(s + 0.008)(s + 0.1646)(s - 0.0049)}{(s - 0.00278)(s + 0.0000356 \pm 0.055j)^2(s + 0.133 \pm 1.20j)^2}$$

$$A_I(s) = \frac{1470}{s^2 + 46s + 1470}$$

$$A(N) = \pm 0.15^\circ \text{ hysteresis}$$

$$A_O(s) = \frac{2210}{(s^2 + 75.4s + 2210)(1 + 0.05s)}$$

$$F_1(s) = \frac{0.175}{(s + 0.175)}$$

$$F_2(s) = \frac{0.25s}{(s + 0.4)}$$

$$F_{HP}(s) = \frac{50s}{(s + 0.5)(s + 50)}$$

$$F_{st}(s) = \frac{(s^2 + 4s + 400)}{(s^2 + 40s + 400)}$$

$$G_Y(N) = \pm 0.1 \text{ deg/sec negative deficiency}$$

$$h(s) = \frac{0.15(s + 8)}{(s + 4)} + \frac{4(s + 1)}{(s + 10.4)(s + 0.077)}$$

$$\delta_{\theta_L} = 3.6$$

Omitting the transmission linkage nonlinearity, $A(N)$, the system was manipulated to an equivalent form, which is presented in figure 54. In the equivalent system, $G'(s)$ combines the SAS and attitude closed-loop transfer functions. To isolate gyro nonlinearity, high-passed pitch rate is depicted as the only feedback loop. In addition, the filter zeros of $F_{st}(s)$ are assumed to cancel the bending mode characteristics.

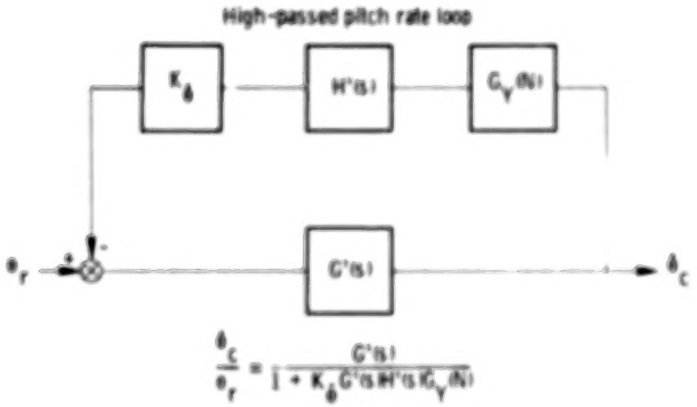

Figure 54. Equivalent modified attitude hold system.

A linear analysis of the equivalent system (fig. 54) was performed with $G_\gamma(N)$ assumed to be 1. The open-loop frequency response, $K_{\dot\theta} G'(s) H'(s)$, is presented in figure 55. The system shows an increase in $\dot\theta/\delta_e$ of 40 decibels per decade at

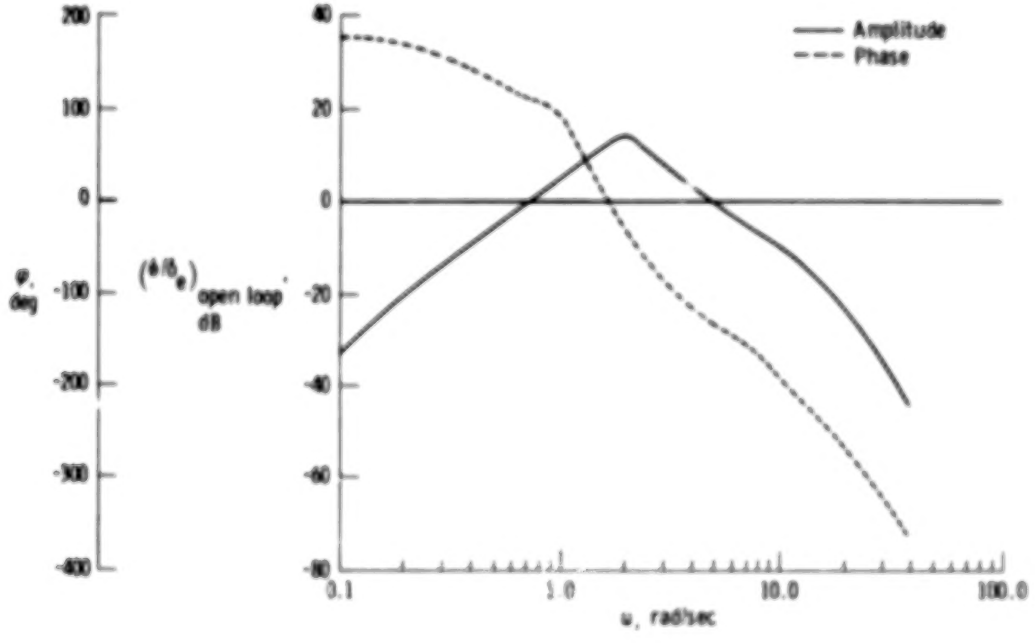

Figure 55. Open-loop frequency response of linear modified attitude hold mode including high-passed pitch rate feedback loop.

the lower frequencies and attenuation of approximately 160 decibels per decade at the higher frequencies. In addition, the expected phase shift accompanies the amplitude variation. For the approximate design gain setting, $K_{\dot{\theta}} = 1.0$, in the high-pass loop, the system has a phase margin of 45° and a gain margin of approximately 10 decibels. In general, the predicted open-loop margins are reasonable for this type of system. Additional gain or phase lag, or both, is required to sustain limit cycles. After considering possible sources, such as transmission linkage hysteresis, gyro location, and gyro nonlinearity, the gyro was believed to be the element most likely to provide the necessary gain and phase lag.

The gyro was removed from the aircraft and mounted on a rate table, and normal oscillations and rate tests were conducted. The input to the rate table was at a frequency of 1 hertz and amplitudes slightly above those normally experienced in flight. As shown in figure 56, when the rate is approximately zero, the output is

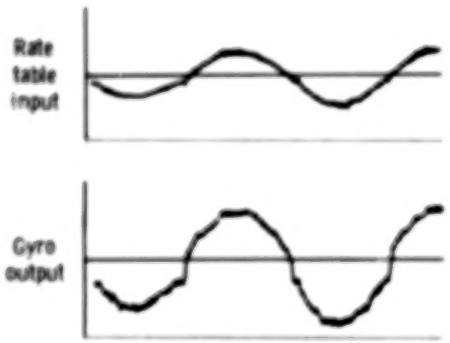

Figure 56. Negative deficiency of gyro used in high-passed pitch rate feedback loop. f = 1 hertz.

particularly different and noticeable as compared to the rest of the cycle. This type of nonlinearity, referred to as negative deficiency, is common to rate sensors, occurring normally with increasing age. Presented in figure 57 are the results of

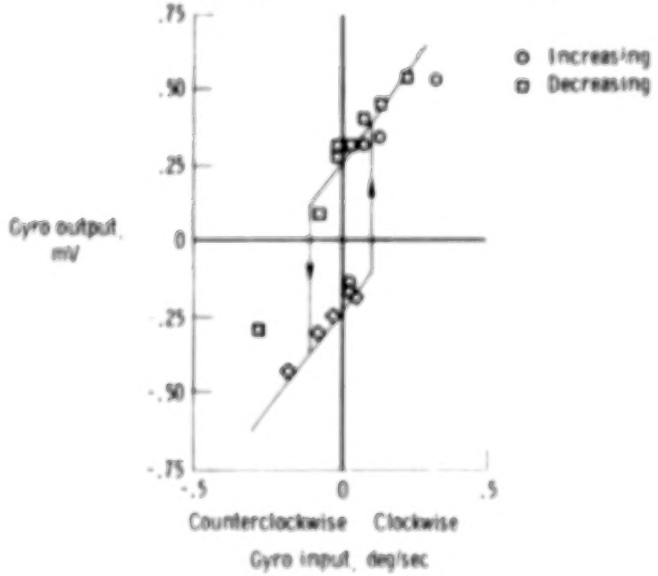

Figure 57. Negative deficiency characteristic of gyro.

constant-rate tests. The maximum input rates are typical of those measured in flight. The input to the rate table is a complete continuous cycle, first increasing in the clockwise direction, then decreasing and increasing through the counterclockwise direction, and finally returning to zero. From the constant-rate tests it is evident that conservative values for the amount of deadband would be within ±0.1 degree per second at low rates. At the higher rates, above 1 degree per second, the sensed rate of 1.7 mV/deg/sec shows good agreement with the design scale factor. The increase in gain and phase lag descriptive of this type of nonlinearity is presented as a describing function in figure 58, which is adapted from

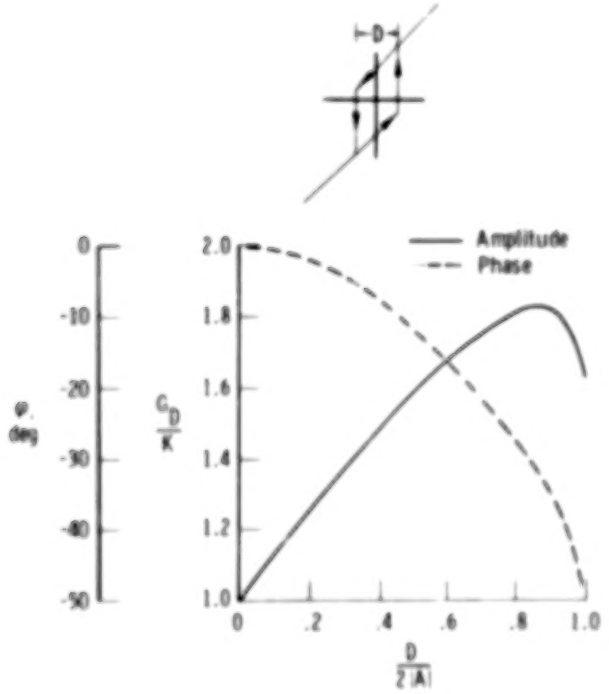

Figure 58. Negative deficiency describing function (adapted from ref. 10).

reference 10. Classical system stability analysis was used with the describing function to predict the limit cycle frequency and amplitude. For example, with reference to figure 54, the nonlinear gyro is manipulated to be cascaded with the other elements into a single loop. Direct application of the Nyquist stability criterion then provides insight regarding the cause and degree of this type of problem.

The Nyquist criterion is essentially concerned with the condition when $K_\theta G'(s)H'(s)G_Y(N)$ equals -1 or when the characteristic equation equals zero. Therefore, when this condition is just satisfied (the magnitude equals 1 and phase equals -180°), the system will be critically stable and able to sustain limit cycle oscillations. The two functions, $K_\theta G'(s)H'(s)$ and $\frac{-1}{G_Y(N)}$, are separated for determining a solution. The open-loop transfer function, $K_\theta G'(s)H'(s)$, is presented in figure 55 as a function of frequency. The function $\frac{-1}{G_Y(N)}$ is the negative reciprocal of the describing function presented in figure 58. In figure 59, the two

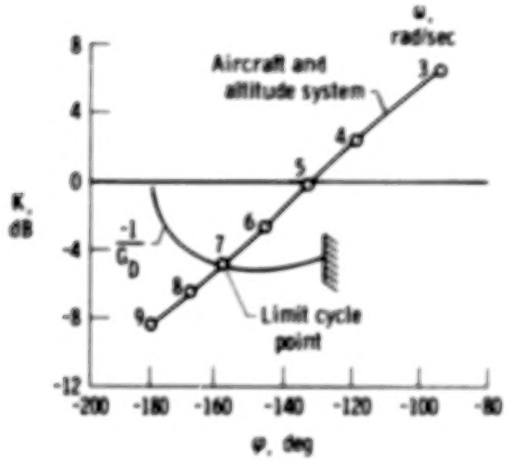

Figure 59. Phase versus amplitude of aircraft with modified altitude hold mode and nonlinearity (negative deficiency) in high-passed pitch rate feedback loop.

functions are plotted as amplitude versus phase and are varied parametrically with frequency and amplitude, respectively. The intersection of the two curves, which occurs at a frequency of approximately 7 radians per second and a pitch rate of approximately 0.15 degree per second, predicts the frequency and amplitude of the limit cycle for a $K_{\dot{\theta}}$ of 1.0. It is evident that if the gain were reduced sufficiently, no intersection would exist; consequently, no residual oscillations would be predicted.

Subsequent flight tests and simulator studies were conducted at the same flight test conditions. Figure 60 is a summary and comparison of data from the flight

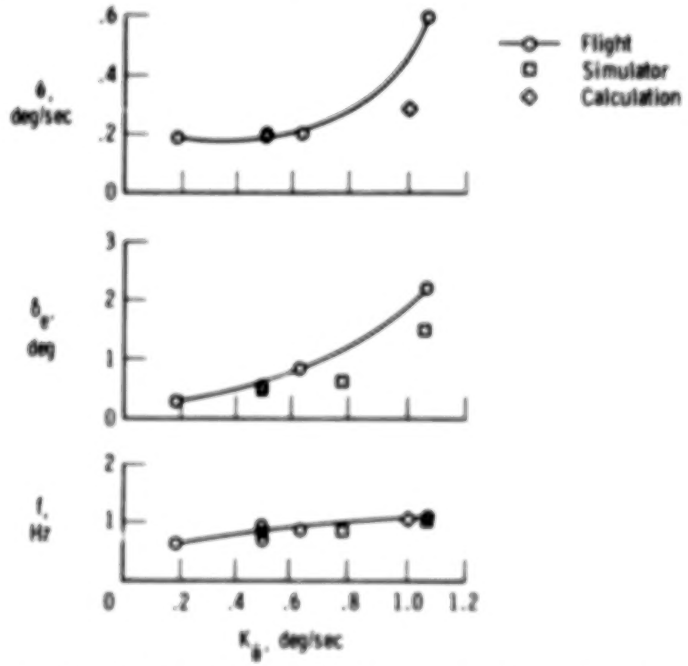

Figure 60. Modified autopilot attitude hold mode peak-to-peak oscillations and frequency versus high-passed pitch rate gain.

tests, simulator studies, and limit cycle calculations. The calculations and simulator studies predicted lower peak-to-peak amplitudes than those experienced in the flight tests. These differences are believed to be caused by the ±0.15° transmission linkage hysteresis between the inboard and outboard elevons. This nonlinearity was not accounted for in the simulator studies or in the limit cycle calculations.

REFERENCES

1. Berry, Donald T.; and Powers, Bruce G.: Flying Qualities of a Large, Supersonic Aircraft in Cruise and Landing Approach. AIAA Paper 70-566, May 1970.

2. Berry, D. T.; and Gilyard, G. B.: Some Stability and Control Aspects of Airframe/Propulsion System Interactions on the YF-12 Airplane. ASME Paper 73-WA/Aero-4, Am. Soc. Mech. Eng., Nov. 1973.

3. Coleman, Herbert J.: Concorde Tour Adds to Operations Data. Aviation Week & Space Technology, vol. 97, no. 6, Aug. 7, 1972, pp. 31-32.

4. Gilyard, Glenn B.; Berry, Donald T.; and Belte, Daumants: Analysis of a Lateral-Directional Airframe/Propulsion System Interaction. NASA TM X-2829, 1973.

5. Gilyard, Glenn B.; Berry, Donald T.; and Belte, Daumants: Analysis of a Lateral-Directional Airframe/Propulsion System Interaction of a Mach 3 Cruise Aircraft. AIAA Paper 72-961, Sept. 1972.

6. Gilyard, Glenn B.; Smith, John W.; and Falkner, Victor L.: Flight Evaluation of a Mach 3 Cruise Longitudinal Autopilot. AIAA Paper 74-910, Aug. 1974.

7. Montoya, Earl J.: Wind-Tunnel Calibration and Requirements for In-Flight Use of Fixed Hemispherical Head Angle-of-Attack and Angle-of-Sideslip Sensors. NASA TN D-6986, 1973.

8. Gilyard, Glenn B.; and Belte, Daumants: Flight-Determined Lag of Angle-of-Attack and Angle-of-Sideslip Sensors in the YF-12A Airplane From Analysis of Dynamic Maneuvers. NASA TN D-7819, 1974.

9. Brown, Stuart C.: Computer Simulation of Aircraft Motions and Propulsion System Dynamics for the YF-12 Aircraft at Supersonic Cruise Conditions. NASA TM X-62245, 1973.

10. Grabbe, Eugene M.; Ramo, Simon; and Wooldridge, Dean E., eds.: Handbook of Automation, Computation, and Control. Volume 1 — Control Fundamentals. John Wiley & Sons, Inc., c.1958.

11. Larson, Terry J.: Compensated and Uncompensated Nose Boom Static Pressures Measured From Two Air Data Systems on a Supersonic Airplane. NASA TM X-3132, 1974.

12. Richardson, Norman R.; and Pearson, Albin O.: Wind-Tunnel Calibrations of a Combined Pitot-Static Tube, Vane-Type Flow-Direction Transmitter, and Stagnation-Temperature Element at Mach Numbers From 0.60 to 2.87. NASA TN D-122, 1959.

13. Northrop Aircraft, Inc.: Methods of Analysis and Synthesis of Piloted Aircraft Flight Control Systems. BU AER Rept. AE-61-4I, Bureau of Aeronaut., Navy Dept., Mar. 1952.

1. Report No.	2. Government Accession No.	3. Recipient's Catalog No.
NASA TP-1180		

4. Title and Subtitle	5. Report Date
RESULTS FROM FLIGHT AND SIMULATOR STUDIES OF A MACH 3 CRUISE LONGITUDINAL AUTOPILOT	April 1978
	6. Performing Organization Code: H-940
7. Author(s): Glenn B. Gilyard and John W. Smith	8. Performing Organization Report No.
	10. Work Unit No.: 516-51-01
9. Performing Organization Name and Address: NASA Dryden Flight Research Center, P.O. Box 273, Edwards, California 93523	11. Contract or Grant No.
	13. Type of Report and Period Covered: Technical Paper
12. Sponsoring Agency Name and Address: National Aeronautics and Space Administration, Washington, D.C. 20546	14. Sponsoring Agency Code

15. Supplementary Notes

16. Abstract

At Mach numbers of approximately 3.0 and altitudes greater than 21,300 meters (70,000 feet), the original altitude and Mach hold modes of the YF-12 autopilot produced aircraft excursions that were erratic or divergent, or both. (Altitude hold was not designed for high altitudes, whereas Mach hold was designed for high Mach number.) Flight data analysis and simulator studies showed that the sensitivity of the static pressure port to angle of attack had a detrimental effect on the performance of the altitude and Mach hold modes. Good altitude hold performance was obtained when a high-passed pitch rate feedback was added to compensate for angle-of-attack sensitivity and the altitude error and integral altitude gains were reduced. Good Mach hold performance was obtained when the angle-of-attack sensitivity was removed; however, the ride qualities remained poor.

17. Key Words (Suggested by Author(s))	18. Distribution Statement
Flight controls Altitude control Mach 3 cruise aircraft YF-12 aircraft	Unclassified—Unlimited Category: 08

19. Security Classif. (of this report)	20. Security Classif. (of this page)	21. No. of Pages	22. Price*
Unclassified	Unclassified	85	$4.75

*For sale by the National Technical Information Service, Springfield, Virginia 22161

NASA-Langley, 1978